TECHNISCHE UNIVERSITÄT MÜNCHEN

Lehrstuhl für Hochspannungs- und Anlagentechnik

Influence of Fillers on Silicone Elastomers for Outdoor Insulation

André Dantas Germano

Vollständiger Abdruck der von der Fakultät für Elektrotechnik und Informationstechnik der Technischen Universität München zur Erlangung des akademischen Grades eines Doktor-Ingenieurs genehmigten Dissertation.

Vorsitzender:		Univ.-Prof. Dr. rer. nat. Thomas Hamacher
Prüfer der Dissertation:	1.	Univ.-Prof. Dr.-Ing. Josef S. Kindersberger
	2.	Univ.-Prof. Dr.-Ing. Ernst Gockenbach, Universität Hannover

Die Dissertation wurde am 15.12.2014 bei der Technischen Universität München eingereicht und durch die Fakultät für Elektrotechnik und Informationstechnik am 11.06.2015 angenommen.

ABSTRACT

Insulating material in outdoor insulation may be exposed directly to the environment and be subject to various stresses like humidity, leakage currents, electrical surface discharges, UV radiation and acid exposure. Usually, micro-sized inorganic fillers are used to improve the resistance of polymeric insulating material to such stresses. For a promising silicone base material the effect of submicron fillers of different types, sizes and amounts is studied on electrical, mechanical and chemical properties. Additionally, the mechanism of action of fillers is explained by models based on their interaction with the base material.

ZUSAMMENFASSUNG

Isolierwerkstoffe für Freiluftanwendungen sind Umwelteinflüssen wie Feuchtigkeit, Kriechströmen, Oberflächenentladungen, Säuren sowie UV-Strahlung ausgesetzt. Um die Beständigkeit polymerer Isolierwerkstoffe zu verbessern, werden üblicherweise anorganische mikroskalige Füllstoffe verwendet. Für ein ausgewähltes Silikonpolymer und verschiedene Füllstoffarten wird in der Arbeit der Einfluss von Partikelgröße und Füllstoffanteil auf die elektrischen, mechanischen und chemischen Eigenschaften untersucht. Mit Hilfe von Modellen, die von einer Wechselwirkung der Füllstoffe mit dem Basismaterial ausgehen, wird der Wirkmechanismus der Füllstoffe beschrieben.

RESUMO

Os isolamentos elétricos de uso externo são tipicamente submetidos a intempéries e a uma série de esforços como umidade, correntes de fuga, descargas superficiais e radiação ultravioleta. Normalmente, preenchimentos inorgânicos em escala micrométrica são empregados para melhorar a resistência dos isolamentos a esses fatores. Visando a melhor qualidade dos materiais baseados em silicone, o efeito de preenchimentos submicrométricos de diversos tipos, tamanhos e quantidades é estudado em propriedades elétricas, mecânicas e químicas. Adicionalmente, o mecanismo de ação desses preenchimentos é explicado através de modelos baseados na interação do preenchimento com o material base.

TABLE OF CONTENTS

LIST OF FIGURES

LIST OF TABLES

LIST OF ABBREVIATIONS

ATH	alumina trihydrate, $Al(OH)_3$, aluminium hydroxide
CI	confidence interval
DDT	dynamic drop test
DSC	differential scanning calorimetry
EDX	energy-dispersive X-ray
EPDM	ethylene propylene diene monomer rubber
EPR	ethylene propylene rubber
ESDD	equivalent salt deposit density
EVA	ethylene-vinyl acetate copolymer
FE-SEM	field emission scanning electron microscope
HCEP	hydrophobic cycloaliphatic epoxy
HCR	high consistency silicone rubber
HTV	high temperature vulcanizing/vulcanized (silicone rubber)
LMW	low molecular weight (silicone components)
LSR	liquid silicone rubber
PC	polycarbonate
PE	polyethylene
PEI	polyetherimide
phr	parts per hundred parts rubber
RTV	room temperature vulcanizing/vulcanized (silicone rubber)
SIR	silicone rubber
TGA	thermogravimetric analysis
UV	ultraviolet light
wt%	percentage by weight

1 INTRODUCTION

Electrical outdoor insulation is an essential part of energy systems, directly influencing their efficiency and reliability. Historically, electrical insulators have been traditionally composed of glass or porcelain; nevertheless, ever since their introduction in overhead transmission lines in the 1980s, polymeric insulators are gaining ground over their ceramic counterparts.

The advantages of polymeric insulation include their improved contamination performance, lower susceptibility to vandalism, light weight, easy handling and reduced installation and maintenance costs [1-3]. Adversely, polymeric insulation possesses low erosion performance and mechanical strength [4-6]. In fact, in the early days of this technology, its use for outdoor insulation was only made feasible by the discovery, in the 1950s, that alumina trihydrate (ATH) increases the tracking and erosion resistance of such material ([7] apud [8]).

Field experience with polymeric insulators associated with the advances in polymer technology allowed an improvement of overall material performance. Initial compositions included ethylene propylene rubber (EPR) [9], which was later added to silicone rubber (SIR). In the late 1980s ethylene propylene diene monomer (EPDM) was introduced, taking advantage of technology improvements in EPDM materials [3].

Early experience with SIR included room temperature vulcanizing (RTV)-SIR, later replaced by high temperature vulcanizing (HTV)-SIR, which had a higher tear resistance of the weathersheds [10]. Among the several choices of polymeric housing materials for outdoor insulation, nowadays SIR is recognized as the most superior and popular material [4], and as a result stands out with an expanding field of research and applications.

Adequate material development and compound formulations can provide higher general performance to polymeric insulators [11]. Fillers and additives are blended with the basic polymer not only to enhance performance, but also to reduce costs and facilitate processing [6,12]. The fillers that are typically employed in the insulation industry are examined in the next section.

1.1 A REVIEW OF CONVENTIONAL FILLERS

Fillers are usually applied in polymer compositions to improve specific properties. As such, ATH is extensively used to improve tracking and erosion resistance to SIR [12-13], while silica (SiO_2) might be used to improve elasticity, tear resistance and tensile strength [12].

Standard grade fillers and additives usually need to be added in high amounts to improve a desired property (up to 80% by weight of the formulation [4]). This might, on the other hand, affect other properties negatively, e.g., despite being a major flame retardant, high amounts of ATH are known to be detrimental to mechanical properties [14-15].

NELSON et al. [16] verified substantial benefits with the use of titanium dioxide (TiO_2) in an epoxy matrix, particularly with regard to improvements in voltage endurance. KIM et al. [17] studied the effects of ATH filler in RTV-SIR coatings, and affirmed that even though the filler imparts tracking and erosion resistance, the diffusion rate of silicone fluid to the surface decreases with increasing filler level. Furthermore, DENG et al. [18] showed that the amount of silicone fluid in the surface also decreases with increasing filler size.

FANG et al. [12] analyzed the electrical and mechanical properties of silicone rubber blends with different levels of ATH and different silica fillers. The results showed that between the 4 silica types tested, fumed silica contributed more on hardness, tensile strength, elongation and tear strength. Regarding ATH, the authors state that at least 100 phr (parts per hundred parts of rubber) are necessary to pass the inclined plane test, however further increase of ATH level after 70 phr already leads to decreased mechanical properties.

Still on the subject of optimum loading level, according to KUMAGAI et al. [19], the critical level of ATH filler in HTV-SIR is 40 wt%: with less than that amount, frequent occurrence of high temperature spots are found to cause tracking and erosion, while highly filled HTV-SIR (> 40 wt% ATH) allow no erosion when exposed to such high temperature spots.

1.2 THE INTRODUCTION OF NANOFILLERS

The definition of nanomaterials is still debated, but these are generally accepted to be materials with at least one dimension under the 100 nm range. Fillers which suit this requirement are, therefore, named nanofillers. Such fillers present themselves a viable alternative to the standard grade ones, due to the comparatively more extensive filler/polymer interface (i.e. larger chemical and physical interaction with the polymer matrix) and the emerging of mesoscopic properties that belong neither to the atomic nor the macroscopic frame.

In this manner, nanofillers are capable of reaching the desired improvements in polymer performance in considerably lower amounts (less than 10%), so avoiding the usual drawbacks of standard grade fillers [15,20-23]. Not surprisingly, the field of nanotechnology has been ever increasing in the last couple of decades, and nanofillers are being widely researched [15-16,20-35].

It was reported, for example, that nano-sized magnesium hydroxide performs better than conventional ATH in RTV in terms of eroded mass, depth, width and length of erosion [24]. Another research shows that the required flame retardation of an RTV-layered silicate nanocomposite can be obtained with an amount of filler equivalent to only one tenth of the conventionally required ATH quantity, with the upside of not degrading other properties like loss factor or permittivity [20].

HAN et al. [15] studied the effects of nanosilica in ethylene-vinyl acetate copolymer (EVA)-ATH composites, concluding that by partially replacing ATH by nanosilica, better thermal stability, tracking and erosion resistance, flame retardancy and tensile properties could be obtained. KOZAKO et al. [21] showed that polyamide nanocomposites are more resistant to partial discharges than pure polyamide or polyamide-microfiller composites.

Notwithstanding these encouraging studies, a large-scale application of nanofillers is mainly limited by factors such as their superior costs [25], difficulty to attain proper dispersion [26-28], the requirement of special safety precautions for their handling [20] and lack of comprehensive understanding of their operation.

Concerning the comparison of nanofillers amongst themselves, MAITY et al. [35] showed that the inclusion of nano-aluminium oxide (n-Al_2O_3) and nano-titanium dioxide (n-TiO_2) in epoxy resin increases the resistance of the material to surface degradation. RAMIREZ et al. [29] compared n-Al_2O_3 with different types of nanosilica, and found out that fumed nanosilica imparts better heat resistance to SIR than natural nanosilica or n-Al_2O_3. However REED [30] stated that the use of n-SiO_2 in polyethylene (PE), polycarbonate (PC) or polyetherimide (PEI) often results in degraded or non-reproducible electrical and mechanical properties.

RAETZKE et al. [31] studied the erosion behavior of both nano and micro-sized SiO_2 and Al_2O_3 fillers in HTV-SIR, concluding that, between them, n-SiO_2 provided better erosion resistance, lowest loss factor and relative permittivity. Further, in [32] the authors compared two different types of n-SiO_2 regarding their resistance to high voltage arcing and tracking and erosion; the results showed that precipitated nanosilica improves both properties especially at 5 wt%, while fumed nanosilica does not enhance any of the properties significantly.

A review chart of relevant research in this field, listing the typically employed micro and nanofillers associated to the base materials and the investigated properties is presented in Table 1.

Table 1. Chart review of typical fillers, base material and investigated properties.

Filler Type	Base Material	Investigated Properties	Reference
ATH	HTV-SIR	Tracking and erosion resistance	[19,36-37]
	RTV-SIR	Leakage current under salt fog	[17-18]
		Surface roughness and LMW diffusion from bulk to surface	[18]
	RTV-SIR coating	Leakage current under salt fog	[38]
	HCR-SIR	Tracking and erosion resistance	[37]
	Silicone rubber	Arcing resistance and Tracking and Erosion Resistance	[39]
		Hydrophobicity and surface roughness	[40]
Magnesium hydroxide	Silicone rubber	Tracking and erosion resistance	[41]
Nano-sized magnesium hydroxide	RTV-SIR	Tracking and erosion resistance	[24]
Nano-sized aluminium oxide	EPDM	Mechanical properties	[41]
	HTV-SIR	Arcing resistance	[31]
	Polymethylmethacrylate	Mechanical properties	[42]
	Silicone rubber	Erosion resistance and mechanical properties	[29]
Nano-sized silicon dioxide	Epoxy	Tracking and erosion resistance	[43-44]
	EVA-ATH	Mechanical properties and thermogravimetric analysis	[15]
	HTV-SIR	Arcing resistance	[31-32,45]
		Tracking and erosion resistance	[32]
	Polyethylene	Dielectric breakdown strength and voltage endurance	[23]
	Polyimide	Partial discharge resistance	[23]
	RTV-SIR	Hydrophobicity and tracking and erosion resistance	[46]
	RTV-SIR coating	Hydrophobicity, surface roughness and tracking and erosion resistance	[47]
	Silicone rubber	Arcing resistance and tracking and erosion resistance	[48]
		Erosion resistance and mechanical properties	[29]
	Silicone rubber coating	Leakage current and ESDD	[49]
Nano-sized titanium dioxide	Epoxy	Dielectric breakdown strength	[16,50-51]
		Resistance to surface discharges	[35]
	Low density polyethylene	Dielectric relaxation	[52]

1.3 MOTIVATION

The ability of polymeric insulators to resist physical and chemical degradation due to voltage stress, heat, rain, salt fog, pollution and ultraviolet radiation is still the focus of a great deal of research. The previous section presented and overview of the state of the art of polymeric insulation for outdoor applications, with an emphasis on the application of inorganic fillers for improvement of electrical properties. Advances in nanotechnology urged its application in this field, and many models are available to try to elucidate how the performance improvements in nanocomposites are reached, although it still remains unclear.

A brief review of research regarding nanofillers was provided, where it is possible to see that studies are focused on the influence of specific fillers on a very limited set of properties, while scattered over quite a few base materials, which makes the cross-referencing of data implausible. With that in mind, the following questions are raised:

- Are the available models capable of explaining the mechanism of action of nanofillers? Is the effect of aggregates and agglomerates accounted for? How significant are they?
- The formulation of compounds is a very intricate process, where the improvement of a set of properties usually happens at the expense of others. Which are these compromises and concessions?
- What is the influence of filler chemical composition and size? Is surface treatment relevant?
- Can standard grade ATH be fully removed from silicone rubber compositions and substituted by nanofillers while maintaining an equivalent performance?

Hence, the current work proposes the investigation of fillers ranging from the nanoscale to the standard grade microfillers, both individually and combined, in respect to a wide range of electric, chemical, thermal and mechanical properties, building an extensive set of data in the hope of obtaining clues to the mechanism of action of submicron fillers and their effect on a sizeable set of properties. Data will be checked against available theoretical models, to analyze whether changes in material properties are reasonably explained by them. Conclusions will be drawn as to whether an optimum filler type and loading level can be determined to reach specific properties.

The current work was developed between 2011 and 2014 at the *Technische Universität München* and LAPP Insulators in Wunsiedel, Germany. Material matrix consisted of HTV and fillers of interest included ATH, silica, titania, alumina and boehmite; investigated properties included resistance to high voltage arcing and tracking and erosion, degree and loss of hydrophobicity, resistance to acid and UV stress, tensile strength and tear resistance. Material and methods are further detailed in Chapter 2; results are presented in Chapter 3 and thoroughly discussed in Chapter 4; pertinent conclusions are drawn in Chapter 5, followed by acknowledgements and a list of relevant bibliography.

2 MATERIAL AND METHODS

2.1 MATERIAL

The investigated material consists of high temperature vulcanized silicone rubber (HTV) compounds. Initially, the fillers listed in Table 2 were mixed to a low viscosity dimethylsiloxane methyl vinyl gum at 17 wt% to produce masterbatches. These masterbatches were then mixed to the base material to produce compounds with nanofiller loading level ranging from 0 to 3 wt% (S1, S2 and A2) or 0 to 5 wt% (T1, A1 and A3). The first base material consists of pure HTV silicone rubber, while the second one consists of HTV silicone rubber containing standard grade ATH (mean particle size of 1.2 µm) at 52 wt%.

Table 2. Description of the six submicron-scale fillers studied.

Filler	Description
S1	Hydrophilic fumed silicon dioxide with mean particle size of 7 nm
S2	Hydrophobic fumed silicon dioxide, octylsilane treated, with mean particle size of 12 nm
T1	Hydrophilic fumed titanium dioxide with mean particle size of 20 nm
A1	Hydrophilic fumed aluminium oxide with mean particle size in the range of 7-20 nm
A2	Aluminium hydroxide with mean particle size of 400 nm
A3	Aluminium oxide hydroxide (boehmite) with mean particle size of 350 nm

All mixing was performed in an industrial sigma blade kneader. Compounds were then pressed in steel moulds and vulcanized, for a cross-linking agent activated by pressure and temperature was used. Three basic sample designs were produced to fit each of the performed tests parameters: 120 x 50 x 6 mm slabs, 140 x 120 x 3 mm and 140 x 120 x 2 mm plates. Other relevant material data, such as the roughness of the samples and the quality of dispersion of the fillers, are discussed in the coming chapters.

2.2 METHODS

In order to characterize and evaluate material, nine methods are proposed in this chapter: initially, surface roughness and filler dispersion are investigated to assure their uniformity. Then tests are chosen taking into account the physical parameters which are more important for polymeric material applied in outdoor insulation according to [53]: degree and loss of hydrophobicity are investigated with contact angle measurements and the dynamic drop test; their resistance to pollution initiated surface discharges is studied via IEC 61621 and IEC 60587; mechanical properties via ISO 34-1 and ISO 37; thermal stability with thermogravimetric analysis, and a new methodology is developed to investigate the effects of UV and acid exposure.

2.2.1 Surface Roughness

The mean roughness depth (R_z) is to be determined using a laser profilometer from the company Nanofocus (µScan AF2000) with vertical measurement range of 1.5 mm and resolution of 25 nm (vertical) and 1 µm (horizontal). The parameter R_z is calculated by measuring the vertical distance from the highest peak to the lowest value within five sampling lengths, then averaging these distances. A more detailed description of the parameter is available in [54] and the experimental procedure is described in [55].

2.2.2 Filler Dispersion Analysis

In order to evaluate particle dispersion in the silicone matrix, a high resolution field emission scanning electron microscope (FE-SEM) is to be used (Zeiss Supra 40 VP). Samples are prepared using the cryogenic fracturing technique, where they are placed in liquid nitrogen for 15 minutes to allow cooling and are subsequently cryogenically sliced. Samples are then gold coated for the microscopy analysis. Energy-dispersive X-ray spectroscopy (EDX) analyses will also performed to identify the chemical element composition of local domains.

2.2.3 High Voltage Arcing

In the high-voltage low-current arc discharges test [56], said arcs are ignited on a 3 mm thick sample by two needle type electrodes placed 6.35 mm apart from each other as displayed in Figure 1. The applied stress is enhanced every 60 s by slowly increasing the duration and the value of the current pulses, following the sequence of Table 3. Samples fail if either the arc disappears, which means current is flowing in the material, or if the sample caches fire. The maximal test duration is 420 s, and the time between the beginning of the test and the extinction of the arc is defined as the arcing time.

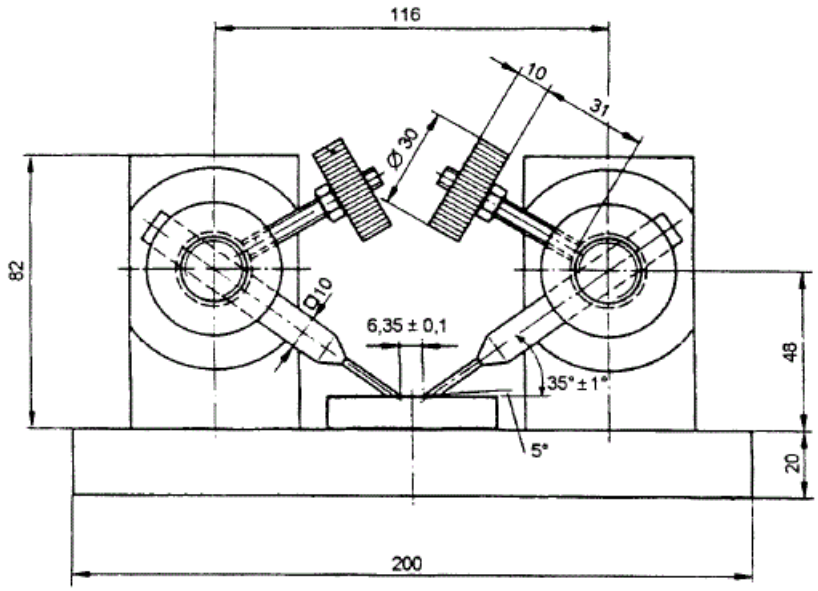

Figure 1. Arrangement of the high-voltage, low-current arc discharges test [56].

Table 3. Sequence of the stages of the high-voltage, low current arc discharges test.

Stage	Current (mA)	Current pulse length (cycles of 1 s)	Beginning and end of stage (in s)
1/8	10	1/8 on, 7/8 s off	0 – 60
1/4	10	1/4 on, 3/4 s off	60 – 120
1/2	10	1/2 on, 1/2 s off	120 – 180
10	10	constantly on	180 – 240
20	20	constantly on	240 – 300
30	30	constantly on	300 – 360
40	40	constantly on	360 – 420

2.2.4 Tracking and Erosion

The test method for evaluating resistance to tracking and erosion as described in [57]. In this test 6 mm thick samples are placed at an angle of 45^{o} to the horizontal plane with electrodes placed 50 mm apart (Figure 2). Test voltage varies between 2.5–4.5 kV (rms), and a contaminant with 395 Ω.cm conductivity flows over the sample with a rate between 0.15 and 9.6 ml/min, depending on the test voltage. The contaminant contains a non-ionic wetting agent, which causes the tested material, here the silicone to (temporarily) lose its hydrophobicity, so that the contaminant flows in a continuous path over the surface, forming a stream.

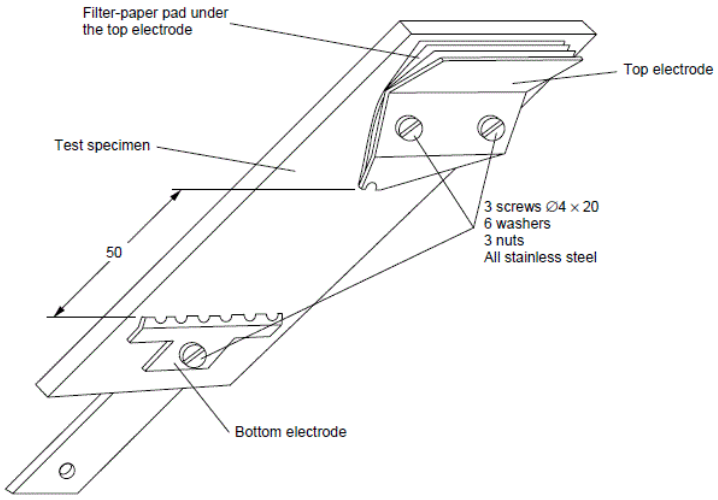

Figure 2. Electrode arrangement of the tracking and erosion test [57].

The test has a maximum duration of 6 h, and a sample is said to fail if tracks longer than 25 mm are formed, erosion breaks through the sample, or a maximum current of 60 mA (rms) is detected at any time for longer than 2 s. Erosion is defined as the loss of material by leakage current or electrical discharges, while tracks are partially conducting paths created by localized deterioration of the surface of an insulating material.

According to IEC 60587, a material is said to fail the test if one or more out of 5 of its samples fail. Besides the pass/fail criteria, the maximum erosion depth should be reported. Other parameters might also help in classifying and comparing material, and are frequently determined, such as the eroded mass, eroded volume and tracking length [37,58-59]. Eroded mass is measured using an analytical scale with precision of 0.1 mg, while erosion depth and tracking length are measured with a vernier caliper with accuracy of 0.01 mm and a depth gauge probe with a 0.5 mm diameter.

2.2.5 Contact Angle Measurement

The IEC/TS 62073 [60] describes the available methods for the measurement of wettability of composite insulators, among them the contact angle method. The static contact angle is measured at the edge of a droplet in relation the solid surface on a horizontal plane (Figure 3).

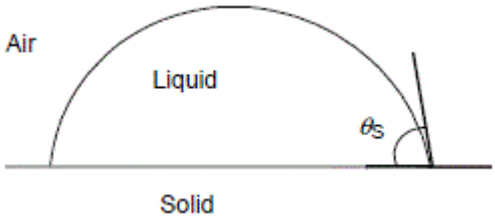

Figure 3. Definition of the static contact angle (θ_s) [60].

In addition to the static contact angle, two dynamic contact angles are defined in an inclined solid surface: the angle formed at the inside of the droplet at its lowest part in relation to the surface is named the advancing contact angle, while the angle inside the droplet at its highest part in relation to the surface is the receding contact angle.

The advancing contact angle can also be determined by adding water to a droplet on a horizontal surface (dynamic sessile drop method). In that case, it corresponds to the angle at the exact moment when the liquid front advances (Figure 4). Likewise, the receding contact angle is the one measured at the moment when the liquid front recedes, when withdrawing water from the droplet.

Figure 4. Advancing (θ_a) and receding (θ_r) contact angles on a horizontal surface determined by the dynamic sessile drop method [61].

The three previously defined contact angles can be used to evaluate de degree of hydrophobicity on the surface of isolating material, and they hold the following relation among themselves: $\theta_a \geq \theta_s \geq \theta_r$. Additionally, it has been verified [62] that from the three contact angles the receding contact angle corresponds best to the electrical performance of wetted surfaces.

The static and dynamic contact angles are determined with the help of the optical contact angle measuring instrument Dataphysics OCA 20.

2.2.6 Dynamic Drop Test

The Dynamic Drop Test (DDT) is proposed to evaluate the loss of hydrophobicity due to pollution and simultaneous electrical stress [63]. The test setup consists of flat material samples tilted by 60^o to the horizontal plane with two electrodes separated by 50 mm (Figure 5). A fluid with conductivity of 1.5 mS/cm drips over the sample in individual droplets, at the rate of 12 drops/minute, until a current of 2 mA (rms) is detected for more than 2 s or the maximum duration of 24 h is reached [64].

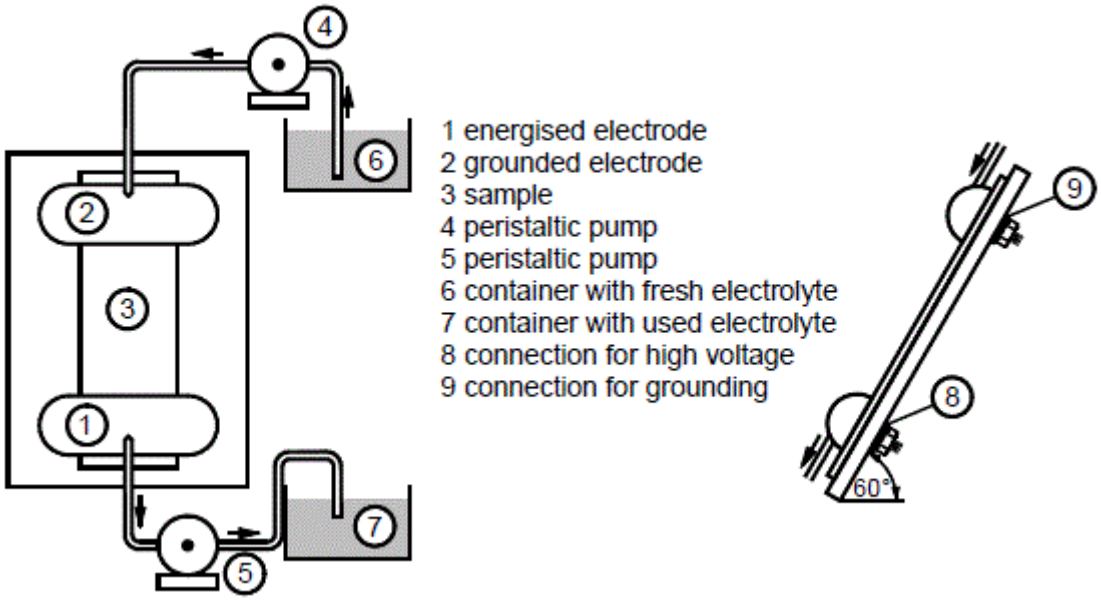

Figure 5. Arrangement of the dynamic drop test [64].

2.2.7 Mechanical Tests

Mechanical tests are performed using a universal testing machine following ISO 37 [65] and ISO 34-1 [66] guidelines. Tensile strength is the maximum stress that a material withstands while being stretched before breaking. In this test, 2 mm thick dumb-bell shaped specimens (Figure 6) are submitted to tension until fracture. The tensile strength value, measured as a force per unit of area, corresponds to the force before breaking divided by the cross sectional area of the test sample.

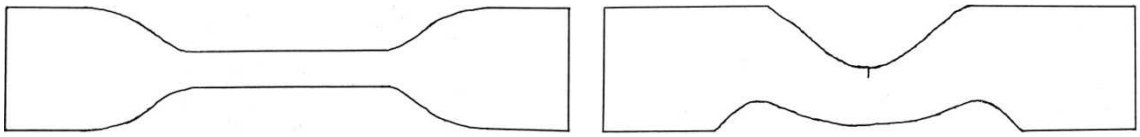

Figure 6. Shape of samples for the tensile strength test (left) and tear resistance test (right).

Tear resistance is a measure of how a material resists the growth of cuts when under tension. In this test 2 mm thick crescent shaped samples are nicked (razor cut) in one of the sides (Figure 6), perpendicular to the applied force, so that as they are elongated the nick extends, until complete tearing occurs. Tear resistance is measured as a force per unit of length, and corresponds to the force before breaking divided by the thickness of the test sample.

2.2.8 Acid and UV Exposure

One major source of degradation of polymeric insulation is ultraviolet light, which is emitted not only by sunlight, but also corona discharges and dry-band activity. It can cause cracking, chalking, discoloration and loss of hydrophobicity [67]. Another cause of degradation of outdoor insulation is acid attack, which can lead to exposure of the rod and further brittle fracture [68].

Sulfuric and nitric acid are constituents of acid rain, and might also be generated in service due to pollution (e.g. industrial pollution of the combustion of fossil fuels), corona discharges, ozone and moisture, water droplet coronas or partial discharges in water filled cracks [69].

In the absence of reference tests or standards when evaluating the influence of acid and ultraviolet exposure, a new method is developed where samples are submitted to 168 h (7 days) of medium to long wavelength (UVA and UVB) ultraviolet radiation, while being sprayed once a day with a solution of 0.1% H_2SO_4 (sulfuric acid). The sprayer is a typical garden spray bottle, which is squeezed once on each sample, from a distance of around 17 cm. The ultraviolet source is a 300 W incandescent lamp placed 17 cm from the samples.

2.2.9 Thermogravimetric Analysis

Thermogravimetric analysis (TGA) is a technique that allows the investigation of the thermal stability of material by monitoring the variation of their mass as temperature increases (or decreases). It is to be performed using a Netzsch STA 449 Jupiter Simultaneous TGA-DSC Analyzer. Samples of 30 mg were tested in nitrogen atmosphere, temperature ranging from 30^{o}C to 500^{o}C at a rate of 10 K/min.

3 RESULTS

Data contained in each graphic represent the mean value of all measurements and their respective 95% confidence interval (CI), except in the Dynamic Drop Test results, where it was found that the probability distribution function that best represents data is the Weibull distribution. Hence, in this particular case, the 63% quantile and its respective 95% CI are displayed. It is also worth pointing out that, in each graphic, individual plots were slightly shifted horizontally to avoid overlapping and facilitate interpretation. Nevertheless loading levels always correspond to the closest truncated integer (i.e. 0, 1, 2, 3 or 5 wt%), unless otherwise specified.

3.1 SURFACE ROUGHNESS

The surface roughness of the samples was determined in order to ensure that possible variations on their surface profile do not cause discrepancies in the results of the proposed tests. The parameters used in these measurements are as follows: resolution of 5 µm over a 5 mm line, resulting in a 1,000 point array. Results of mean roughness depth, R_z, are presented in Figures 7 and 8.

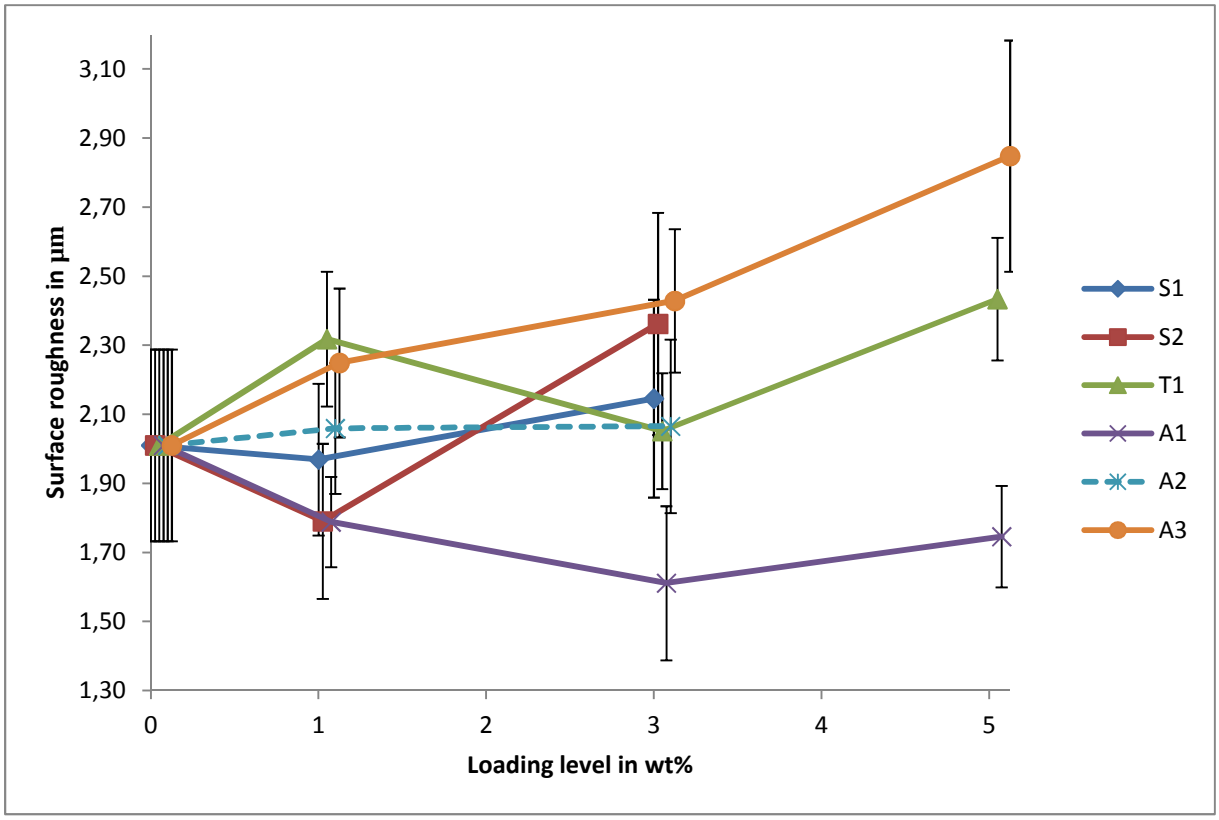

Figure 7. Surface roughness R_z of samples without ATH depending on nanoparticle filling level (mean values and 95% CI of n = 8 samples).

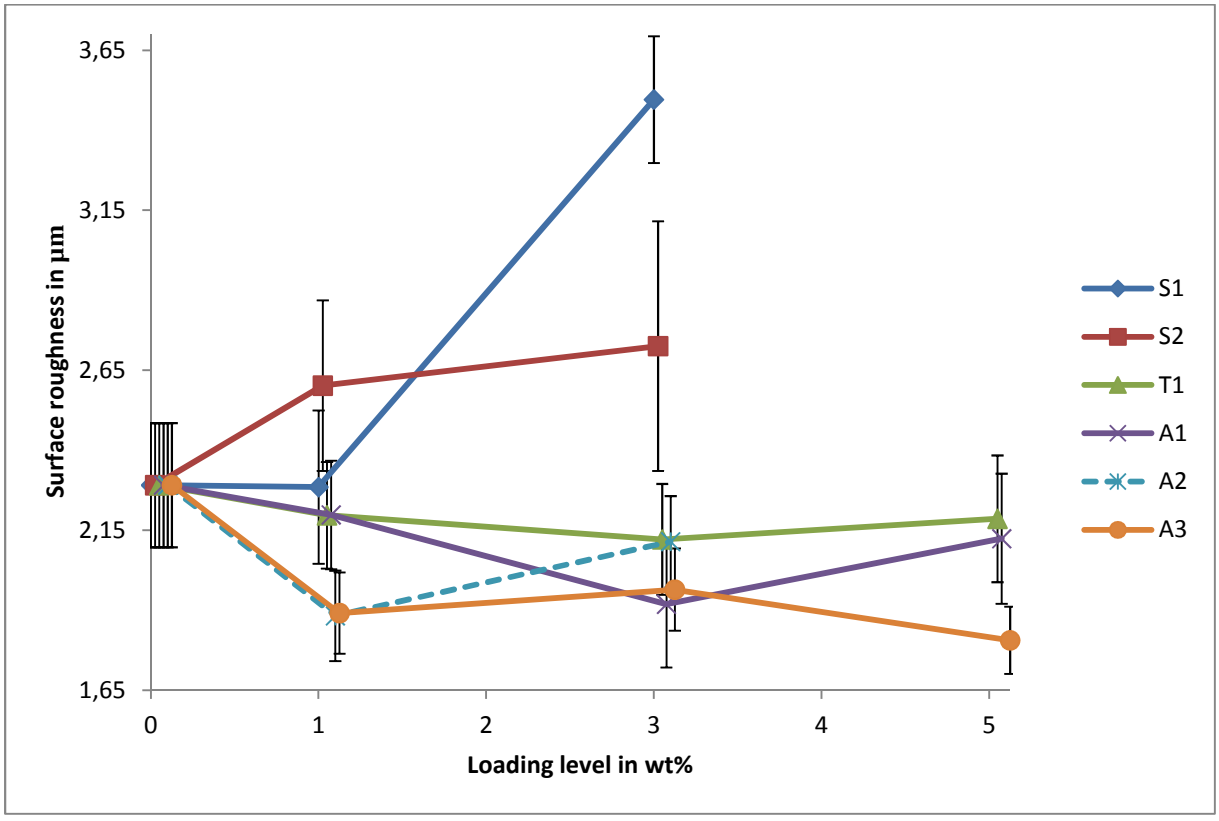

Figure 8. Surface roughness R_z of samples containing ATH depending on nanoparticle filling level (mean values and 95% CI of n = 8 samples).

3.2 FILLER DISPERSION ANALYSIS

Initial microscopies were performed with an unfilled reference sample (*'0'* without standard grade ATH), and the morphology of the specimen at 50,000 x magnification is shown in Figure 9.

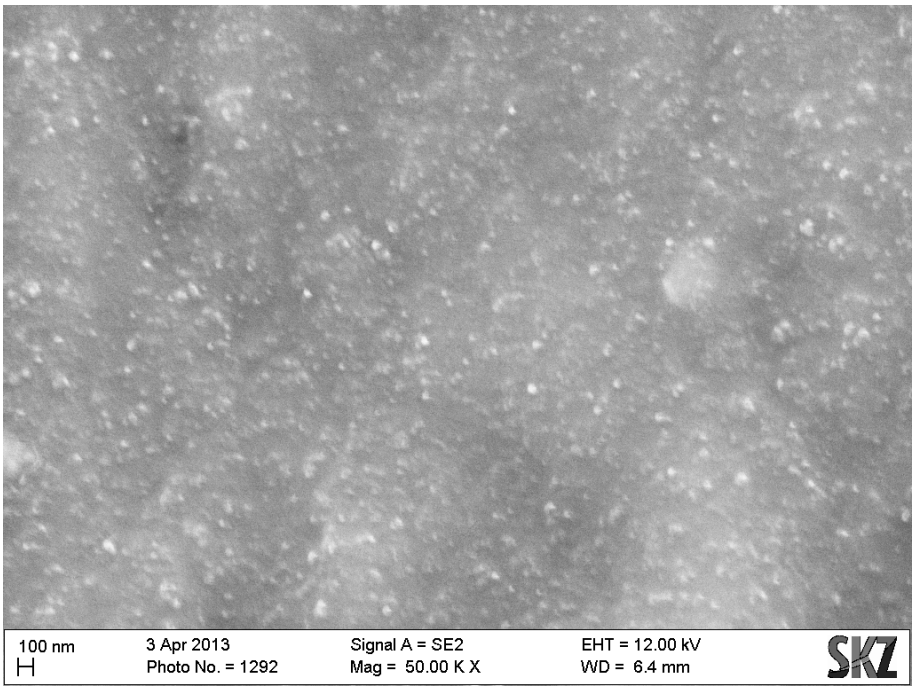

Figure 9. Morphology of reference specimen *'0'* without standard grade ATH taken by FE-SEM with a magnification of 50,000 x.

It can be seen in Figure 9 that the tested silicone sample, to which neither standard grade ATH nor any other filler was added, already possesses "highly dispersed silica" in an amount believed to be between 10 wt% and 15 wt% (more precise information is not divulged by supplier).

Secondly, a detailed analysis of specimen *S1-3wt%* without standard grade ATH and results are shown in Figures 10 and 11.

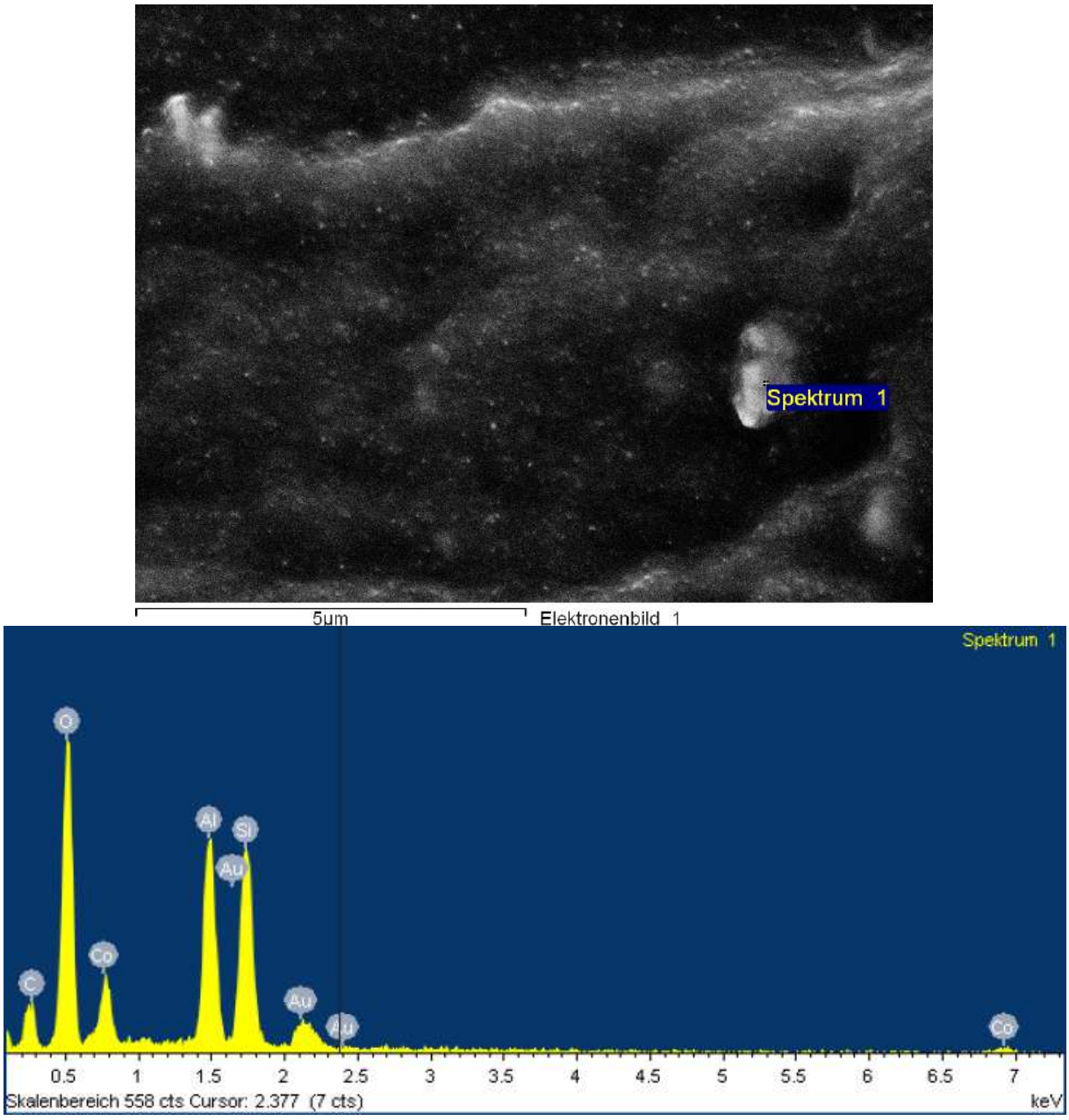

Figure 10. FE-SEM and EDX analysis of specimen *S1-3wt%* without standard grade ATH.

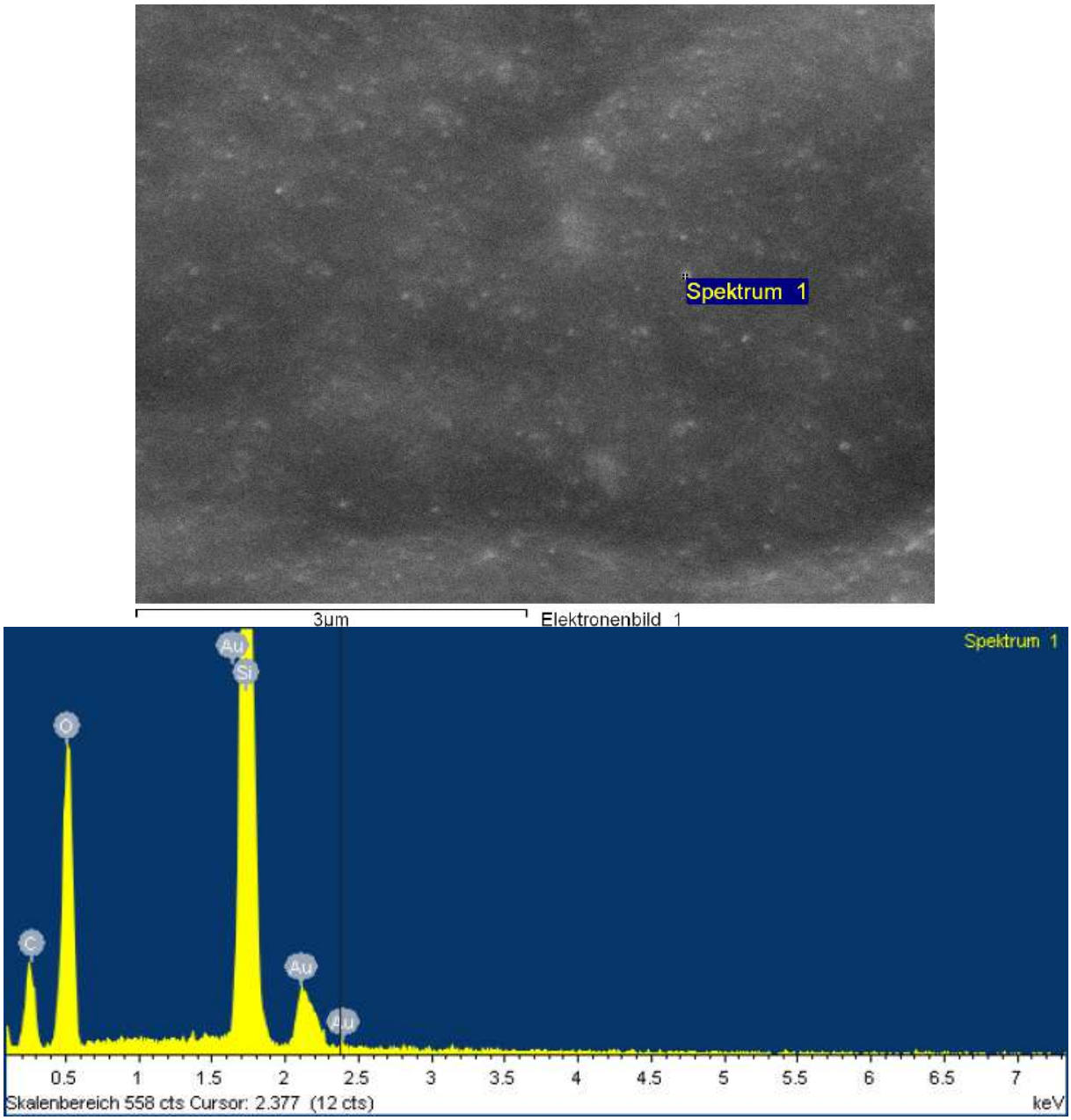

Figure 11. FE-SEM and EDX analysis of specimen *S1-3wt%* without standard grade ATH.

EDX analysis of the micro-particle domain in Figure 10 indicates the presence of atoms of cobalt (Co) and aluminium (Al), which are elements routinely used in pigment masterbatches. A further EDX analysis of the domain in Figure 11, on the other hand, identified uniquely C, O, Au and Si, indicating that these are indeed the investigated silicon dioxide particles.

Further microscopies were performed at 50,000 x magnification to analyse filler dispersion, and an illustrative example of these is shown in Figure 12.

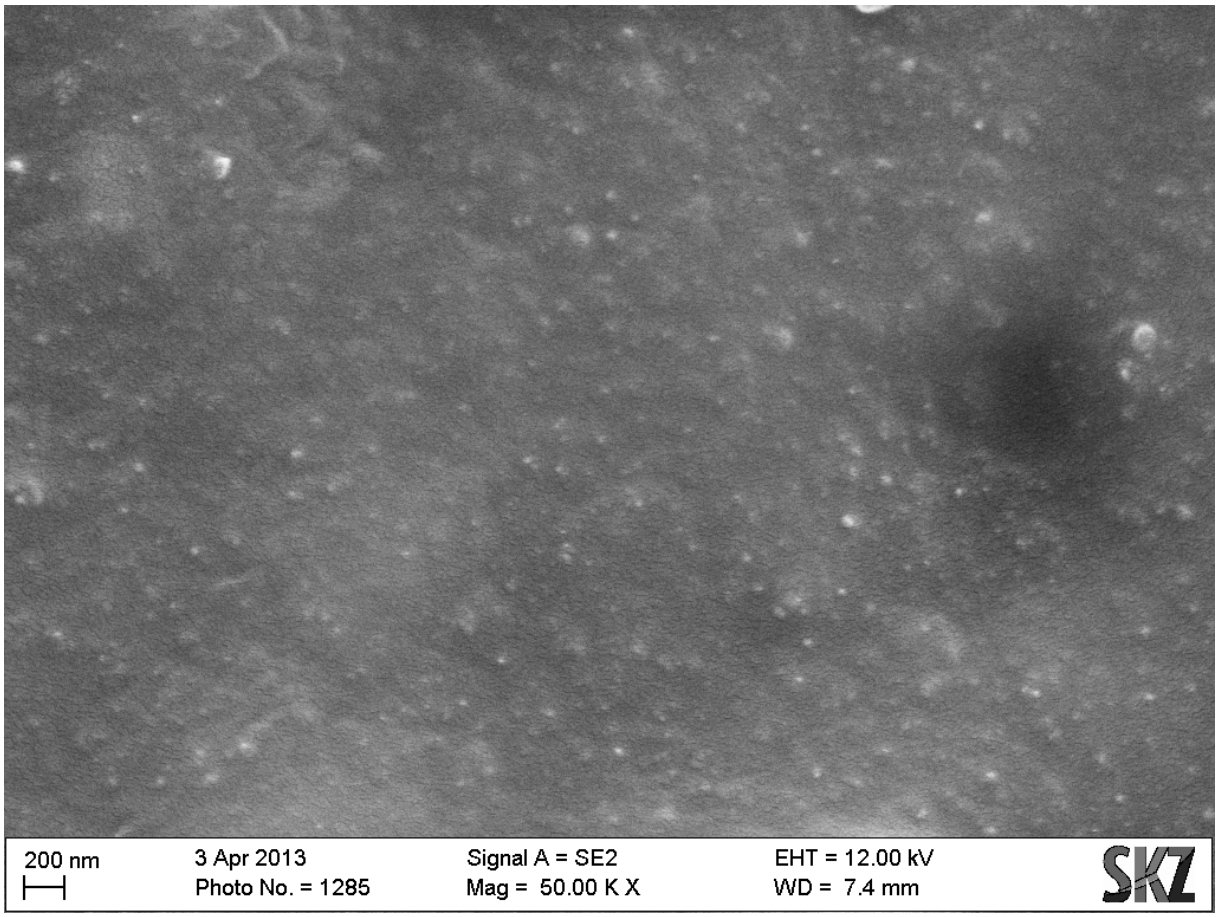

Figure 12. Morphology of specimen *S2-3wt%* without standard grade ATH taken by FE-SEM with a magnification of 50,000 x.

Filler seems properly dispersed, although aggregates of single particles can be found in Figure 12, with an average diameter of 40 nm. These results will be revisited and discussed in the next chapter.

3.3 HIGH VOLTAGE ARCING

Resistance to high voltage arcing was evaluated according to IEC 61621. Samples were rinsed using isopropanol followed by distilled water, and left to rest for at least 24 h in a controlled environment with temperature of (23 ± 2)°C and humidity of (50 ± 5)%. Ten samples of each composition were tested, measuring 15 x 30 x 6 mm. Results are presented in Figures 13 and 14.

Additional compositions containing standard grade ATH and alternative nanofiller loadings (namely, 0.25 wt%, 0.50 wt% and 0.75 wt%) were submitted to the high voltage arcing test. This made the results in Figure 14 to some extent clustered in the range between 0 and 1 wt%. For this reason, a new plot highlighting this specific area is presented in Figure 15.

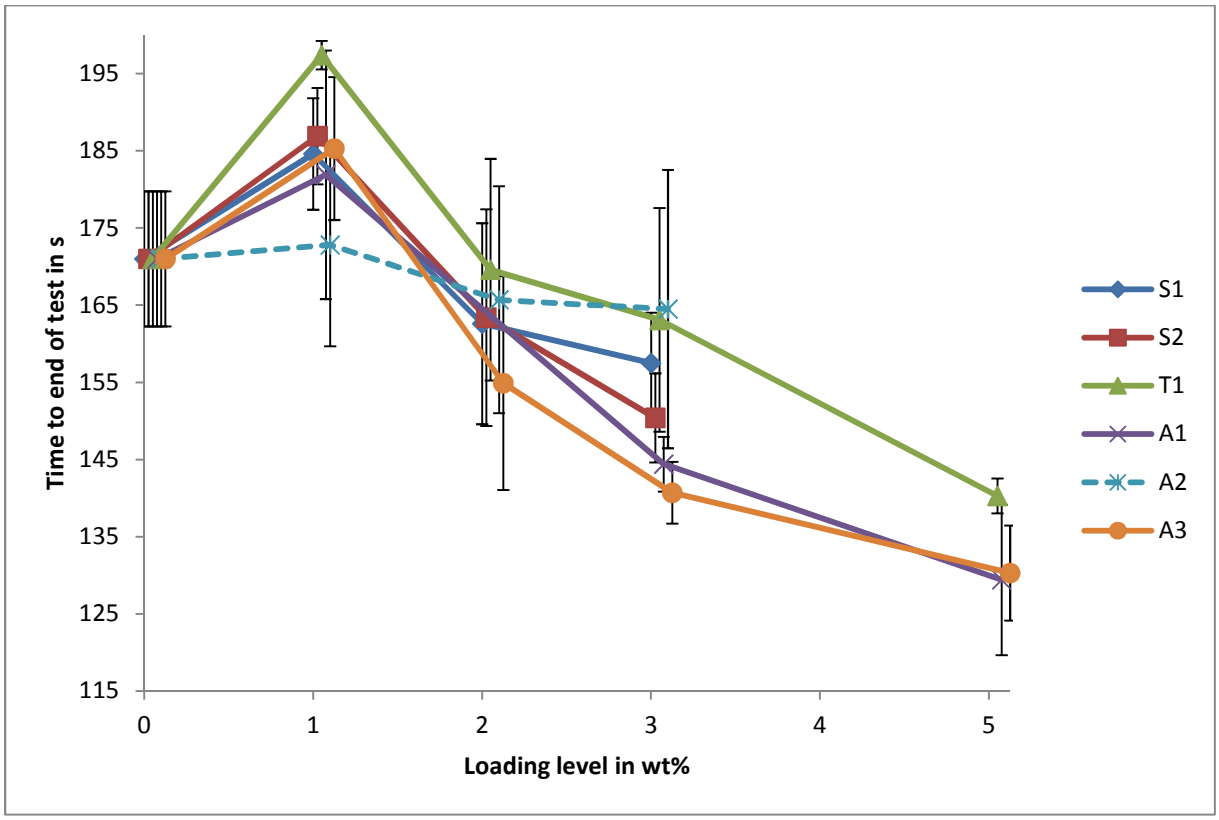

Figure 13. Time to end of the high voltage arcing test of compositions without standard grade ATH depending on nanoparticle filling level (mean values and 95% CI of n = 10 samples).

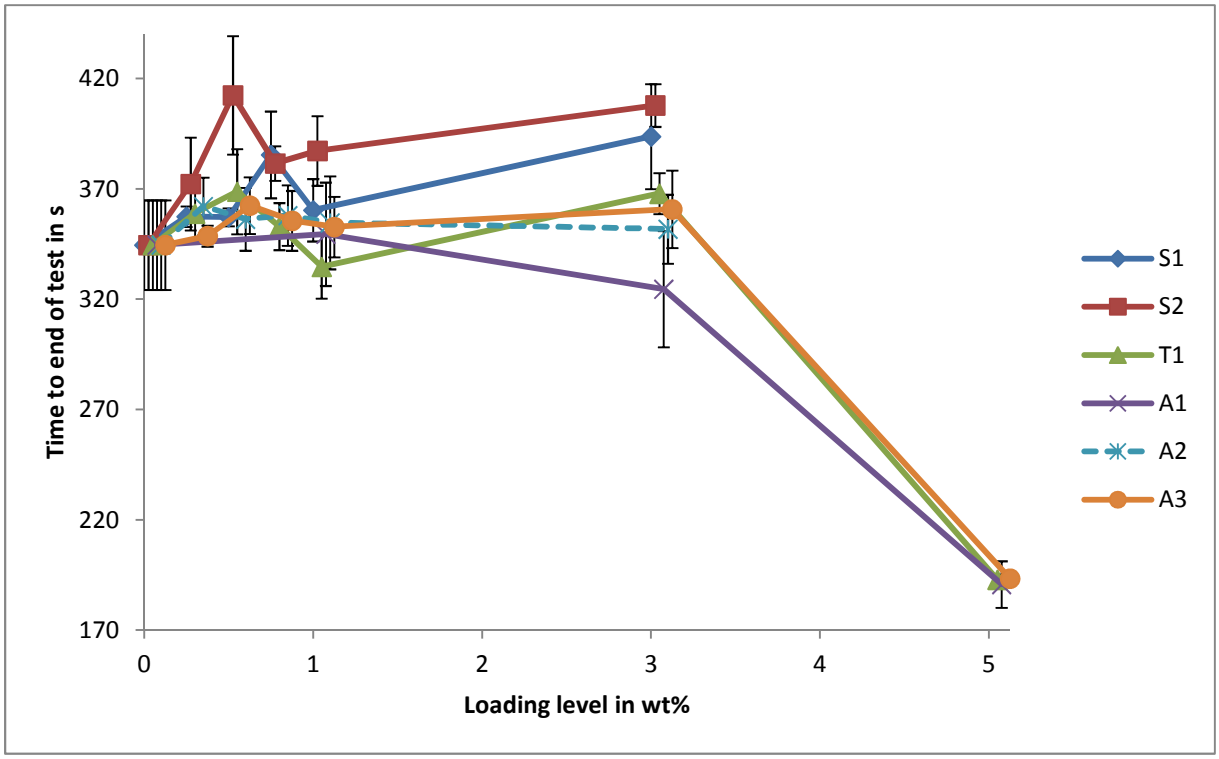

Figure 14. Time to end of the high voltage arcing test of compositions containing standard grade ATH depending on nanoparticle filling level (mean values and 95% CI of n = 10 samples).

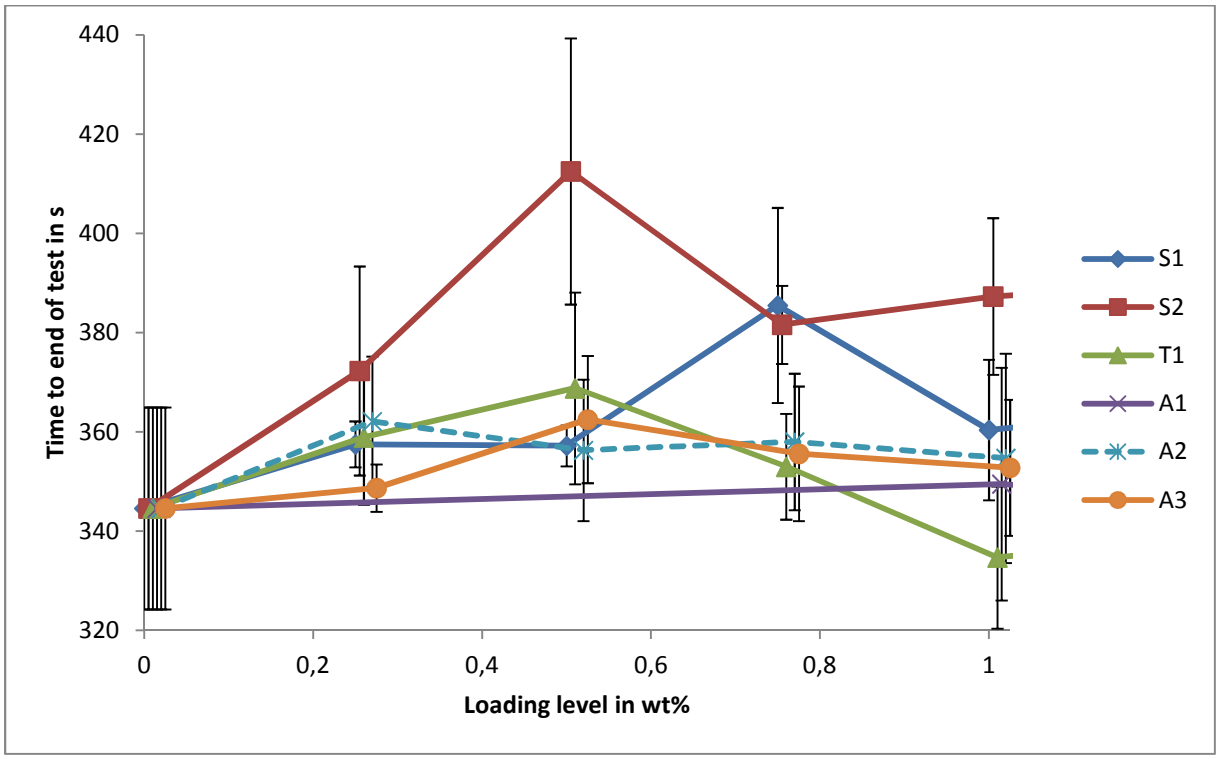

Figure 15. Time to end of the high voltage arcing test of compositions containing standard grade ATH depending on nanoparticle filling level (mean values and 95% CI of n = 10 samples). Magnification of the area between 0 and 1 wt%.

3.4 TRACKING AND EROSION

Tracking and erosion resistance was evaluated according to IEC 60587. Five samples of each composition (120 x 50 x 6 mm) were rinsed using isopropanol followed by distilled water. Samples were stored for at least 24 h before testing in a controlled environment with temperature of (23 ± 2)^{o}C and humidity of (50 ± 5)%. Compositions without standard grade ATH were tested at 2.5 kV, whereas compositions with ATH were tested at 3.5 kV. Material was evaluated by means of eroded mass (Figures 16 and 17), tracking length (Figures 18 and 19) and erosion depth (Figures 20 and 21).

The two different voltage levels were required because compositions without standard grade ATH have such a lower erosion performance than compositions containing it, that initial trials performed with the reference sample (*'0'*) without ATH at 3.5 kV led to failure of all five samples either by perforation or by reach of the maximum current. On the other hand, a test executed at 2.5 kV with material *'0'* containing ATH proved it to be too low to lead to any visible degradation.

Following the aforementioned choice of parameters, all compositions were effectively submitted to 6 hours of stress, i.e. at no point the maximum current criterion was reached. Nevertheless the compositions *T1-5wt%* and *A3-5wt%* containing ATH failed to attend the 25 mm maximum tracking length criterion, as shown in Figure 19.

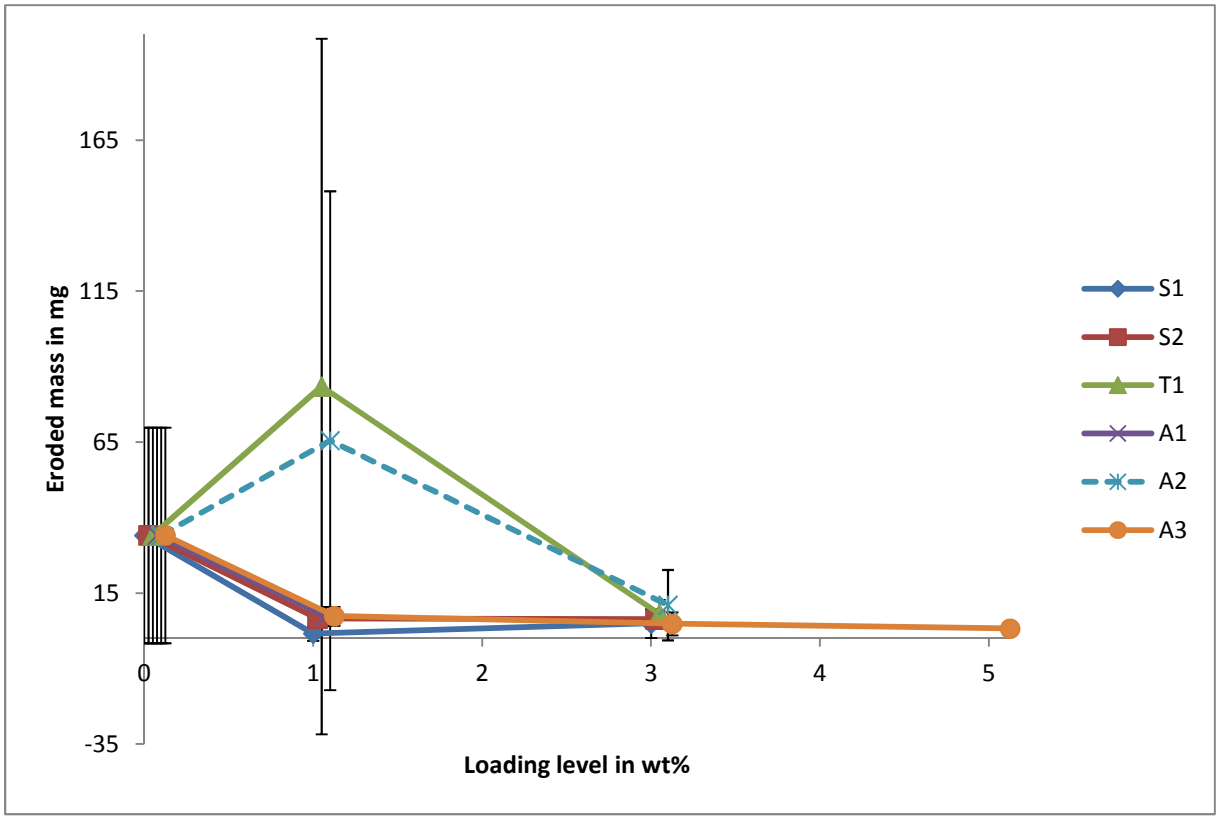

Figure 16. Eroded mass in the tracking and erosion test at 2.5 kV for compositions without standard grade ATH depending on nanoparticle filling level (mean values and 95% CI of n = 5 samples).

Not displayed in Figure 16 due to their exceedingly high eroded mass and CI values are compositions *A1-3wt%* (167.3±191.7 mg), *A1-5wt%* (89.1±155.4 mg) and *T1-5wt%* (130.7±248.9 mg). The problem is grounded on the small number of specimens, even though in agreement with standard requirements (e.g. material *A1-3wt%* individual measurements: 13.2 mg, 5.1 mg, 6.5 mg, 377.9 mg, 433.9 mg).

Negative values as those found in Figure 16, which are evident physical impossibilities, originate from the fact that the normal distribution is symmetric about its mean value, and highly dispersed data (as that mentioned in the previous paragraph) might lead to a 95% confidence interval larger than the mean.

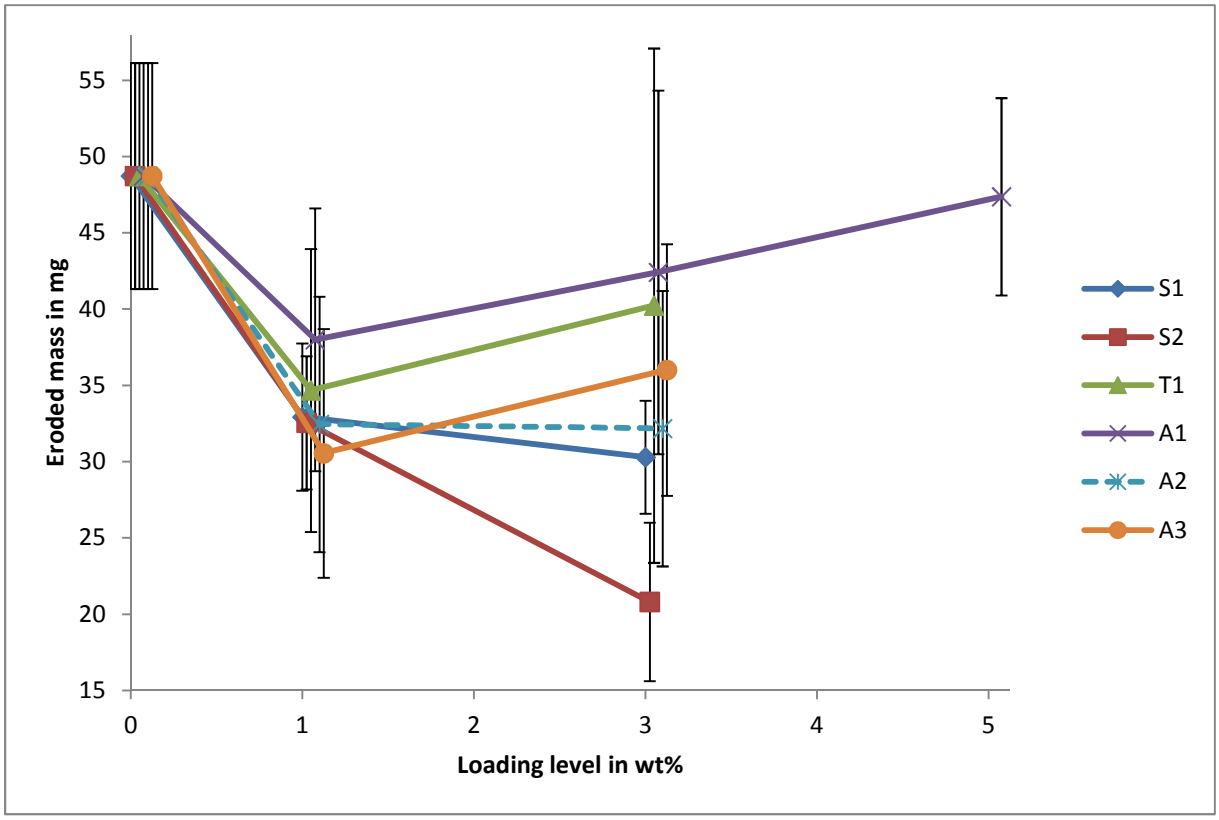

Figure 17. Eroded mass in the tracking and erosion test at 3.5 kV for compositions containing standard grade ATH depending on nanoparticle filling level (mean values and 95% CI of n = 5 samples).

Not displayed in Figure 17 due to their exceedingly high eroded mass are the two compositions which failed the test: *T1-5wt%* (1974.6 mg) and *A3-5wt%* (1306.8 mg).

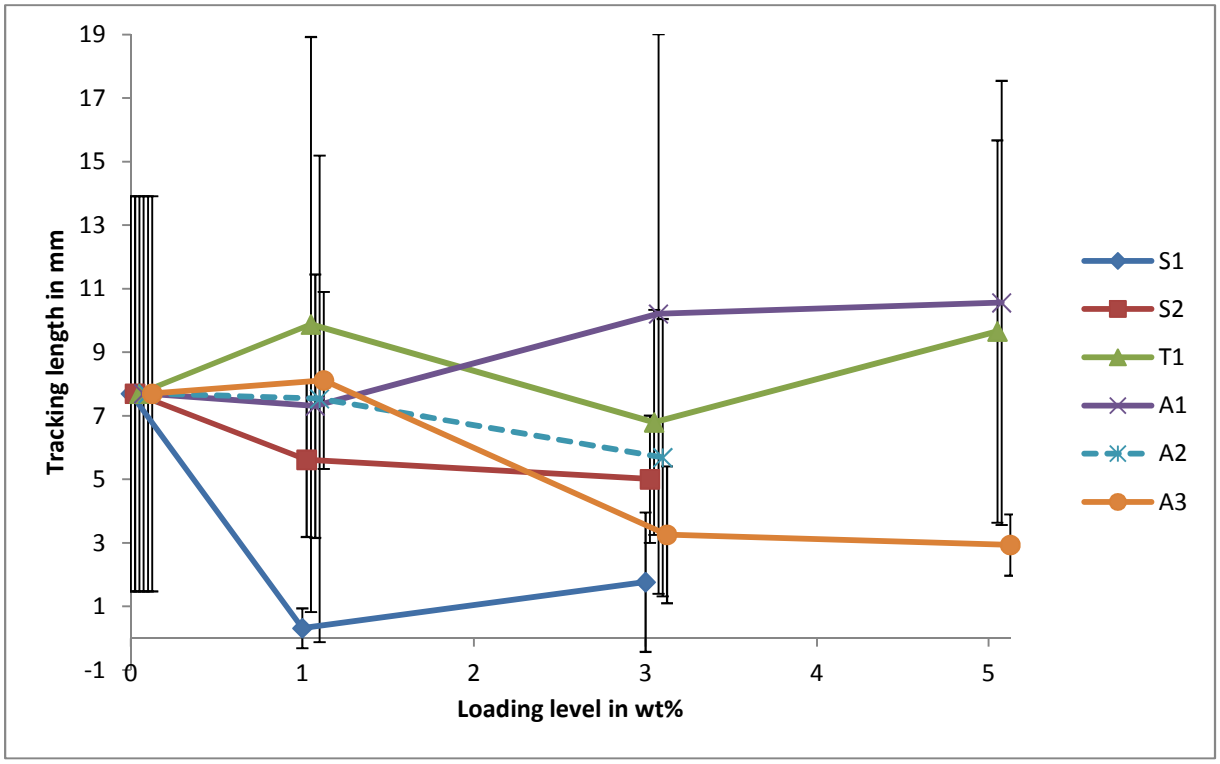

Figure 18. Tracking length in the tracking and erosion test at 2.5 kV for compositions without standard grade ATH depending on nanoparticle filling level (mean values and 95% CI of n = 5 samples).

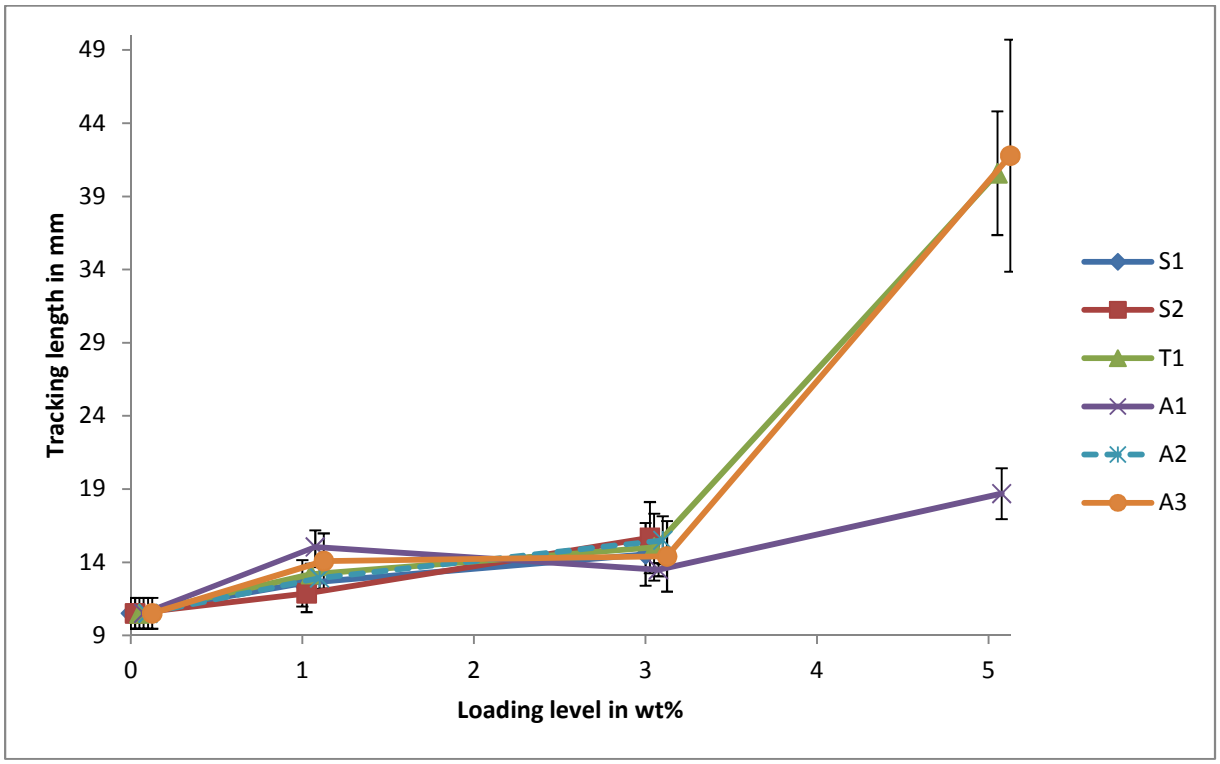

Figure 19. Tracking length in the tracking and erosion test at 3.5 kV for compositions containing standard grade ATH depending on nanoparticle filling level (mean values and 95% CI of n = 5 samples).

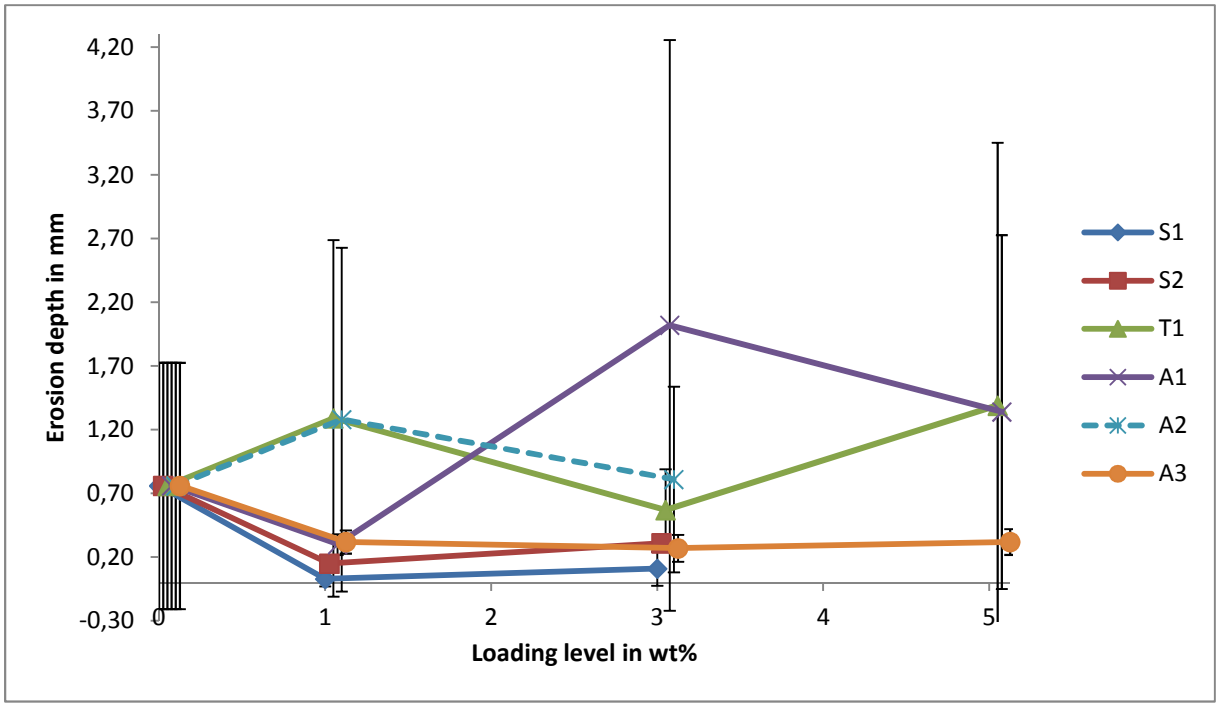

Figure 20. Erosion depth in the tracking and erosion test at 2.5 kV for compositions without standard grade ATH depending on nanoparticle filling level (mean values and 95% CI of n = 5 samples).

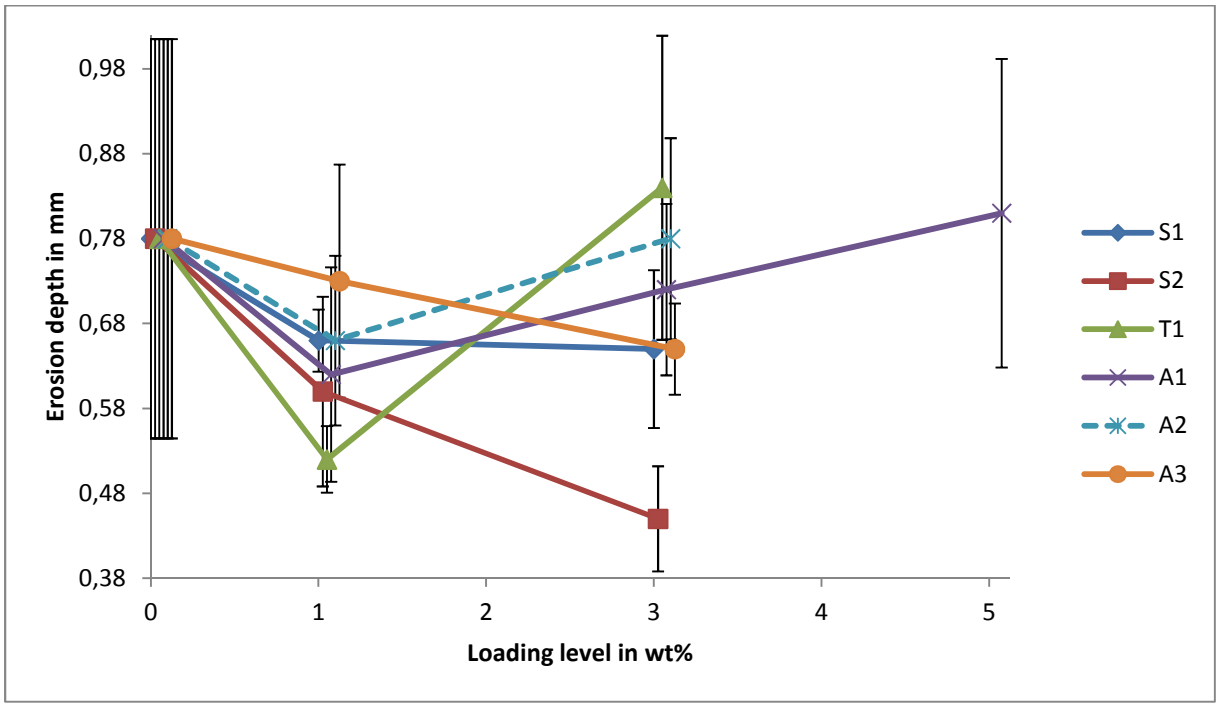

Figure 21. Erosion depth in the tracking and erosion test at 3.5 kV for compositions containing standard grade ATH depending on nanoparticle filling level (mean values and 95% CI of n = 5 samples).

Not displayed in Figure 21 due to their exceedingly high erosion depth are the two compositions which failed the test: *T1-5wt%* (4.80 mm) and *A3-5wt%* (5.05 mm).

3.5 CONTACT ANGLE MEASUREMENT

Measurements of the static, advancing and receding contact angles were performed in the various HTV compositions and are presented in Figures 22 to 27.

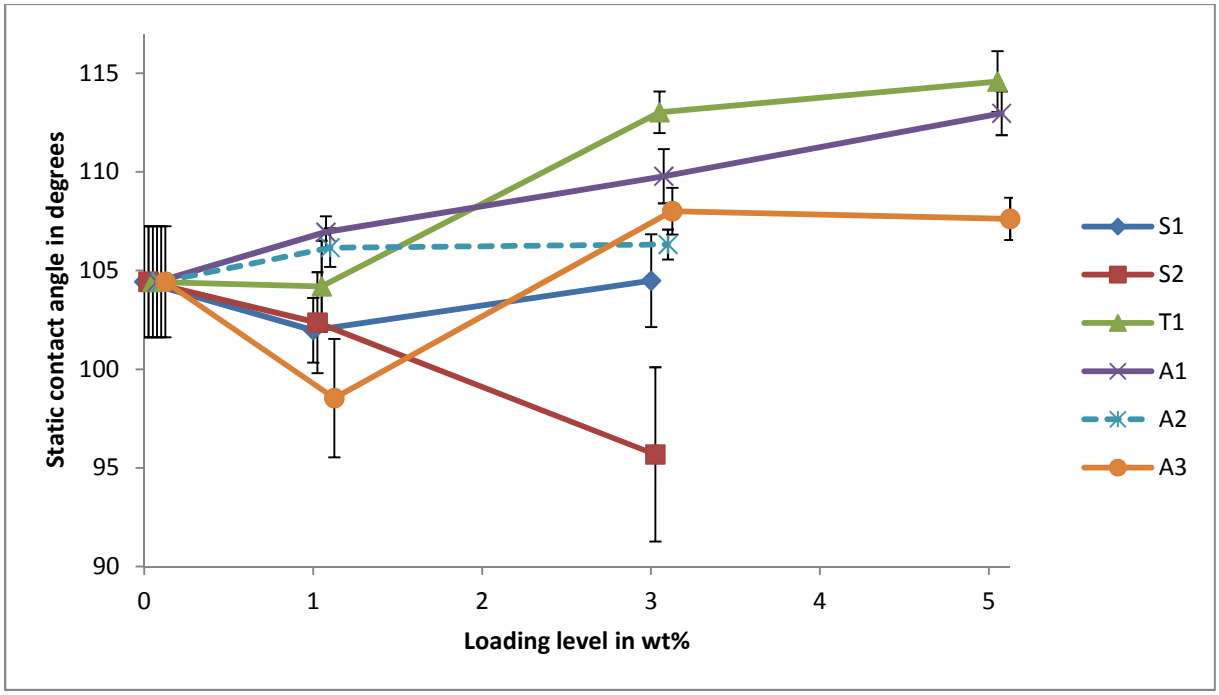

Figure 22. Static contact angles of compositions without ATH depending on nanoparticle filling level (mean values and 95% CI of n = 8 samples).

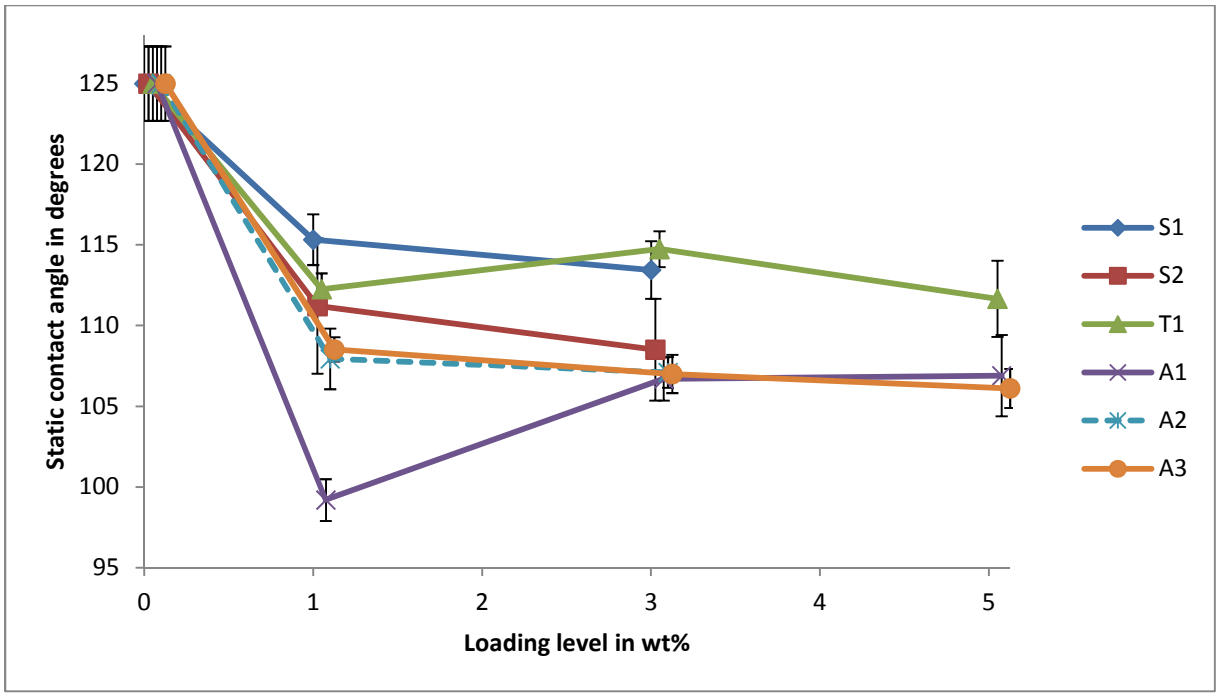

Figure 23. Static contact angles of compositions containing ATH depending on nanoparticle filling level (mean values and 95% CI of n = 8 samples).

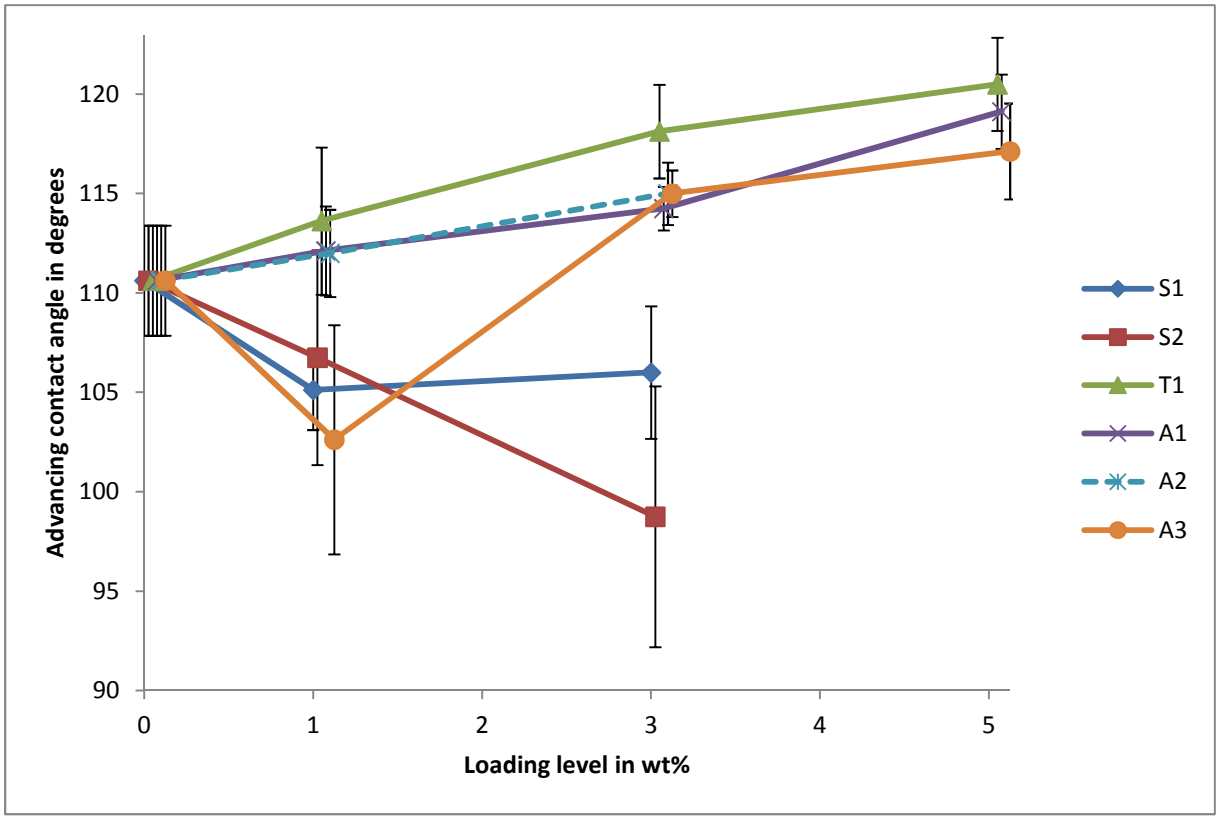

Figure 24. Advancing contact angles of compositions without ATH depending on nanoparticle filling level (mean values and 95% CI of n = 8 samples).

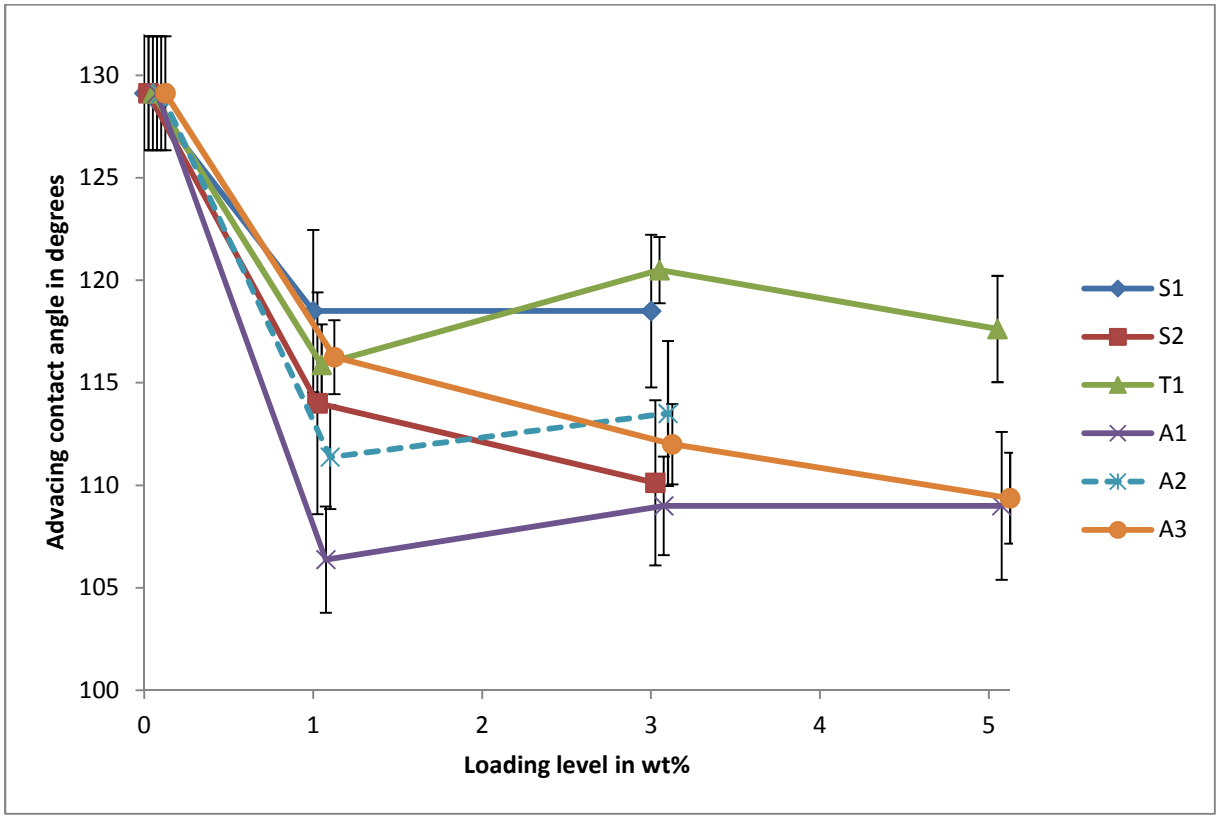

Figure 25. Advancing contact angles of compositions containing ATH depending on nanoparticle filling level (mean values and 95% CI of n = 8 samples).

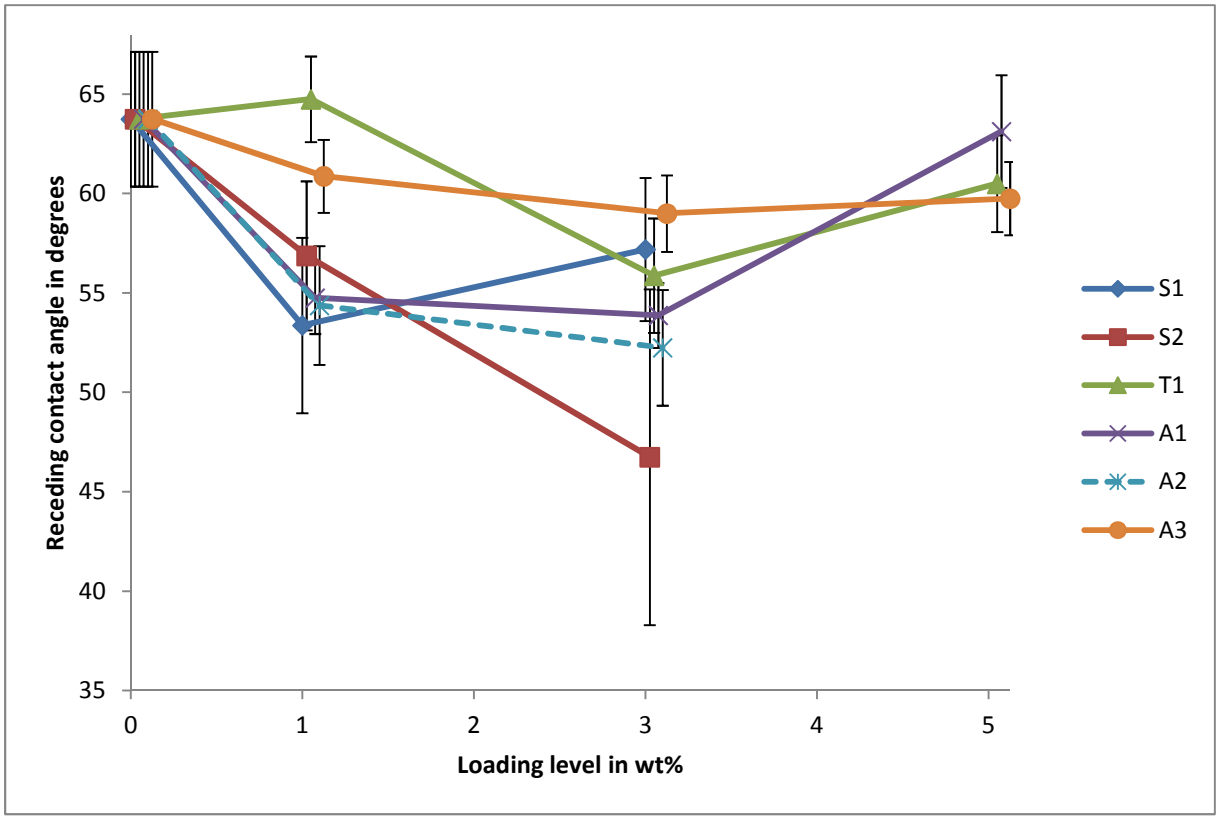

Figure 26. Receding contact angles of compositions without ATH depending on nanoparticle filling level (mean values and 95% CI of n = 8 samples).

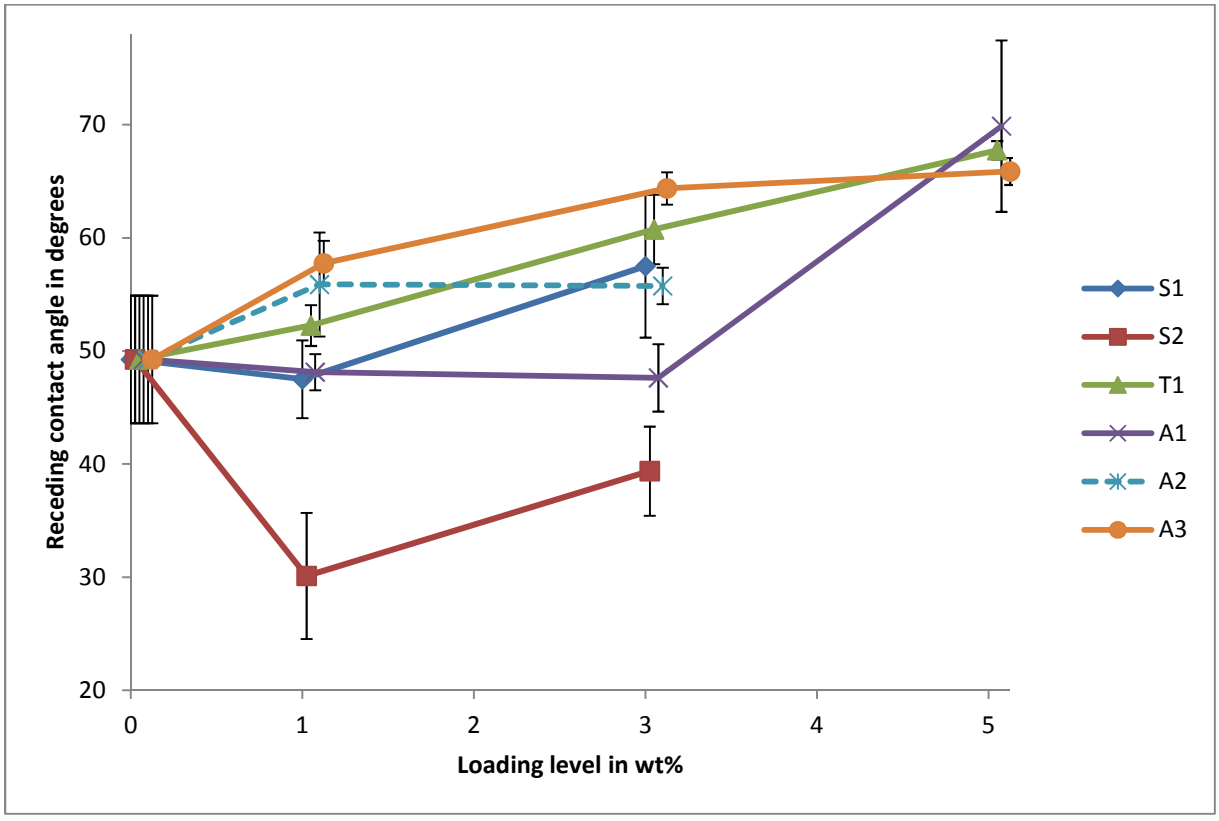

Figure 27. Receding contact angles of compositions containing ATH depending on nanoparticle filling level (mean values and 95% CI of n = 8 samples).

3.6 DYNAMIC DROP TEST

Retention of hydrophobicity was evaluated through the Dynamic Drop Test (DDT). Samples were cleaned with isopropanol and distilled water and stored under room conditions for at least 24 h before testing. Eight samples of each material were tested.

Different parameters were chosen because initial trials with all compositions at the same voltage level lead to clusters either in the lower or the upper limits (i.e. 0 and 24 h) and no statistical difference among filler types or amounts could be observed. For example, at 4 kV all compositions tested without standard grade ATH reached the maximum test duration of 24 h (1440 min). When the voltage level was raised to 5 kV, on the other hand, all compositions tested containing ATH failed in the first 15 min of test.

Therefore, compositions without standard grade ATH were tested at the voltage level of 5 kV (Figure 28) and compositions containing standard grade ATH were tested at 4 kV (Figure 29). Despite the different test parameters, the superior performance of compositions without ATH is noticeable, for even with the higher voltage level, time to end of test of compositions is still higher.

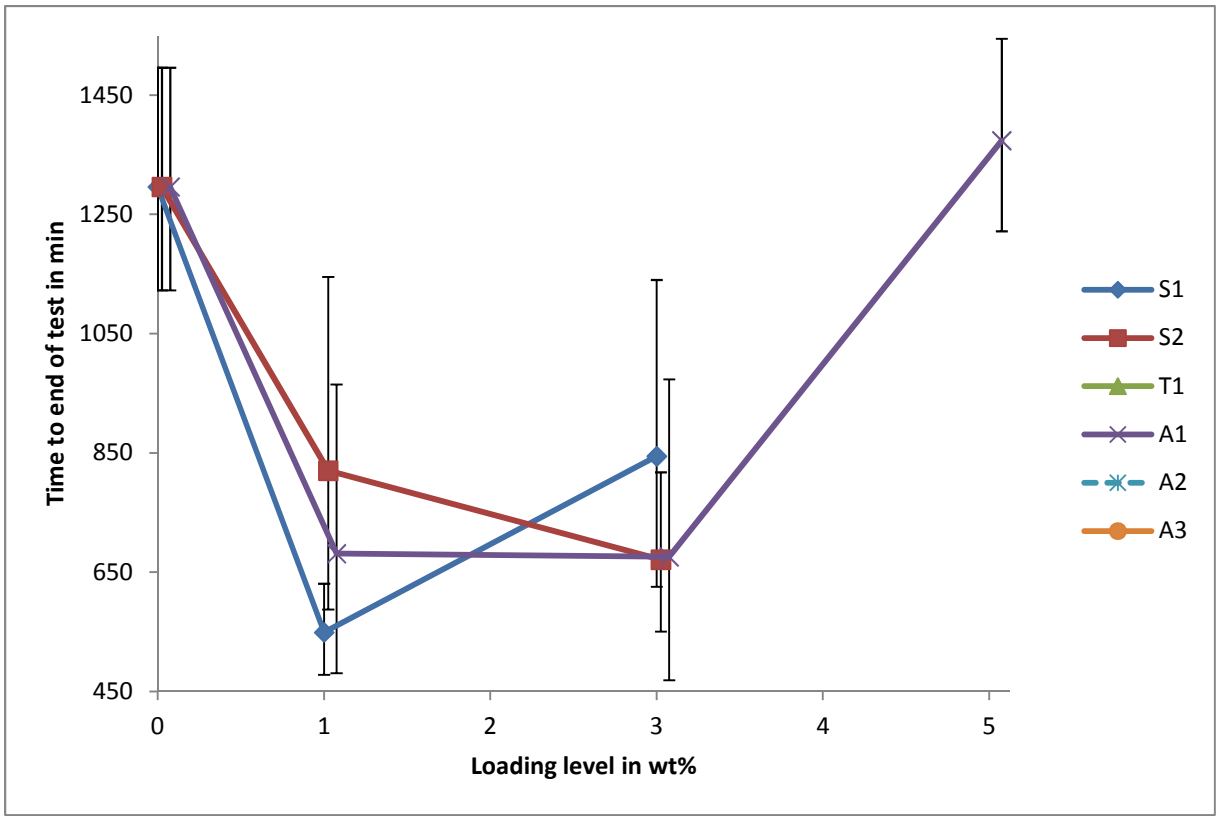

Figure 28. Time to end of the DDT at 5 kV for compositions without standard grade ATH depending on nanoparticle filling level (63% quantile and 95% CI of n = 8 samples).

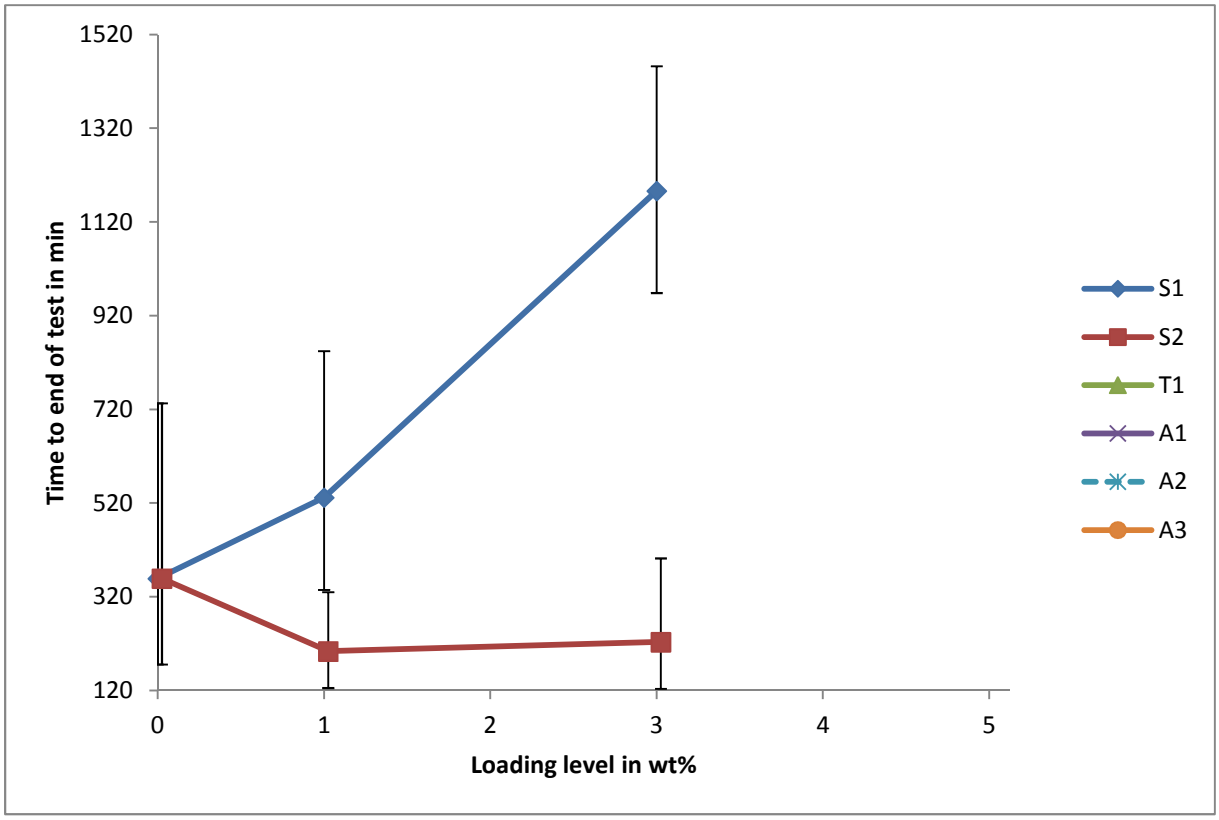

Figure 29. Time to end of the DDT at 4 kV for compositions containing standard grade ATH depending on nanoparticle filling level (63% quantile and 95% CI of n = 8 samples).

3.7 MECHANICAL TESTS

Mechanical tests were performed according to ISO 37 and ISO 34-1. Results of tensile strength measurements are shown in Figures 30 and 31 for compositions without and containing ATH, respectively, and tear resistance measurements are shown in Figures 32 and 33.

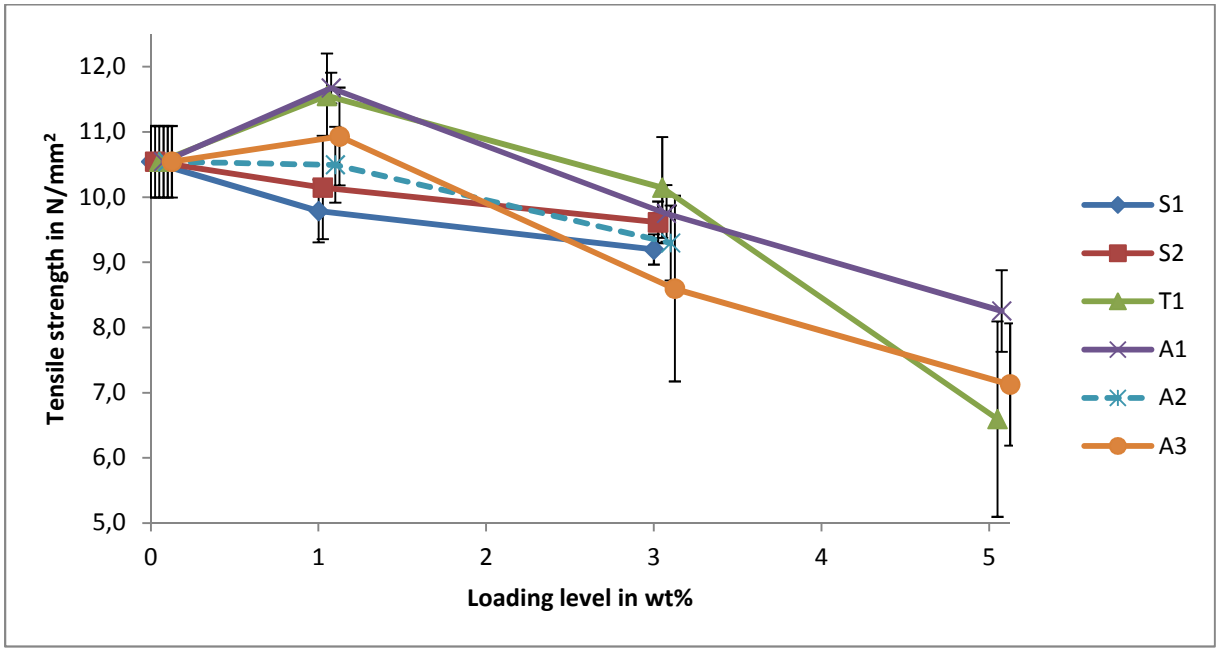

Figure 30. Tensile strength of compositions without standard grade ATH depending on nanoparticle filling level (mean values and 95% CI of n = 3 samples).

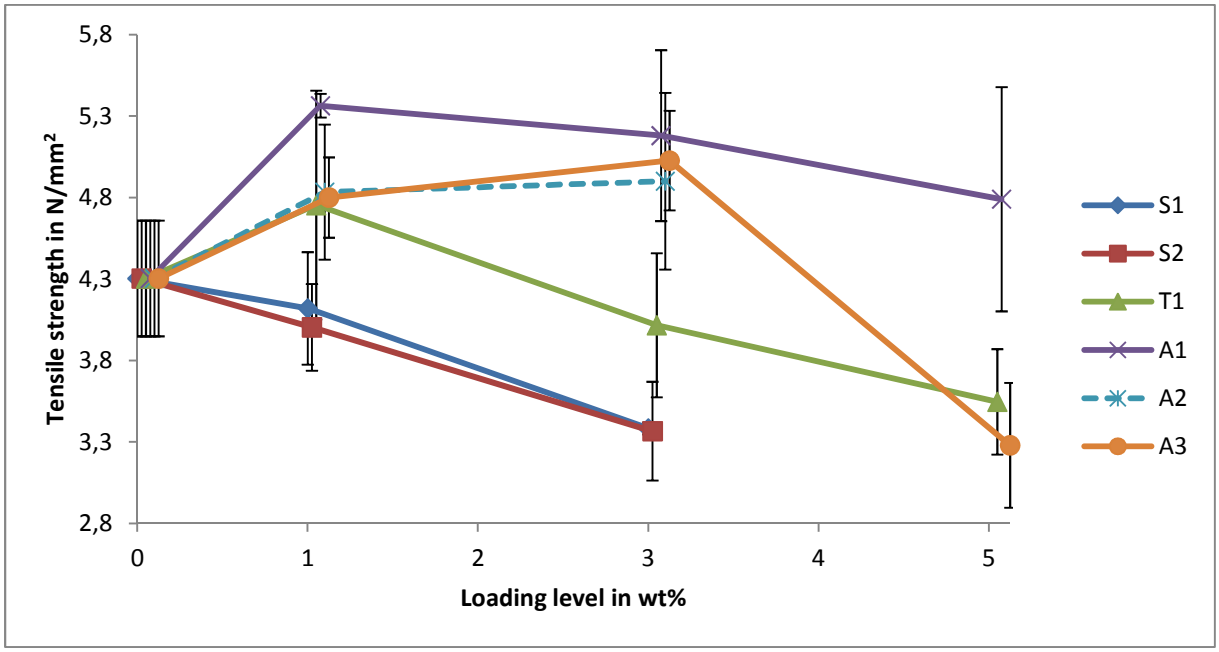

Figure 31. Tensile strength of compositions containing ATH depending on nanoparticle filling level (mean values and 95% CI of n = 3 samples).

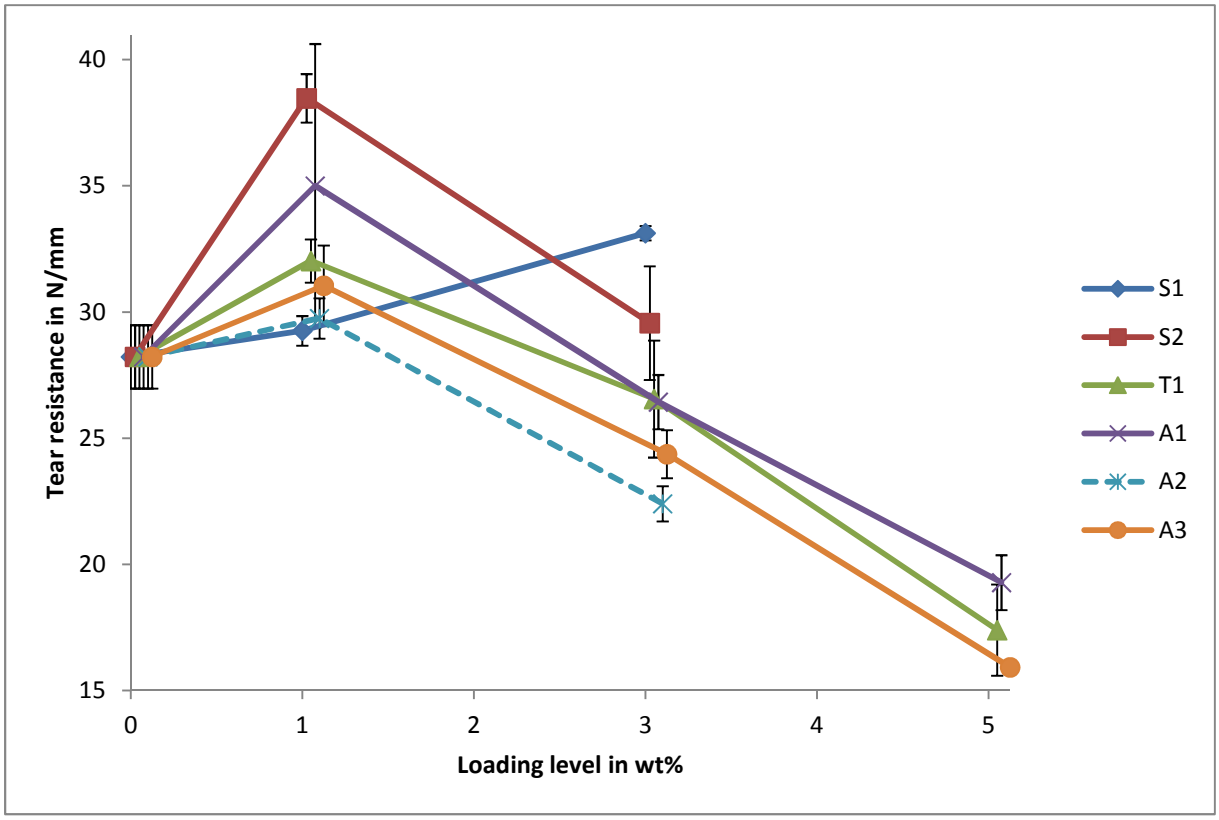

Figure 32. Tear resistance of compositions without standard grade ATH depending on nanoparticle filling level (mean values and 95% CI of n = 3 samples).

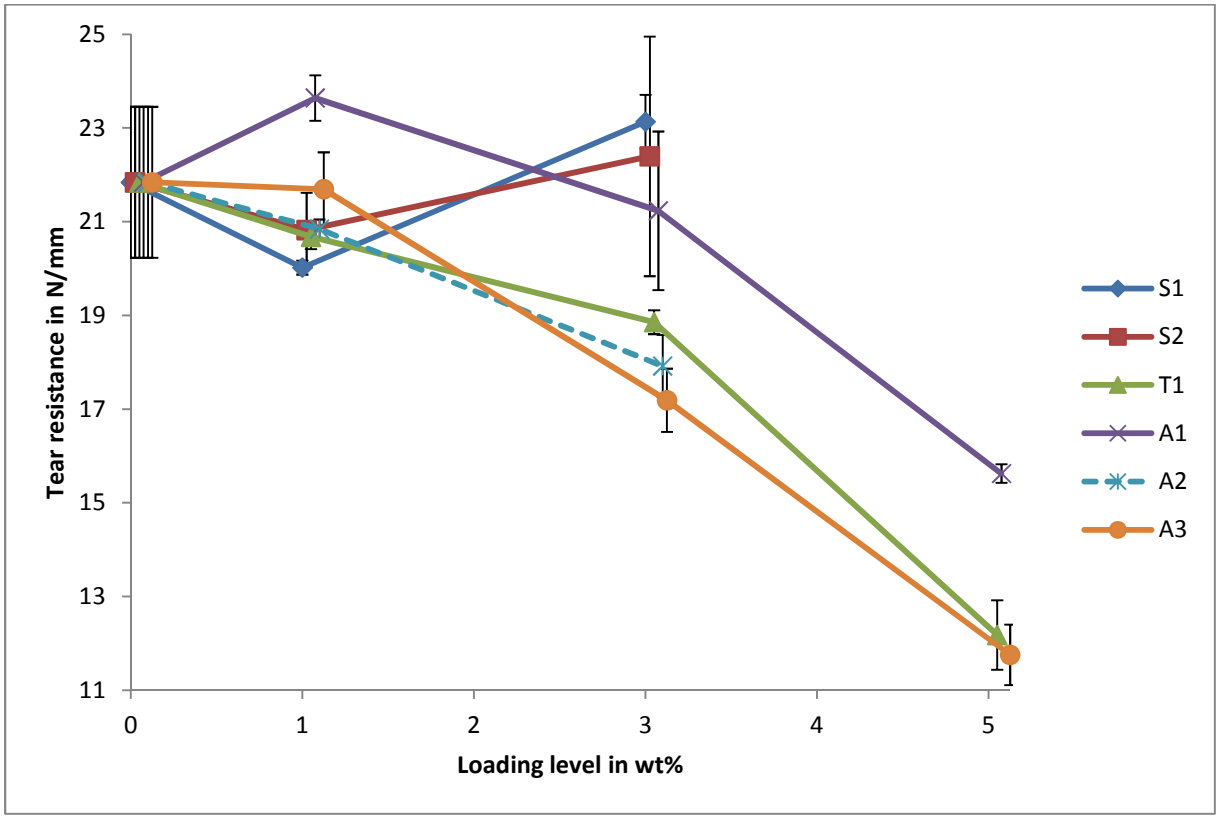

Figure 33. Tear resistance of compositions containing ATH depending on nanoparticle filling level (mean values and 95% CI of n = 3 samples).

3.8 ACID AND UV EXPOSURE

Only one sample of each material was tested in the ultraviolet and acid stress test. Samples were inspected visually, both by naked eye and by means of an optical microscope. The evaluation and classification of samples is, therefore, qualitative rather than quantitative. Pictures of the samples after the test are presented in Figures 34 to 43.

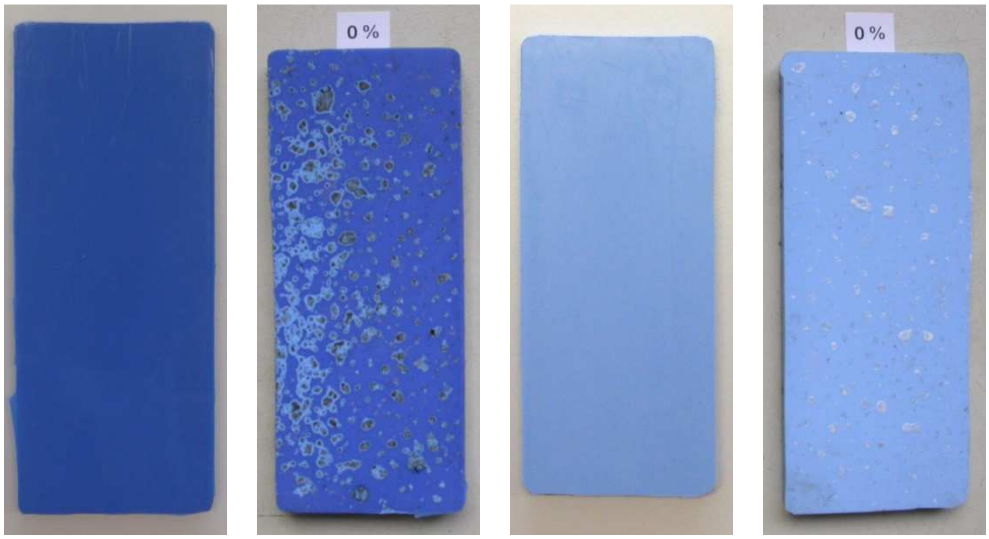

Figure 34. Reference samples (*'0'*) without standard grade ATH (120 x 50 mm) before and after UV and acid stress and containing ATH before and after UV and acid stress (from left to right).

The ATH filled sample in Figure 34 presents small and protuberant spots, which can be scraped; they result from accumulation and hardening of residues of the acid spray. The spots on the unfilled sample, on the other hand, are no deposit; they are the result of the discoloration of the surface of the sample due to the acid attack and ultraviolet exposure.

The sample without ATH is softer than the one containing it, and after the UV and acid stress it suffered a much more severe hardening of the surface, becoming brittle and displaying streaks and grooves on the surface that cannot be seen in the sample containing ATH. The lateral profile of the samples without ATH is also altered, i.e. at the end of the test the sample is concave. That effect is much reduced in the sample containing standard grade ATH.

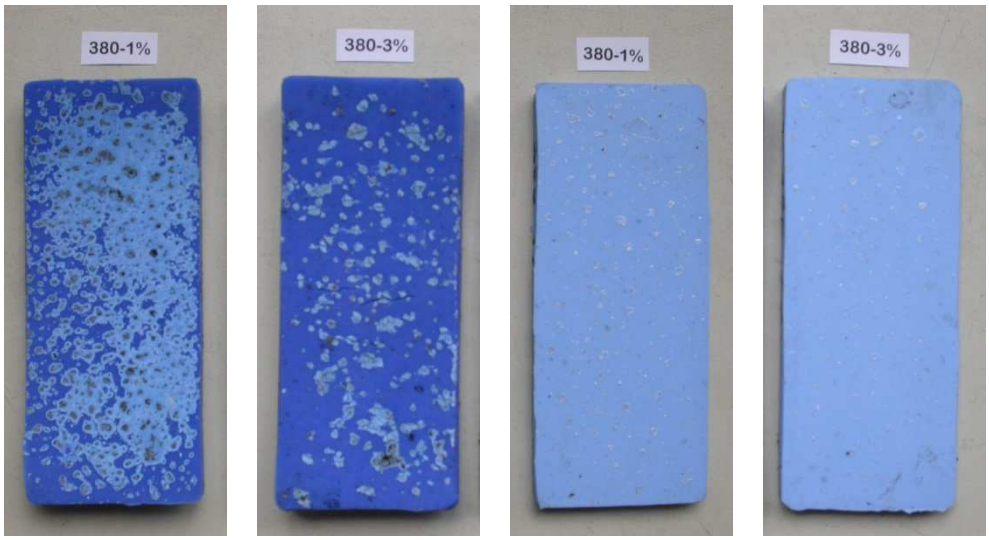

Figure 35. Samples of filler S1 without standard grade ATH (120 x 50 mm) at 1 wt% and 3 wt% and containing ATH at 1 wt% and 3 wt% (from left to right) after UV and acid stress.

The 1 wt% sample without ATH in Figure 35 is completely covered with discoloration spots, while the 3 wt% composition displays the deepest and longest grooves on the surface. The two samples containing S1 and ATH (Figure 35, right) do not deviate considerably from the reference sample in Figure 34, except for the fact that spots are somewhat smaller, but also higher in number throughout the surface of the sample.

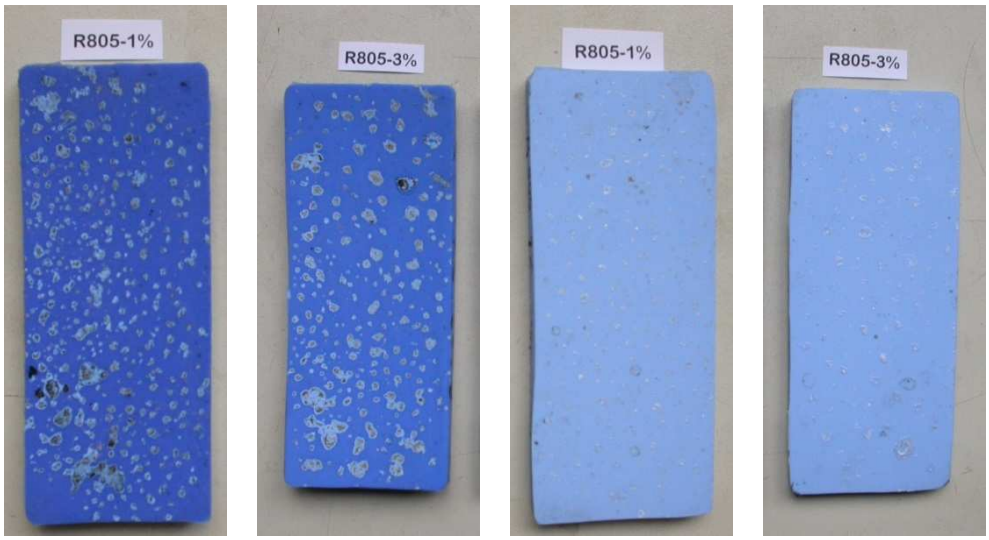

Figure 36. Samples of filler S2 without standard grade ATH (120 x 50 mm) at 1 wt% and 3 wt% and containing ATH at 1 wt% and 3 wt% (from left to right) after UV and acid stress.

In samples filled with hydrophobic silica S2 (Figure 36), even though some grooves can be found in the surface of the two samples without ATH, those are definitely not as deep or extensive as those found in sample *S1-3%*.

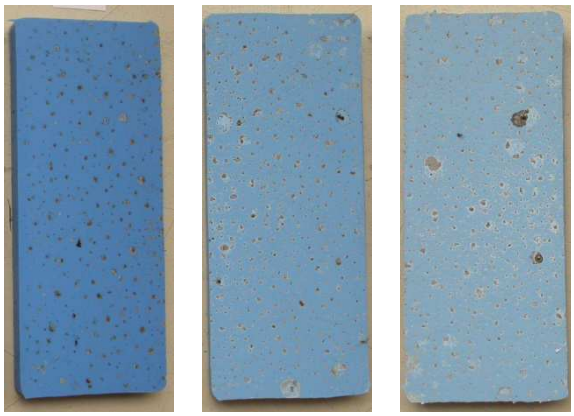

Figure 37. Samples of filler T1 without standard grade ATH (120 x 50 mm) at 1 wt% (left), 3 wt% (middle) and 5 wt% (right) after UV and acid stress.

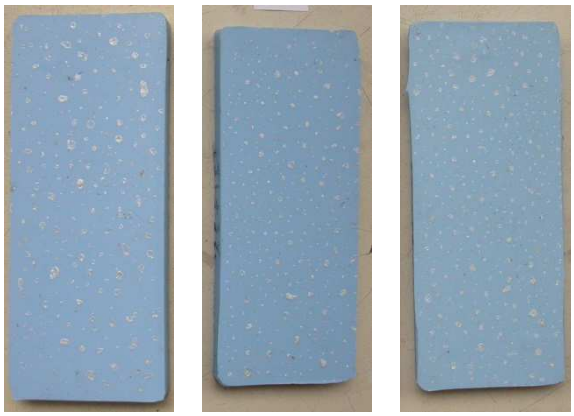

Figure 38. Samples of filler T1 containing standard grade ATH (120 x 50 mm) at 1 wt% (left), 3 wt% (middle) and 5 wt% (right) after UV and acid stress.

Samples filled with titanium dioxide T1 without standard grade ATH (Figure 37) present several small scratches on the surface, but these are all short and shallow.

Figure 39. Samples of filler A1 without standard grade ATH (120 x 50 mm) at 1 wt% (left), 3 wt% (middle) and 5 wt% (right) after UV and acid stress.

The samples in Figure 39 are severely attacked. The pattern of the white spots is particularly different than the other compositions; the spots are much smaller and present much sharper edges.

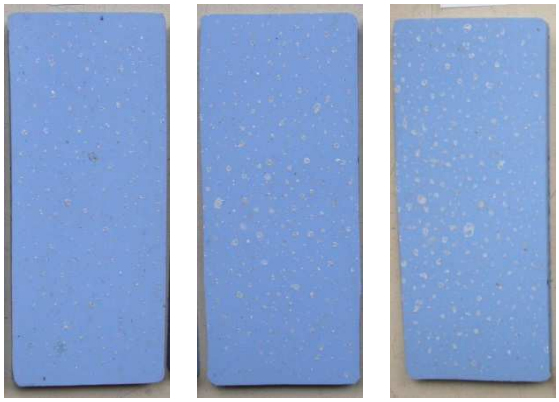

Figure 40. Samples of filler A1 containing standard grade ATH (120 x 50 mm) at 1 wt% (left), 3 wt% (middle) and 5 wt% (right) after UV and acid stress.

Figure 41. Samples of filler A2 without standard grade ATH (120 x 50 mm) at 1 wt% and 3 wt% and containing ATH at 1 wt% and 3 wt% (from left to right) after UV and acid stress.

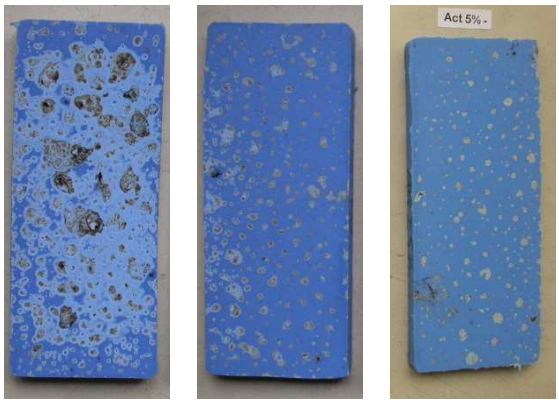

Figure 42. Samples of filler A3 without standard grade ATH (120 x 50 mm) at 1 wt% (left), 3 wt% (middle) and 5 wt% (right) after UV and acid stress.

Samples filled with aluminium oxide hydroxide A3 are very severely damaged, particularly the 1 wt% sample in Figure 42. The discoloration spots are not any more restricted to the spots were the acid drops were concentrated, but spread over the whole surface, connecting adjacent spots in such a way that the sample is almost completely discolored.

Figure 43. Samples of filler A3 containing standard grade ATH (120 x 50 mm) at 1 wt% (left), 3 wt% (middle) and 5 wt% (right) after UV and acid stress.

3.9 THERMOGRAVIMETRIC ANALYSIS

Thermogravimetric analyses were performed with the following parameters: temperature range from 30°C to 500°C at a rate of 10 K/min in nitrogen atmosphere; average sample mass of 30 mg. Results of the test are shown in Figures 44 to 55.

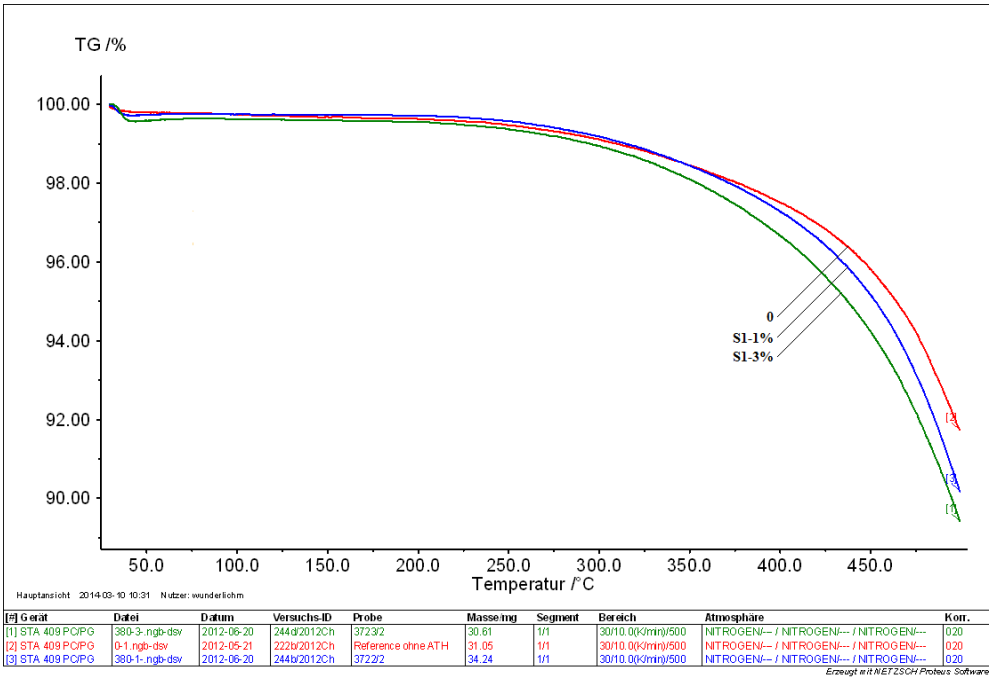

Figure 44. Thermogravimetric analysis of silicone compositions containing filler S1 without standard grade ATH depending on nanoparticle loading level.

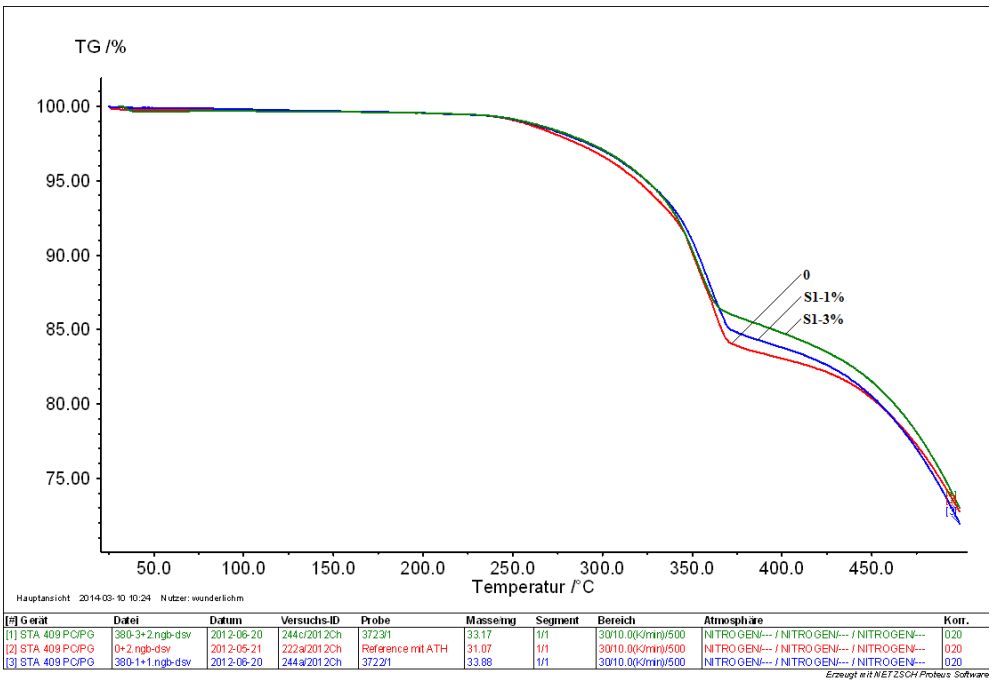

Figure 45. Thermogravimetric analysis of silicone compositions containing filler S1 and with standard grade ATH depending on nanoparticle loading level.

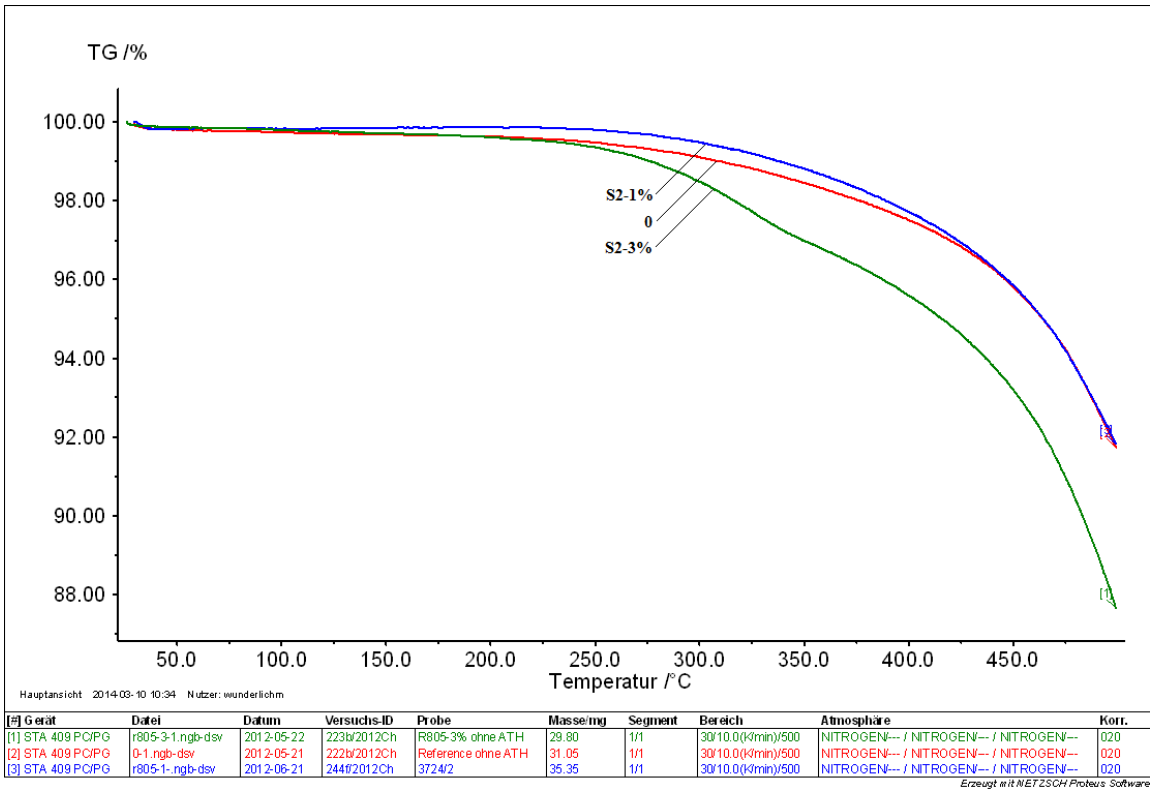

Figure 46. Thermogravimetric analysis of silicone compositions containing filler S2 without standard grade ATH depending on nanoparticle loading level.

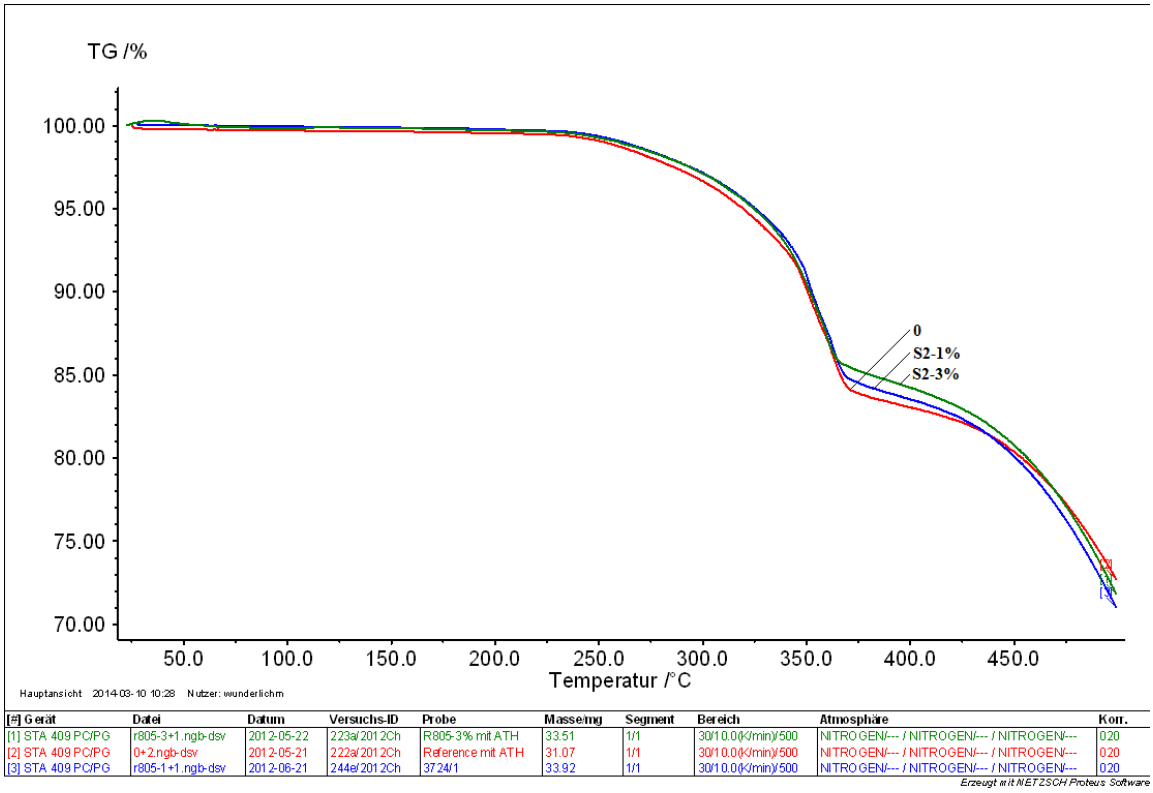

Figure 47. Thermogravimetric analysis of silicone compositions containing filler S2 and with standard grade ATH depending on nanoparticle loading level.

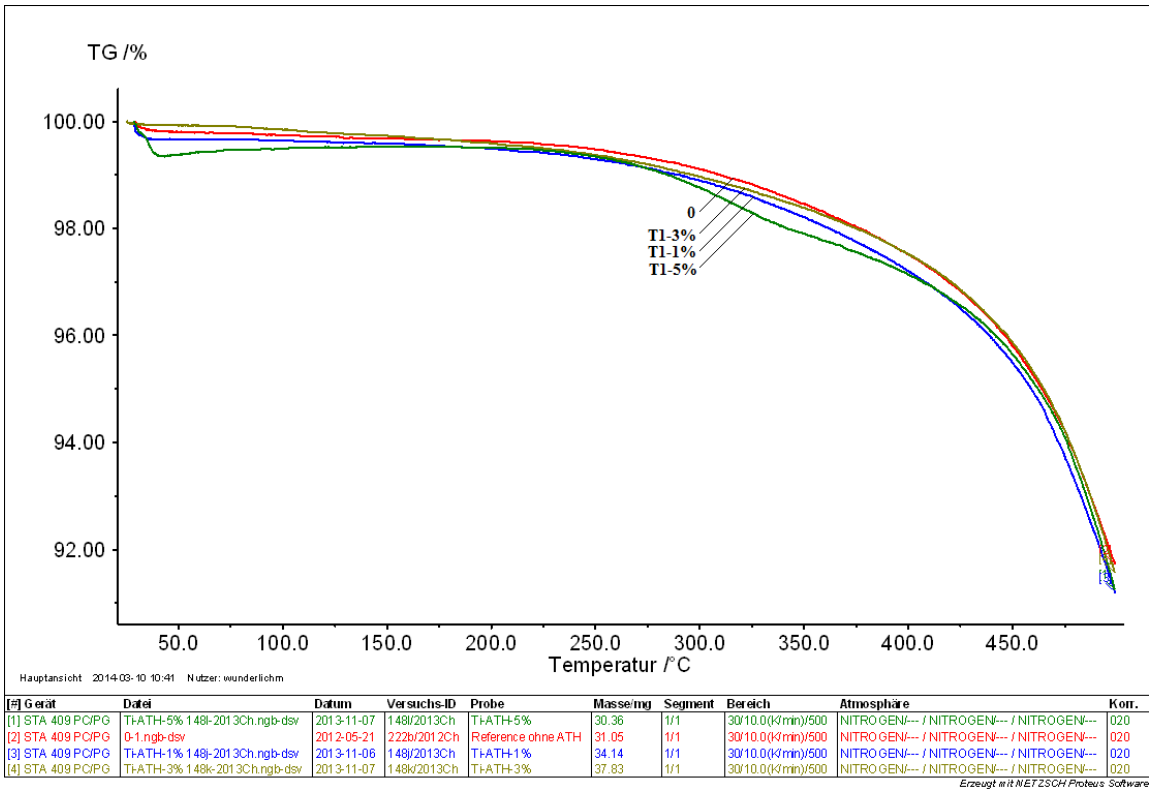

Figure 48. Thermogravimetric analysis of silicone compositions containing filler T1 without standard grade ATH depending on nanoparticle loading level.

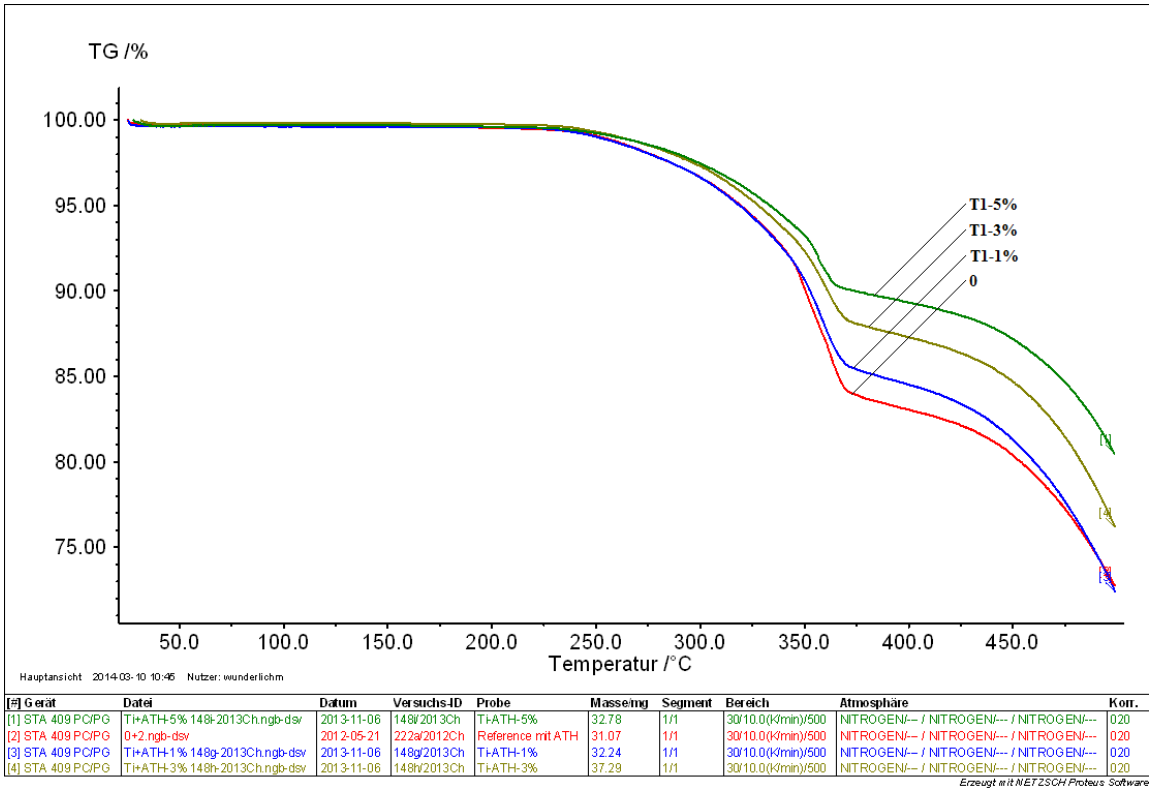

Figure 49. Thermogravimetric analysis of silicone compositions containing filler T1 and with standard grade ATH depending on nanoparticle loading level.

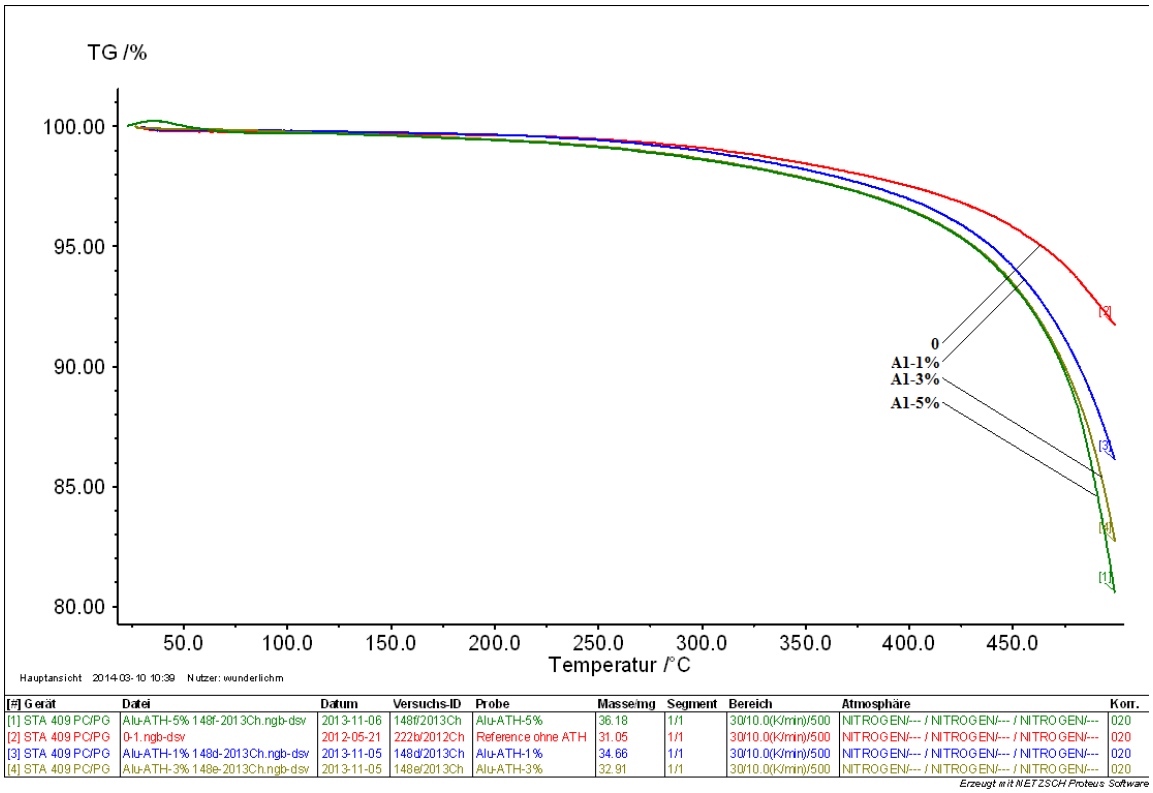

Figure 50. Thermogravimetric analysis of silicone compositions containing filler A1 without standard grade ATH depending on nanoparticle loading level.

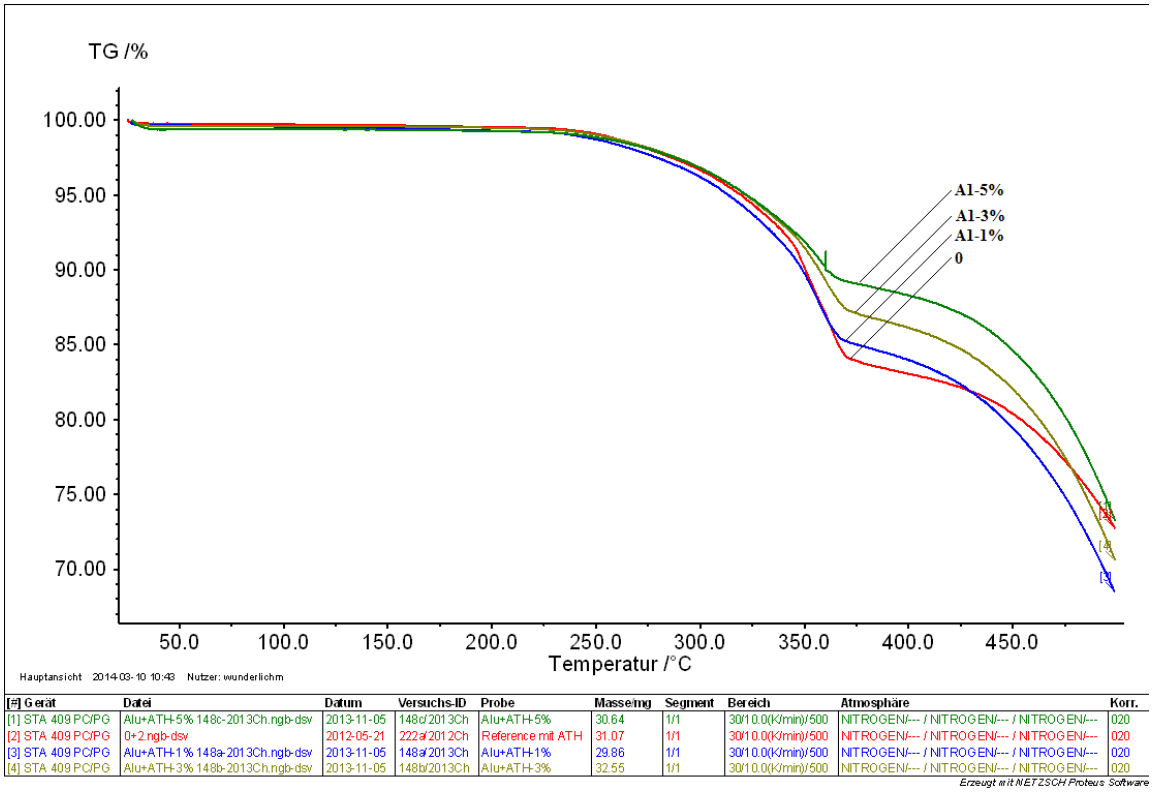

Figure 51. Thermogravimetric analysis of silicone compositions containing filler A1 and with standard grade ATH depending on nanoparticle loading level.

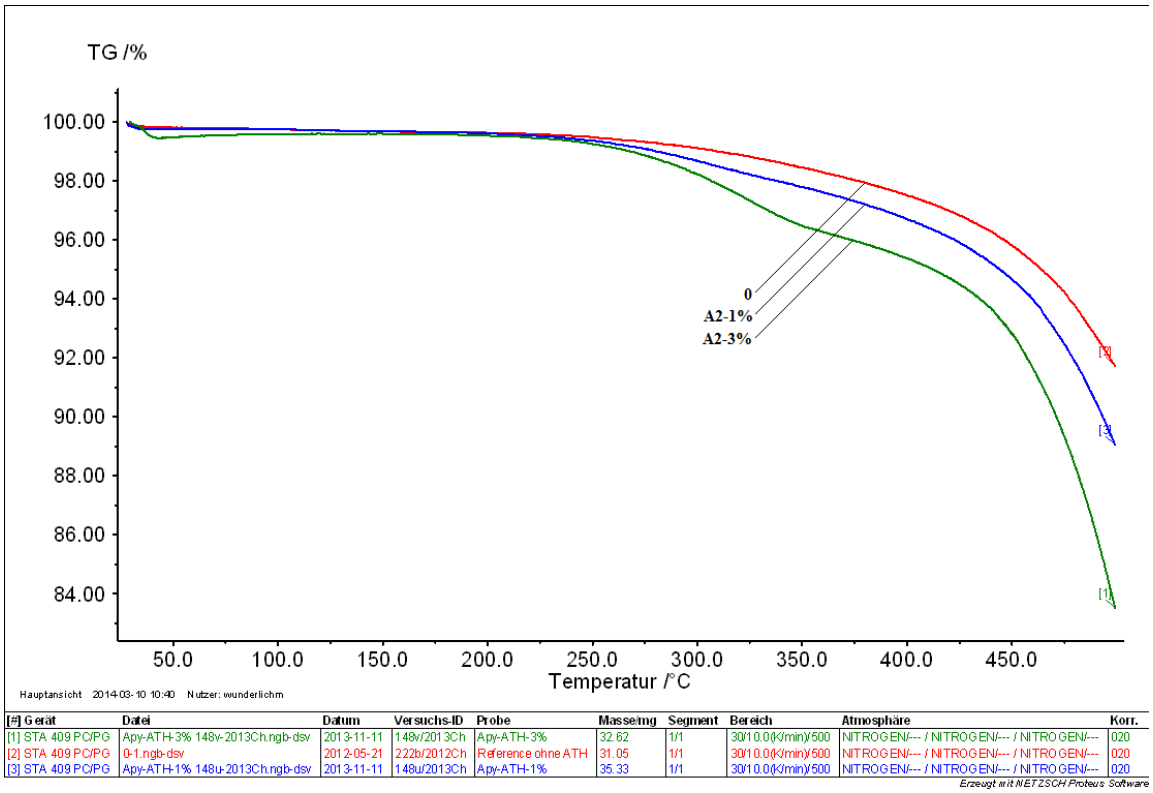

Figure 52. Thermogravimetric analysis of silicone compositions containing filler A2 without standard grade ATH depending on nanoparticle loading level.

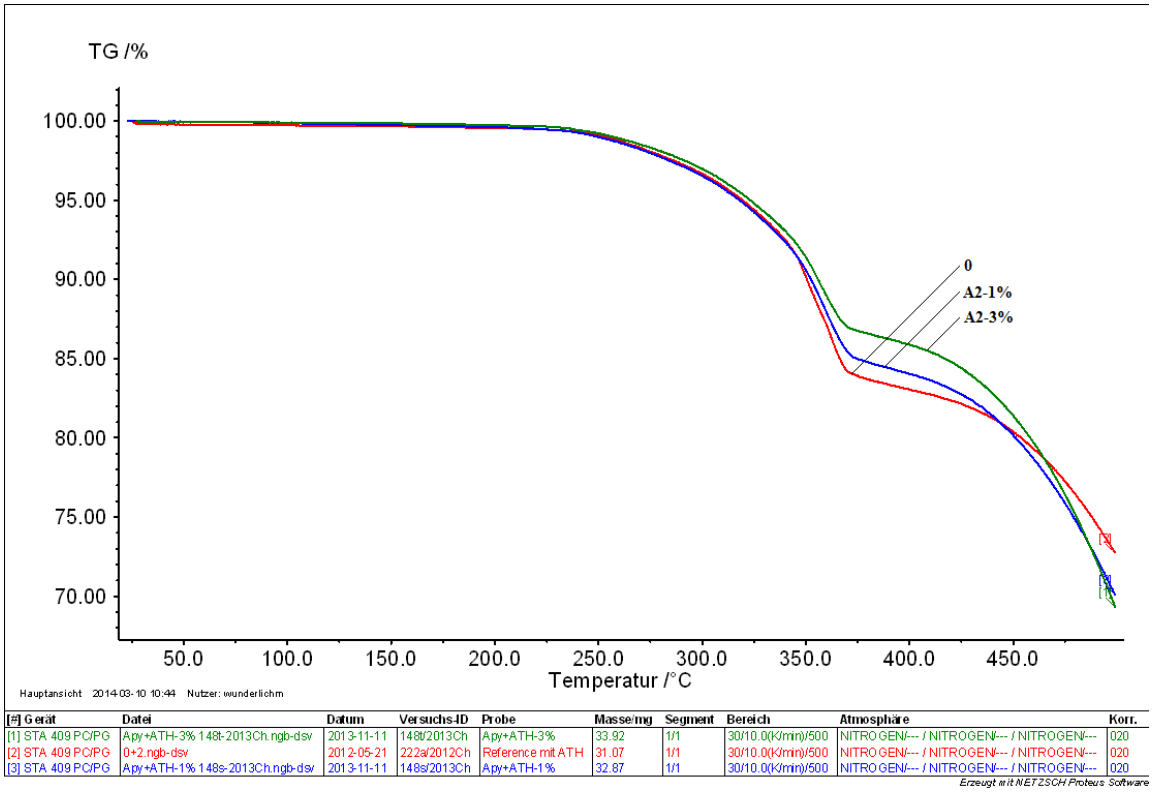

Figure 53. Thermogravimetric analysis of silicone compositions containing filler A2 and with standard grade ATH depending on nanoparticle loading level.

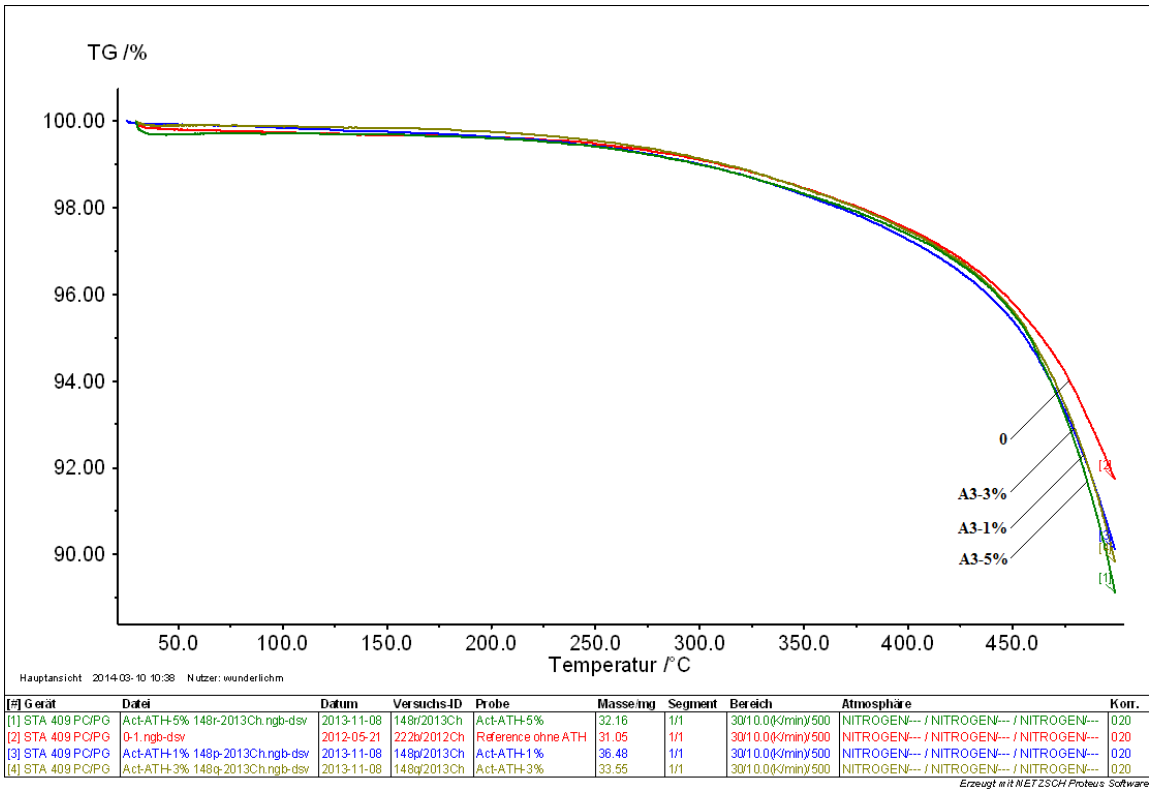

Figure 54. Thermogravimetric analysis of silicone compositions containing filler A3 without standard grade ATH depending on nanoparticle loading level.

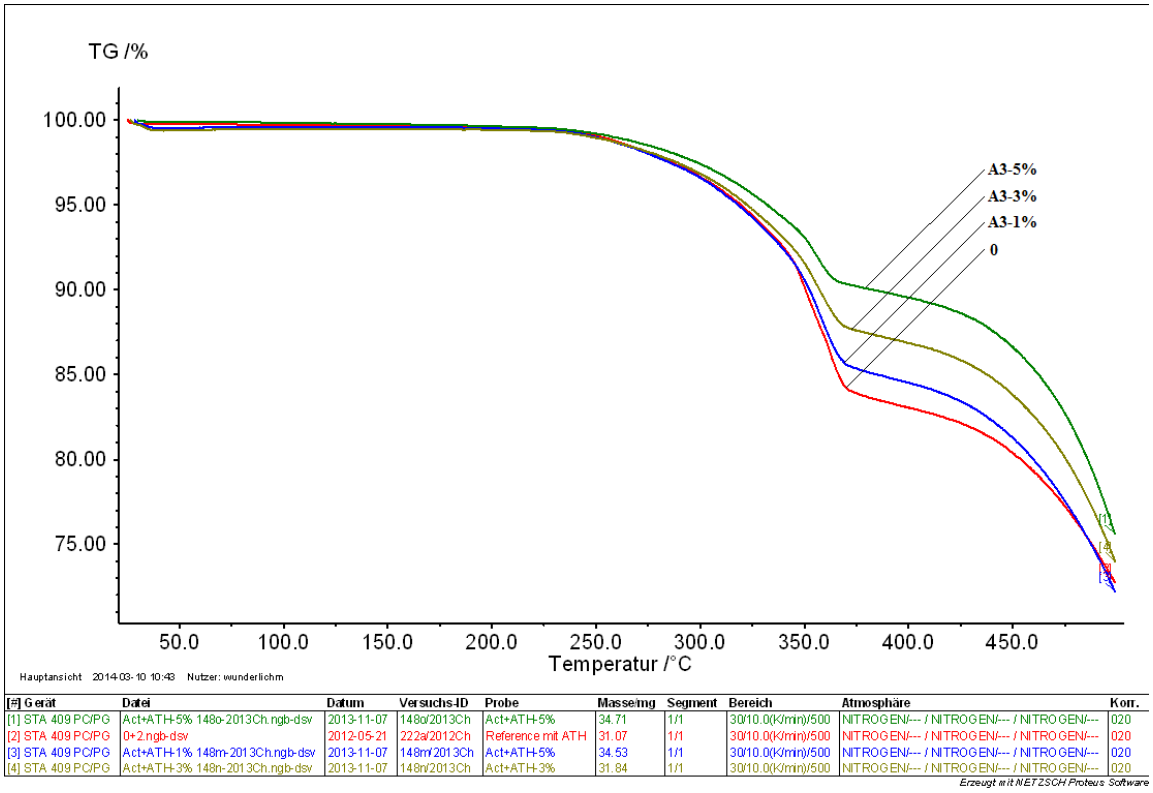

Figure 55. Thermogravimetric analysis of silicone compositions containing filler A3 and with standard grade ATH depending on nanoparticle loading level.

4 DISCUSSION

4.1 DESCRIPTION OF THE INTERPHASE VOLUME MODEL

There are several models available to try to explain the influence of nanofillers, such as the Intensity Model by LEWIS [70], the Multi-Core Model by TANAKA [71], the Polymer Chain Alignment Model by ANDRITSCH [72] and the Interphase Volume Model by RAETZKE [73]. The premise shared by these models is that between a filler particle and the matrix material there is a region with specific properties inherent to neither of these; each author naturally having studied a different set of fillers, base materials and properties, and believing this region has a different numbers of layers and average thicknesses.

In comparison to the other theories, the Interphase Volume Model takes a step further defining a set of equations to determine the exact volume of the interphase, accounting for the overlapping areas due to neighbor particles as filler loading level increases. The assumptions made by this model are that filler particles are spherical, have the same diameter, are uniformly dispersed in the matrix material and around each of them an interphase of constant thickness is generated.

This interphase is relevant because it is believed that in it, the structure of polymer chains differs from the rest of the base material, and this might yield properties not observed on the uninfluenced base material. These properties will reflect more on overall material performance the greater the interphase volume is considered to be.

RAETZKE's model derives from the analysis of the basic element displayed in Figure 56, a cube with edge length a_0.

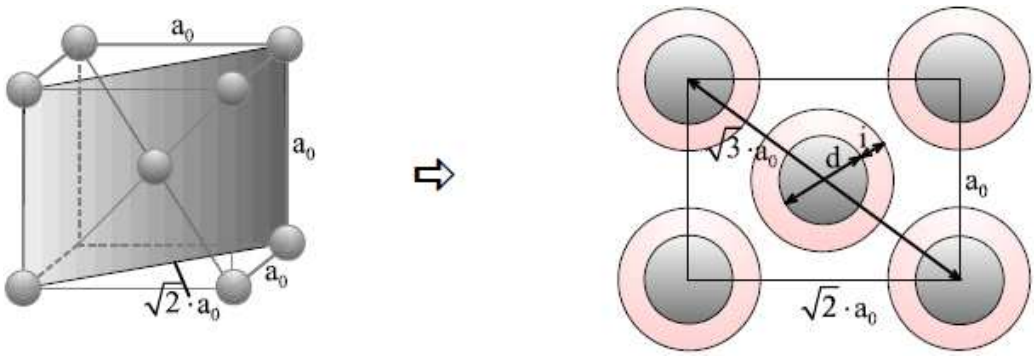

Figure 56. Basic element of the Interphase Volume Model, highlighting the diagonal plane of the cube [73].

$$a_0 = d \cdot \sqrt[3]{\frac{\pi}{3p}}$$; where:

d diameter of the filler particles;

p volume fraction of the filler;

i thickness of the interphase.

Considering the particle diameter *d* is constant, the edge length of the cube a_0 decreases as filler level *p* increases. As a_0 decreases, the particles are brought closer together and the interphase surrounding neighboring particles (red regions on Figure 56) start to overlap. RAETZKE defined a set of equations to determine the interphase content in four different areas of consideration as straight line segments defined as follows:

If $\frac{2}{\sqrt{3}}(d+2i) \leq a_0$, then: $p_i = p \left[\left(1+\frac{2i}{d}\right)^3 - 1\right]$;

if $(d+2i) \leq a_0 < \frac{2}{\sqrt{3}}(d+2i)$, then: $p_i = p \left[\left(1+\frac{2i}{d}\right)^3 - 1 - 8\left(\frac{1}{2}+\frac{i}{d}-\frac{\sqrt{3}a_0}{4d}\right)^2\left(2+\right.\right.$ *4id+3a02d*;

if $\frac{2\sqrt{2}}{3}(d+2i) < a_0 < (d+2i)$, then: $p_i = p \left[\left(1+\frac{2i}{d}\right)^3 - 1 - 8\left(\frac{1}{2}+\frac{i}{d}-\frac{\sqrt{3}a_0}{4d}\right)^2\left(2+\right.\right.$ *4id+3a02d−612+id−a02d22+4id+a0d*;

if $a_0 \leq \frac{2\sqrt{2}}{3}(d+2i)$, then: $p_i = 1 - p$.

Where:

d diameter of the filler particles;

i thickness of the interphase;

a_0 edge length of the cube;

p_i volume fraction of the interphase;

p volume fraction of the filler.

As seen above, in the model proposed by RAETZKE all the calculations are performed considering the volume fraction of the filler (*p*). Whenever necessary, the mass fraction of the filler, p_w, is determined as follows:

$$p_w = \frac{\rho_{filler}}{\rho_{filler} + \rho_{matrix}\left(1/p - 1\right)};$$

where:

p_w	mass fraction of the filler;
ρ_{filler}	density of the filler;
ρ_{matrix}	density of the matrix material;
p	volume fraction of the filler.

According to the previous equations, considering a fixed particle diameter *d*, the thicker the interphase *i* is, the faster the highest interphase volume is reached as filler loading level increases. For example: consider a particle with diameter *d = 20 nm* (Figure 57); at an assumed interphase thickness *i = 20 nm* the highest interphase is reached at a filler content of 5 vol%; an interphase thickness *i = 30 nm*, though, leads to highest interphase content at 2 vol%.

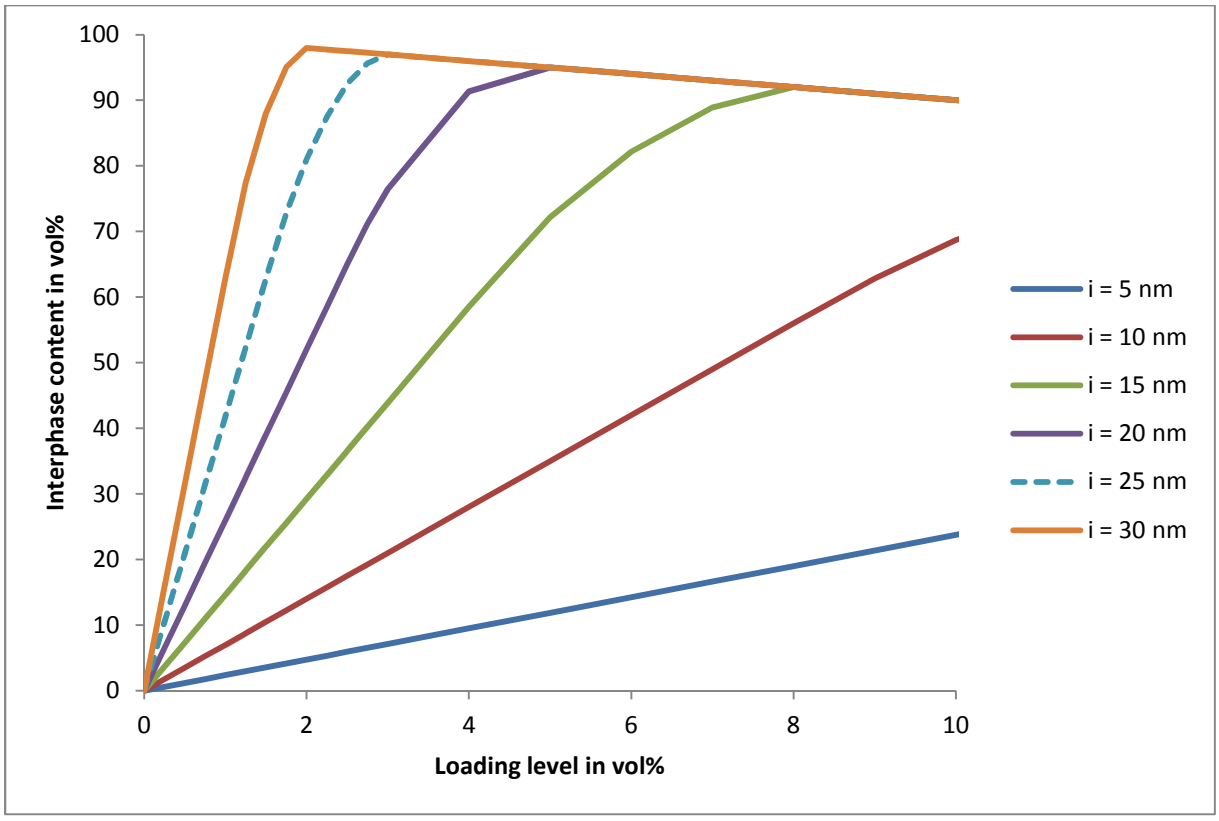

Figure 57. Interphase content p_i depending on nanoparticle filling level *p* for a particle with diameter *d = 20 nm*, considering different interphase thicknesses (*i*).

In both cases, if the loading level is further increased past the highest interphase content, the interphase volume slowly decreases, for the entire polymer matrix already consists of interphase, and a further addition of filler would only reduce the overall amount of base material.

If a constant interphase thickness *i* is now considered, and particle diameter *d* is changed instead, the larger the filler particle is, the higher the loading level *p* at which the peak in interphase volume occurs. Consider, for example, the previous interphase thickness *i = 30 nm* on a particle with diameter *d = 20 nm*, where the highest interphase volume is reached at 2 vol%. It can be seen in Figure 58 that another particle with a diameter of *d = 30 nm* under the same conditions would in fact lead to highest interphase content at 5 vol%.

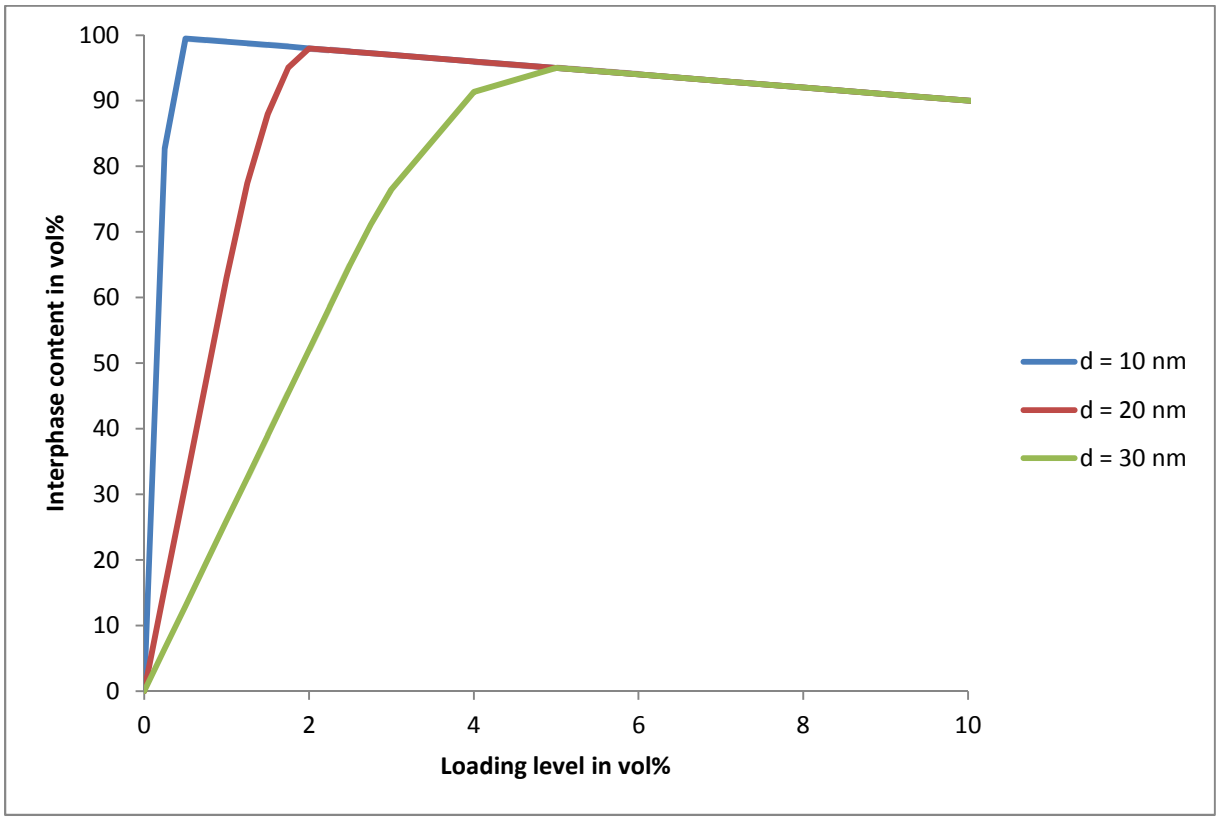

Figure 58. Interphase content p_i depending on nanoparticle filling level *p* for an interphase thickness *i = 30 nm*, considering different particle diameters (*d*).

4.2 THE EFFECT OF PARTICLE CLUSTERS IN THE PROPOSED MODEL

Because of their high surface energy, nanoparticles tend to agglomerate easily. The proper dispersion of fillers has been the focus of a great deal of research [28,74-75], although the existence of agglomerates was not considered in any of the models discussed in the previous section. Aiming to determine if and how they might affect the interphase content, the Interphase Volume Model has been expanded to account for particle clusters. Cluster is a general denomination used in this work to refer to groups of particles that may be gathered in the form of aggregates (chemically bonded primary particles) or agglomerates (aggregates gathered by weaker surface forces). These terms might be interchanged throughout the work, since these clusters are considered as a whole, despite the exact nature of the bonding.

The assumptions regarding particle clusters are the same as those previously made for regular filler particles in the model proposed by RAETZKE, i.e. perfectly dispersed spherical particles with the same diameter. The clusters are defined by two parameters: their size (diameter d) and amount (a), defined as the volume fraction of these clusters in relation to the total filler content.

Assume that the interphase content by volume (p_i) of a material containing primary particles and clusters in the total amount of p ($p = p_{primary\ particles} + p_{clusters}$) is defined as a function of filler content (p), particle diameters (d) and interphase thickness (i), $p_i = f(p, d_{primary\ particles}, d_{clusters}, i)$, which is unknown. The influence of the primary particles and clusters can be analyzed individually and then superimposed (Figure 59).

In this scenario, the total interphase content is determined by adding up the interphase content generated by the single particles alone (as shown in Figure 59b) and the interphase content produced by the clusters (Figure 59a). This approximation does not account for the overlapping of interphases generated by clusters and interphases generated by single particles. In other words, certain areas where single particles and clusters are close enough might belong to the interphase of both particles; in the individual analysis, these sections are computed in both equations, leading to a total interphase content higher than the real amount.

The error in this approximation will be quantified later, but it can already be advanced that: a) it increases with filler content and cluster amount (a high value of either of these means more interphase overlap); and b) it cannot be higher than the interphase contribution of clusters alone (the size of the intersection between two groups cannot be higher than the size of the smallest group).

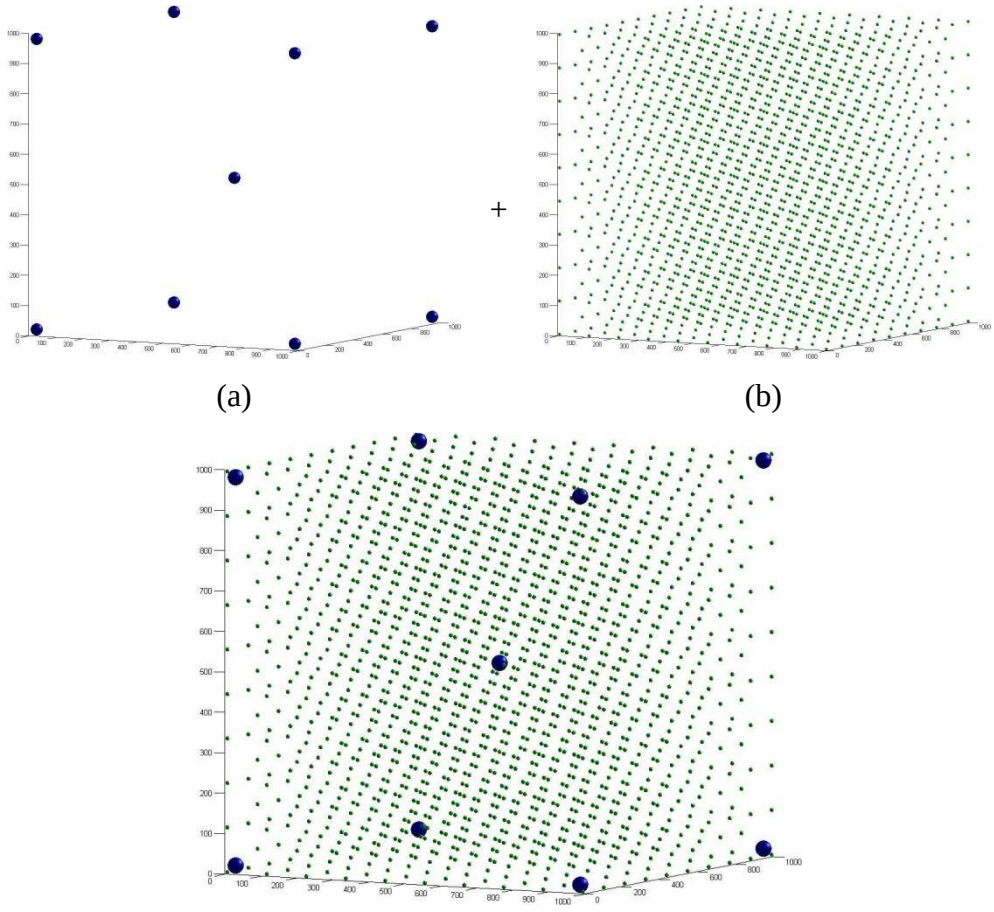

(a) (b)

(c)

Figure 59. Dispersion of a filler content of 0.2 vol% consisting of single particles (*d = 10 nm*) and clusters (*d = 40 nm*) in an amount of *a = 20%* per volume: a) distribution of particle clusters; b) distribution of single particles; c) superimposed representation.

In the individual analysis $p_{clusters} = a \cdot p$ and $p_{primary\ particles} = (1-a) \cdot p$; the unknown function $p_i = f(p, d_{primary\ particles}, d_{clusters}, i)$ can be approximated as:

$$p_i = f_1(a \cdot p) + f_2\big((1-a) \cdot p\big);$$

where:

p_i: total interphase content;

p: total filler content;

a: volume fraction of clusters (in relation to the total filler content);

$f_1(a \cdot p)$: interphase content determined as a function of clusters alone $f_1(a \cdot p) = f(p_{clusters}, d_{clusters}, i)$;

$f_2\big((1-a) \cdot p\big)$: interphase determined as a function of primary particles alone $f_2\big((1-a) \cdot p\big) = f(p_{primary\ particles}, d_{primary\ particles}, i)$;

If $a = 0$, $p_i = f_2(p)$, and the function $f_2(p)$ suits the original model proposed by RAETZKE, where all filler particles in the matrix are primary particles (Figure 59b). If $a = 100\%$, all particles in the matrix are clusters, and $p_i = f_1(p)$. In this scenario, the function $f_1(p)$ can again be determined by the original model proposed by RAETZKE, if only the particle size is the diameter of the clusters (Figure 59a). These two situations are illustrated in Figure 60, assuming a primary particle diameter of 10 nm and clusters of 40 nm (determined from the FE-SEM microscopies described in Section 2.2.2).

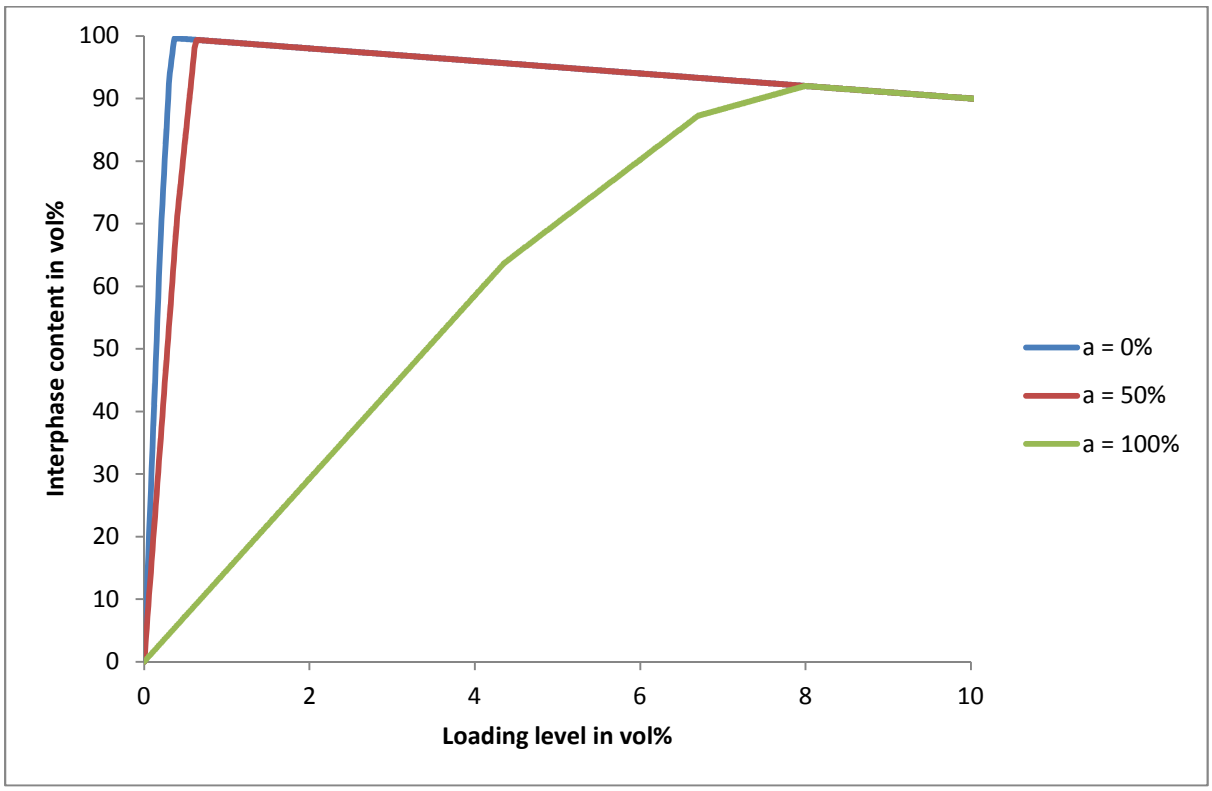

Figure 60. Interphase content p_i depending on filler loading level p for a particle with diameter $d = 10$ *nm* and clusters of 40 nm (both with interphase $i = 30$ *nm*) considering increasing cluster amounts (a).

Notice that the horizontal axis in Figure 60 (and relevant figures afterwards) representing the filler loading level is represented in percentage by volume (p). The reason is that when the horizontal and vertical axes are expressed in the same dimensionless quantity (vol%) it is easier to grasp how the amount of each material relates to the whole compound and to each other. That is, it is clearer, for example, observing the green curve in Figure 60 ($a = 100\%$), that if 5% filler generates 70% interphase content, the other 25% of the compound consists of uninfluenced base material; or that if 8% filler generates 92% interphase, the highest interphase content has been reached (and uninfluenced base material content amounts to 0).

Also displayed in Figure 60 is the curve for a cluster amount *a = 50%*, meaning that half of the volume of the filler is in the form of primary particles (*d = 10 nm*), and the other half as clusters (*d = 40 nm*). In this scenario $p_i = f_1(1/2\, p) + f_2(1/2\, p)$. The function $f_1(p)$, which governs the influence of particle clusters corresponds to the curve *a = 100%* in Figure 60, and $f_2(p)$ corresponds to the curve *a = 0*.

The determination of the curve *a = 50%* is broken into sections, to facilitate understanding. Individual calculations in key points are made below:

1. **Filler loading level of 0.5%:** This means that 0.25% of material consists of 10 nm filler particles and 0.25% consists of 40 nm clusters. The blue curve in Figure 60 gives us the coordinates (0.25, 80.3). This means that the individual contribution of 10 nm particles in an amount of 0.25% is of 80.3% interphase content. Analogously, the green curve gives us the coordinates (0.25, 3.7), meaning that the individual contribution of the 40 nm clusters in an amount of 0.25% is of 3.7% interphase content. Adding these values, the interphase content for a total filler loading level of 0.5% (0.25% single particles + 0.25% clusters) is 84% (80.3% + 3.7%). Thus, the point (0.5, 84) of the red curve is determined.
2. **Filler loading level of 0.64%:** This means that 0.32% of material consists of 10 nm filler particles and 0.32% consists of 40 nm clusters. The curve of the 10 nm particle gives us (0.32, 95) and that of the 40 nm cluster gives us (0.32, 4). Therefore, the interphase content for a filler loading level of 0.64% is 99% (95 + 4), giving us the point (0.64, 99) of the red curve. Notice that this point is critical: at 0.64% filler content, the total amount of matrix material is 99.36% (100% - 0.64%), which is equal to the interphase content, ignoring round-off errors. This means that at this point all matrix material consists of interphase, and thus, the maximum interphase content and the corresponding filler amount are determined.
3. **Filler loading level of 10%:** This means that 5% of material consists of 10 nm filler particles and 5% consists of 40 nm clusters. Nonetheless, there is no need to account for each particle's individual contribution, for once the maximum interphase volume is reached, the total amount of interphase equals the amount of matrix material, which is merely the total volume of the compound minus the total amount of filler (100% - 10%). That is how the point (10, 90) is found. Indeed, this analysis is valid for any filler amount past the previously determined critical filler content of 0.64%.

Accordingly, performing these calculations for the whole range of filler content, the interphase content p_i depending on filler loading level p for a cluster amount of 50% is found. For any other cluster amount the process is analogous, and in this manner Figure 61 is plotted.

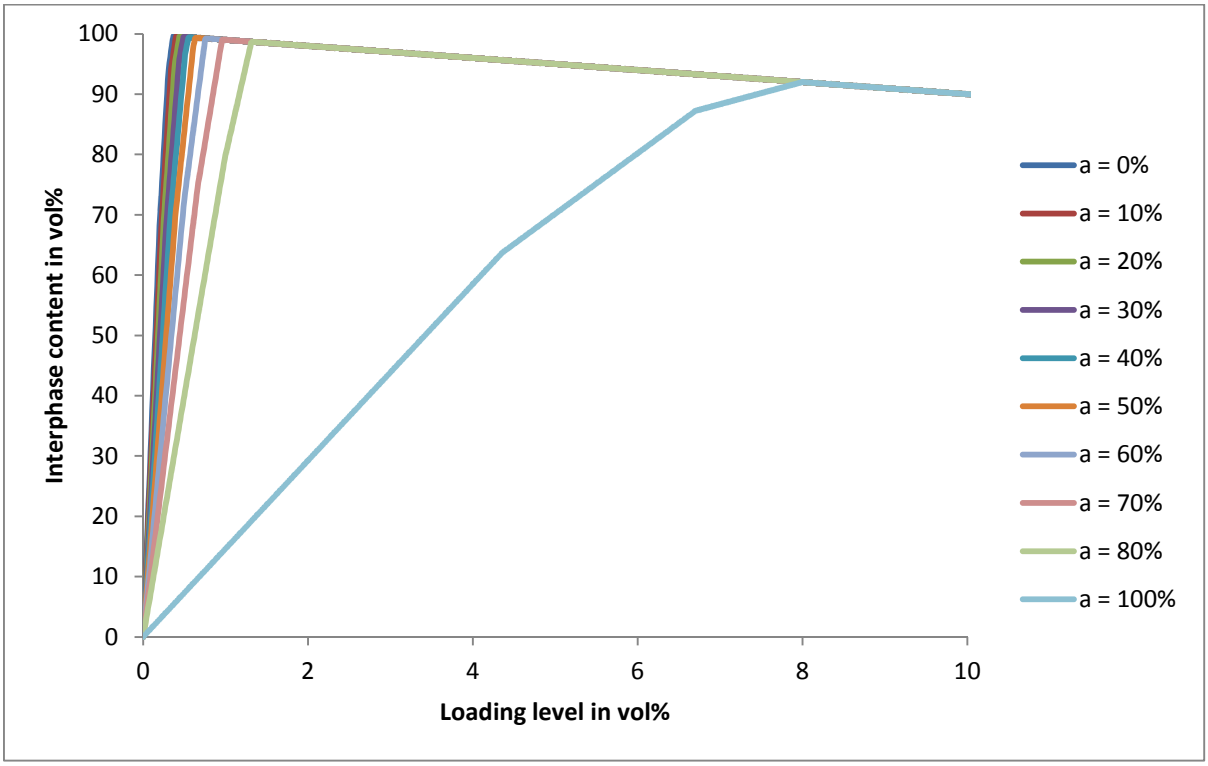

Figure 61. Interphase content p_i depending on filler loading level p for a particle with diameter $d = 10\ nm$ and clusters of 40 nm (both with interphase $i = 30\ nm$) considering increasing cluster amounts (a).

Even at extremely high cluster amounts (e.g. 80%), the amount of primary particles, small as it may, is still enough to provoke extreme effects in the interphase content. If primary particles were neglected (meaning $a = 100\%$, light blue curve) the total interphase content at 1% would be 14%. Considering them, though ($a = 80\%$, light green curve), the total interphase content at 1% is 80%. The contribution of the 0.8% cluster (80% of 1%) is 12% interphase content, while the 0.2% primary particle content (20% of 1%) alone leads to 68% interphase.

At this point the matter of the error in this model can be better explained. It was mentioned that the error consists in not accounting for the overlapping of interphases between single particles and clusters. If one assumes that the whole interphase content generated by clusters consists of overlap (worst case scenario), this means that this interphase was already accounted for in the single particle's calculation and therefore cannot be recounted in the total content.

It was shown in the previous page that when $a = 80\%$, at 1% total filler content the contribution of clusters was 12% interphase content. The maximum error in this scenario, though, would occur at an exact filler content of 1.32%, when the contribution of clusters is 15% interphase content, while single particles contribute with roughly 84% interphase content. One must notice, though, that this estimation of 15% is the maximum error possible, considered only because it could not be determined analytically.

This maximum error is in fact reduced as the volume fraction of clusters, a, decreases: it is 9% for $a = 70\%$ (this highest point is hit when $p = 0.96\%$). For any aggregate content equal to or lower than 60%, the maximum error in interphase estimation is lower than 6%, which validates the proposed method as an accurate estimation of interphase content, particularly for lower cluster amounts.

Now, it was said that the clusters are defined by two parameters (a and d), and only one of them was altered in the previous simulations, the cluster amount a. In order to verify the influence of larger cluster diameters, new simulations were performed with a cluster size of 400 nm, this being a very extreme case, where aggregates and agglomerates are 40 times larger than the primary particle size. Results are shown in Figure 62.

The major difference when such large clusters are considered is that their contribution to the total interphase content is minimal, which is very clear observing the light blue curve ($a = 100\%$) in Figure 62, where the clusters are singularly responsible to the total interphase content. This lesser contribution of clusters improves the precision of the method: the maximum error, even at $a = 90\%$, is only 1.5%.

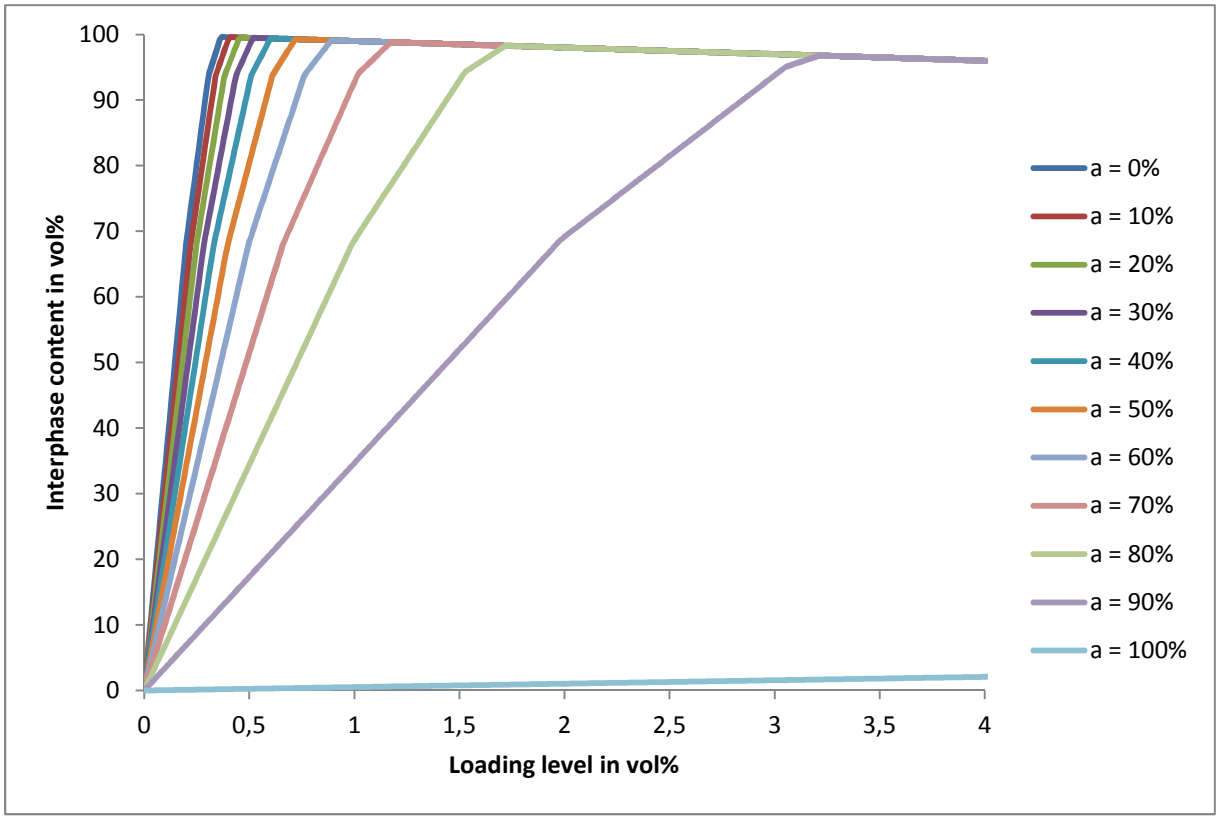

Figure 62. Interphase content p_i depending on filler loading level p for a particle with diameter $d = 10\ nm$ and clusters of 400 nm (both with interphase $i = 30\ nm$) considering increasing cluster amounts (a).

Now, taking into account single particle diameters, interphase thicknesses, cluster diameters and cluster amounts corresponding to the material used in the current work, the following considerations are made: a) it was previously determined from the available microscopies that cluster diameters are no larger than 40 nm; b) precise volume fractions of clusters could not be determined from available data, but assuming they are limited to less than $a = 60\%$, which seems reasonable, the loading level in which the peak in interphase content occurs (which is our greatest interest in this work) varies less than 0.42 wt% in relation to the reference curve ($a = 0$, when clusters are ignored).

In fact, for a cluster amount of $a = 40\%$, this shift in the filler loading level is limited to 0.29 wt%. Taking into account these very low margins, especially when contrasted with the discrete steps taken in filler content during material preparation (which are usually of 1 wt%), in the next sections the Interphase Volume Model will be applied disregarding the presence of particle clusters, which greatly simplifies the analysis of data with little impairment of precision.

4.3 SURFACE ROUGHNESS

As observed in Figures 7 and 8 (Page 29), mean surface roughness values range from $R_z = 1.6\ \mu m$ to $R_z = 2.7\ \mu m$, except for the material filled with standard grade ATH and *S1-3wt%*, which reaches $R_z = 3.5\ \mu m$. All the samples were produced on the same plates, and the range of variation is considered small, therefore surface roughness is uniform. Regarding material *S1-3wt% + ATH*, its performance throughout the tests is in accordance with the general trend observed in the other compositions, so its discrepancy is considered irrelevant.

4.4 FILLER DISPERSION ANALYSIS

Field emission scanning electron microscopies show that even though aggregates of particles are seen, larger agglomerates are not found. Since aggregates (being chemically bonded) are not segregated by the application of shear forces, and therefore cannot be improved by better dispersion techniques, dispersion quality is considered satisfactory.

4.5 HIGH VOLTAGE ARCING

In the high voltage arcing test, compositions without standard grade ATH (Figure 13, Page 34) display a peak in performance at 1 wt% of nanofiller (except for A2), which slowly decreases up to 5 wt%. Compositions containing ATH, on the other hand (Figure 14) perform rather stably between 0 and 3 wt%, showing a severe descent at 5 wt%. Examination of the zoomed area between 0 and 1 wt% (Figure 15) shows a peak of performance for filler S1 at 0.75 wt% and S2 at 0.50 wt%. Variations of fillers T1, A2 and A3 in this interval are rather minor, especially taking into account the confidence intervals.

It is assumed that the highest interphase volume for material in Figure 13 is reached at around 1 wt%, leading to the highest time to end of test. Simulations of interphase content of the base material without standard grade ATH according to the model proposed by RAETZKE are illustrated in Figures 63 and 64, for fillers S1 and S2, respectively.

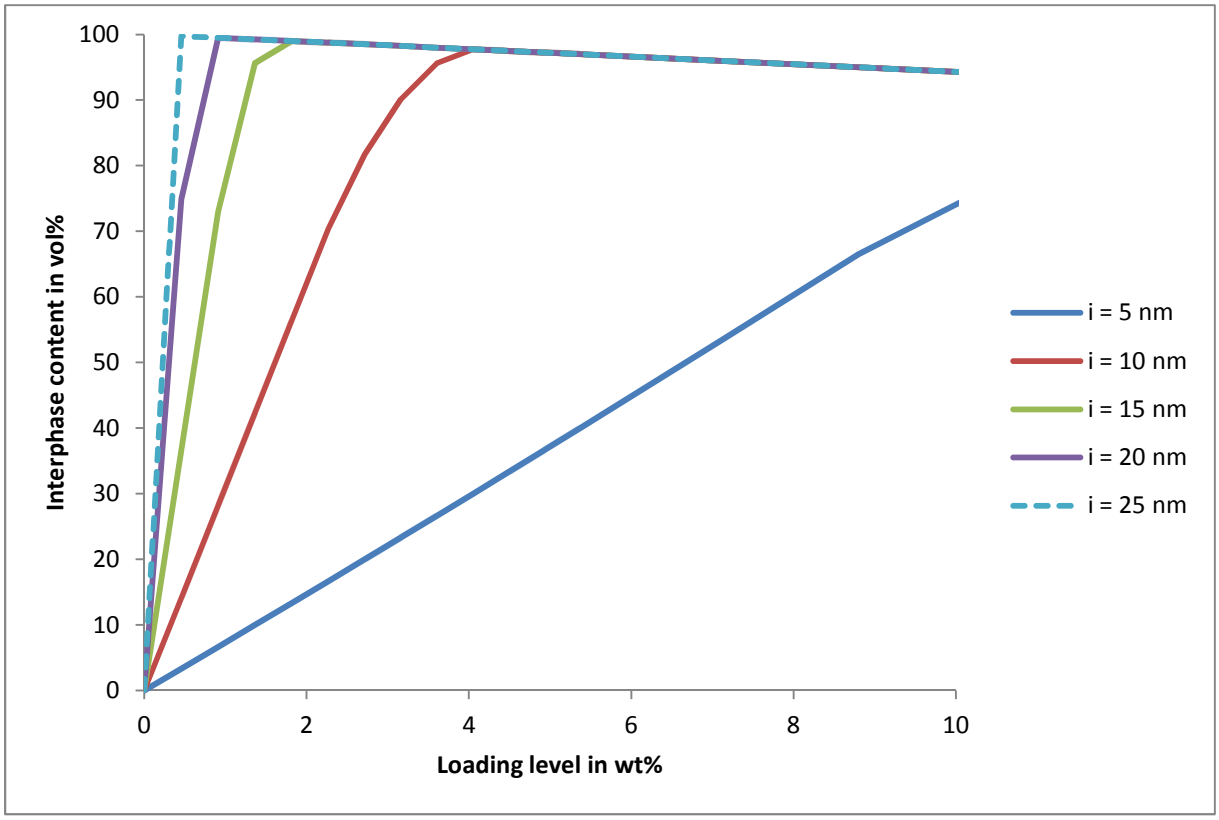

Figure 63. Interphase content depending on filling level of S1 on the base material without standard grade ATH for different assumed interphase thicknesses (*i*).

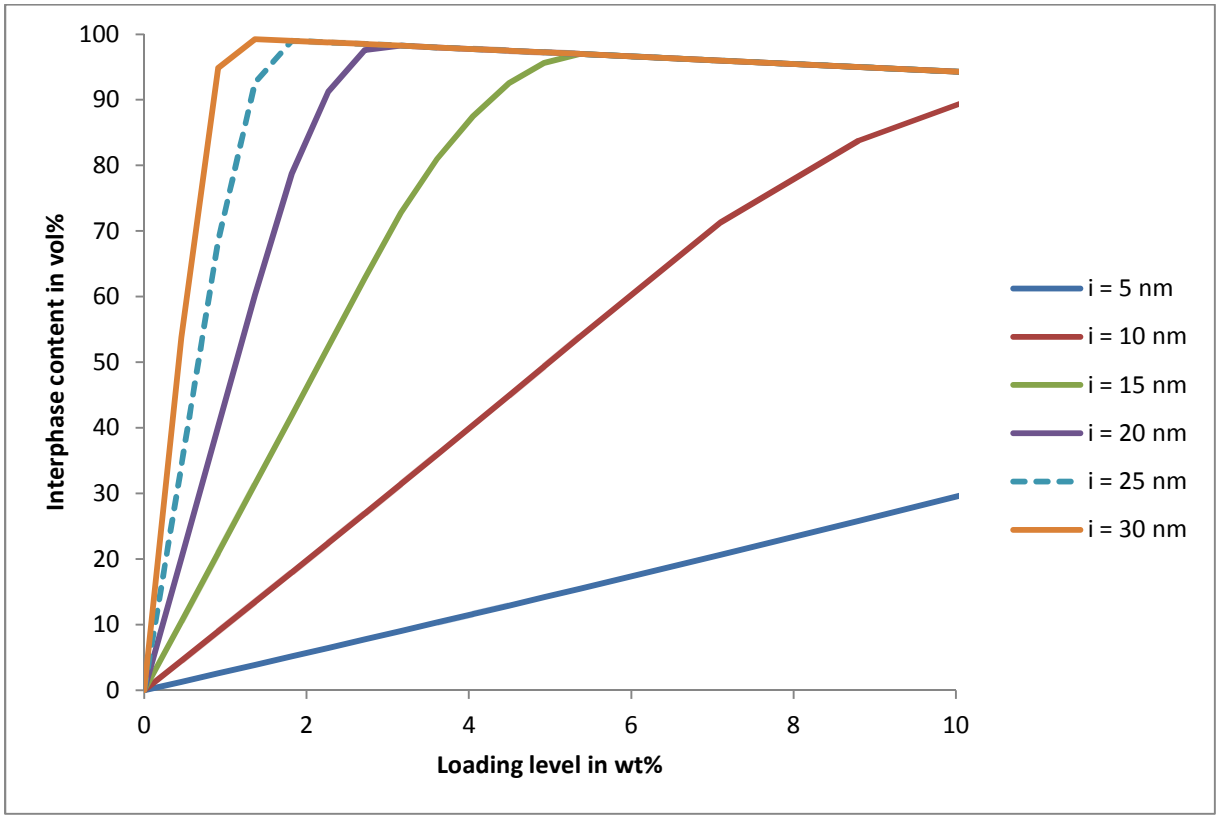

Figure 64. Interphase content depending on filling level of S2 on the base material without standard grade ATH for different assumed interphase thicknesses (*i*).

An assumed interphase thickness between 15 nm and 20 nm for filler S1 (Figure 63) would lead to highest interphase content at 1 wt%. Filler S2, on the other hand, fulfills the same condition for an interphase thickness of 30 nm (Figure 64). Hydrophobic silica S2 is surface treated to provide better interaction between filler and matrix, which can validate the assumption of a larger interphase thickness for filler S2 than for S1.

Simulations of interphase volume for the aforementioned fillers on the base material containing standard grade ATH are shown in Figures 65 and 66. It can be seen that an assumed interphase slightly larger than 15 nm for filler S1 would lead to the highest interphase content at 0.75 wt%, while the previously assumed interphase thickness of 30 nm for filler S2 leads to highest interphase content at 0.5 wt%. These assumptions fit satisfactorily the assumptions made in the previous paragraph as well as the measurements of time to end of the high voltage arcing test on Figures 14 and 15.

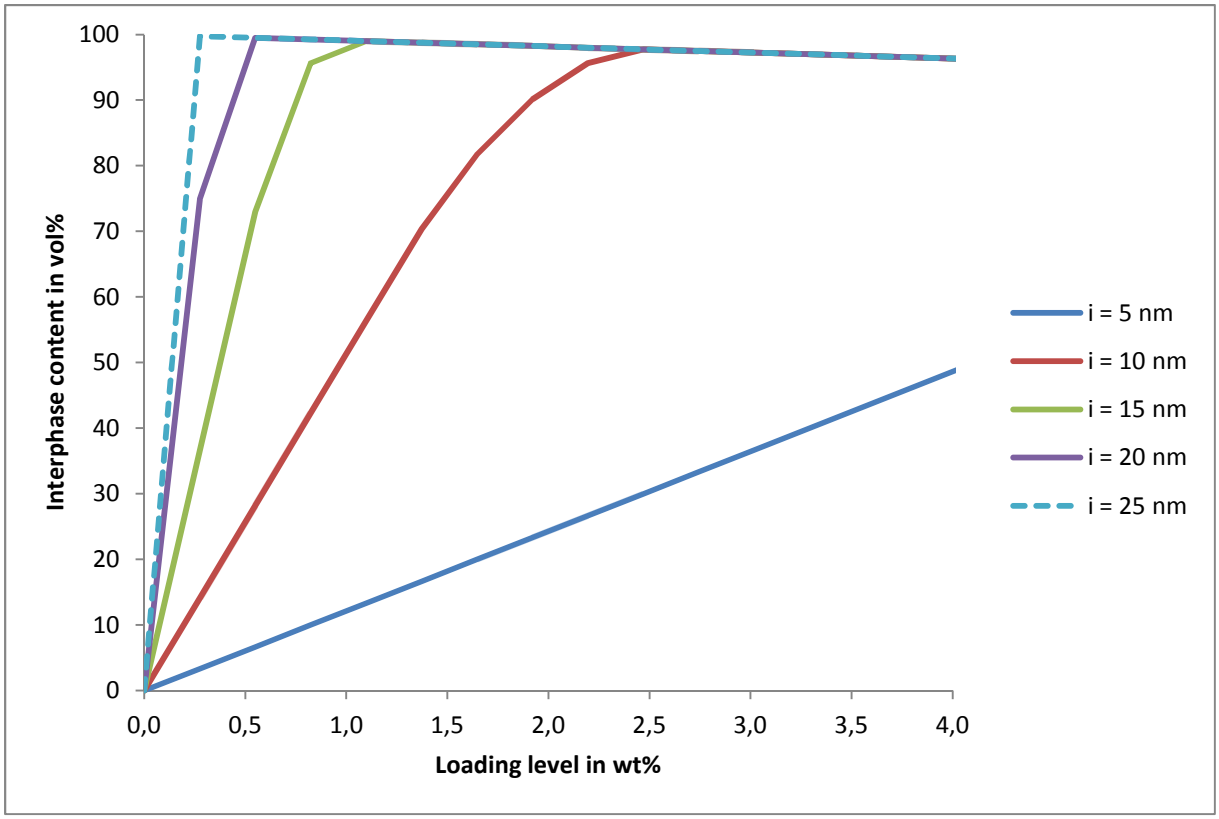

Figure 65. Interphase content depending on filling level of S1 on the base material containing standard grade ATH for different assumed interphase thicknesses (*i*).

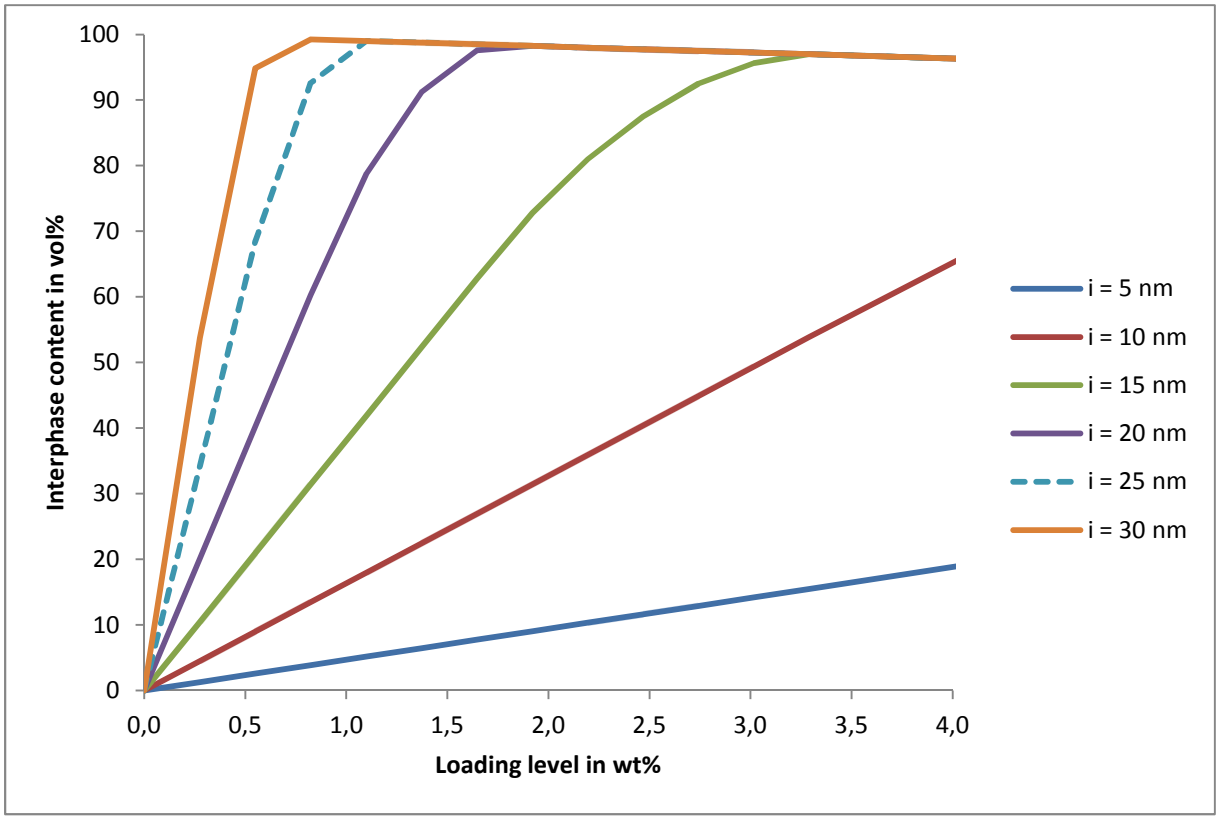

Figure 66. Interphase content depending on filling level of S2 on the base material containing standard grade ATH for different assumed interphase thicknesses (*i*).

Regarding fillers T1, A2 and A3, which do not display a distinct peak in performance between 0 and 3 wt%, the following must be considered: the interphase volume simulation for filler T1 corresponds, in fact, to the previously displayed Figure 57 (Page 61). In that case, any interphase thickness smaller than 25 nm would lead to a straight line between 0 and 3 wt%, with no local maximum in this interval. The other fillers, which have a diameter at least one order of magnitude greater, would present interphase volumes monotonically increasing at even slower rates (straight lines with smaller slope angles).

4.6 TRACKING AND EROSION

Primarily it is imperative to mention that the wide confidence intervals and the overlapping of different sets of data related to the tracking and erosion test makes the analysis of these results challenging, for it cannot always be proven that different sets of data belong in fact to different statistical populations. With that in mind, tracking and erosion data is analyzed as a whole, comparing the different parameters measured to each other, and generally trying to identify variation trends.

Eroded mass of compositions without ATH (Figure 16, Page 37) generally decreased with increasing nanoparticles loading level up to 3 wt%. The greater reduction is observed at 1 wt%, and further variation is rather small. This is largely true for material containing fillers S1, S2 and A3. For the other fillers, high eroded mass values were occasionally obtained, though the associated confidence intervals are exceedingly high. So high in fact that most of this data is not displayed in the graphics to avoid overshadowing relevant data.

At 1 wt% two out of the six compositions displayed higher than average mass losses (*T1-1wt%* and *A2-1wt%*), although at 3 wt% the eroded masses are as low as those of the other fillers at the same amount. At 3 wt% the only atypical measurement is that of A1 (167.3±191.7 mg), which also happens to perform poorly at 5 wt% (89.1±155.4 mg). The only material with a good performance at 5 wt% was A3 (3.3±1.5 mg). It is worthwhile mentioning that despite the occasionally high eroded masses, none of these compositions failed the tracking and erosion test. Compositions containing ATH (Figure 17) display a noticeably reduced eroded mass at 1 wt% and 3 wt%, with an increase at 5 wt%.

Erosion depth measurements of compositions without and containing ATH (Figure 20 and Figure 21, respectively) correlate thoroughly to the measurements of eroded mass, so that the analysis in the previous paragraphs remains true. Regarding tracking length measurements, compositions without ATH (Figure 18) have all very similar results, in spite of filler type or loading level, with the exception of filler S1 that presented smaller than average tracking lengths. Compositions containing ATH (Figure 19) display steadily increasing tracking length with loading level; slowly up to 3 wt%, but much greater at 5 wt%.

With regard to the possible correlation of data contained in this section with that of the previous one, and its compatibility with the Interphase Volume Model: a) the resistance to erosion of compositions without standard grade ATH is highest at 1 wt%, in accordance with the considerations made in Section 4.5; and b) although compositions containing standard grade ATH were not thoroughly studied in the loading range of 0 to 1 wt%, measurements at 1 wt% and 3 wt% still only improve marginally (compared to *‘0’*), with a sharp decline of the property in question at 5 wt%, which is in agreement with the results and assumptions of the previous section.

4.7 CONTACT ANGLE MEASUREMENT

Static contact angles of compositions without ATH (Figure 22, Page 41) increase steadily with nanoparticle filler level, except for hydrophilic silica S2. Filler A3 also presents an atypical reduction of the static contact angle at 1 wt%, but it is regularized at further loading levels. Compositions containing ATH (Figure 23), on the other hand, display a steady decrease of the static contact angle with increasing loading level. Filler A1 displays a lower than average static contact angle at 1 wt%. Advancing contact angles for compositions with and without ATH (Figures 24 and 25, respectively) correlate well to static contact angle measurements.

Receding contact angles for compositions without ATH (Figure 26) slowly decrease with increasing loading level up to 3 wt%, with an increase at 5 wt% that takes it back to the range of the unfilled material. The receding contact angles of compositions containing ATH (Figure 27) steadily increase with loading level. Material filled with filler S2 displays particularly low receding contact angle values. These results will be revisited in the next section.

No mention to the Interphase Volume Model was made in this section, nor will it be in the next ones. That is on account of the fact that these tests are a measure of surface properties, while the studied model accounts for bulk material properties.

4.8 DYNAMIC DROP TEST

Time to end of Dynamic Drop Test (DDT) for compositions without ATH (Figure 28, Page 44) decreases significantly for compositions containing 1 wt% and 3 wt% of nanofillers, but normalize at 5 wt%. In compositions containing ATH (Figure 29), filler S2 once again provoked a reduction in time to end of test, although filler S1 improved performance at both loading levels.

Dynamic drop test data was used for correlation analyses with contact angle measurements. The correlation coefficient between each set of contact angles and the equivalent DDT result is presented in Table 4. This standardized coefficient varies between -1 and +1 (if the variables are inversely or directly proportional, respectively), being close to zero if variables are unrelated.

Table 4. Correlation factors among contact angle measurements and time to end of DDT.

Formulation / Correlation Factor	**Static CA**	**Advancing CA**	**Receding CA**
S1, without standard grade ATH	0.778	0.969	0.999
S1, containing standard grade ATH	-0.768	-0.662	0.933
A1, without standard grade ATH	0.131	0.332	0.989
S2, without standard grade ATH	0.828	0.880	0.921
S2, containing standard grade ATH	0.963	0.951	0.926

The work of HOFMANN [62] was previously mentioned for the discovery of the correlation between the receding contact angle and the electrical performance of wetted surfaces. Furthermore, data on Table 4 shows that the receding contact angle holds a very high correlation (at least 92.1%) with the evaluation of retention of hydrophobicity by the Dynamic Drop Test, with the advantage of being much less time-consuming (less than 5 minutes, against up to 24 h of the DDT) and yielding results with intrinsically narrower confidence intervals (e.g. comparison of Figures 27 and 29, with the same sampling size).

Comparing time to end of DDT and contact angle data with high voltage arcing (IEC 61621) and tracking and erosion (IEC 60587) results, it is noticeable that the lower loading levels of 1 wt% and 3 wt% have better high voltage arcing and tracking and erosion resistance, though usually presenting poor hydrophobicity, while the higher loading level of 5 wt%, which presented the worst performance on IEC 61621 and IEC 60587 in fact displays the best time to end of DDT.

Furthermore, material filled with S2 and ATH, with receding contact angles below average (Figure 27) and performance below the reference material in the dynamic drop test (Figure 29), presents the best time to end of the high voltage arcing test. This compromise in the formulation of silicone rubbers between hydrophobicity maintenance and erosion performance has been well documented [4-5,17-18,76-77].

It is believed that the addition of fillers affects hydrophobicity negatively on silicone elastomers because they slow the process of migration of low molecular weight silicone chains (LMW) from bulk to surface. It is worth mentioning that the work of JAHN [13] also detected decline in loss of hydrophobicity with increasing filler content (ATH) in the tracking wheel and dynamic drop tests, which was attributed to the presence of grains of the filler on the surface of the material, which are hydrophilic.

Nevertheless in the same work JAHN [13] found improvements in hydrophobicity recovery (through measurement of the dynamic contact angles after exposure to corona) and hydrophobicity transfer (measuring the dynamic contact angles on a pollution layer made of silica). The author theorizes that these benefits are due to the ionic behavior of ATH, which produces a change in the chemical equilibrium of the polymer, promoting a breakage of the silicone chains and releasing additional LMW compounds.

4.9 MECHANICAL TESTS

Comparison of the mechanical properties of compositions without ATH (Figures 30 and 32) with the compositions containing ATH (Figures 31 and 33) clearly show the lesser performance of the latter, as discussed in Chapter 1 (the detrimental effects of ATH to mechanical properties). The addition of the nanofillers, however, do not deteriorate either tensile strength or tear resistance at 1 wt% and 3 wt%, although at 5 wt% consistently weakened properties are seen.

4.10 ACID AND UV EXPOSURE

Comparison of samples without standard grade ATH and containing it clearly shows that such filler improves the resistance to acid and UV stress. ATH filled samples only presented acid residues on the surface, while compositions without it suffered from discoloration, hardening and cracking, which in operational conditions might lead to humidity infiltration and exposure of the rod.

Regarding the addition of the nanofillers, the lower filling levels of 1 wt% and 3 wt% perform better than 5 wt%. Moreover, titanium dioxide filled samples display the best resistance to acid and UV stress, while samples filled with S1 and A3 presented the weakest performances.

4.11 THERMOGRAVIMETRIC ANALYSIS

A distinct trend can be observed comparing the thermogravimetric analyses of compositions without ATH and compositions with ATH: in the latter, the addition of nanofillers usually leads to a delayed degradation onset; and the higher the loading level, the better the performance (e.g. Figure 49, Page 55). Knowing the applied fillers intrinsically have better resistance to thermal degradation than silicone rubber and taking into consideration the very high standard grade ATH content (52 wt%) in addition to the 1 wt% to 5 wt% of nanofillers, the results of compositions containing ATH are anticipated, and in accordance with [12,32,78].

However, in the compositions without ATH, addition of nanofillers actually lowers the temperature onset, proportionately with the loading level (e.g. Figure 50). No explanation can be provided for the negative impact of nanofillers on the compositions without standard grade ATH, especially since the addition of nanofillers in such compositions was shown to provide better performance in the high voltage arcing and tracking and erosion tests, presumably due to an improvement in thermal resistance.

Nevertheless, a lower temperature onset due to the addition of fillers has been observed with nanoscale titanium dioxide in epoxy resin [79] as well as with silica in PDMS elastomers [80], and it is agreed not to be an indication of a poor material composition. Moreover, the degradation process under air and nitrogen atmosphere is known to differ [19,81-82], and therefore if any conclusion is to be drawn about the thermal stability of the currently researched material, results of high voltage arcing and tracking and erosion carry more weight when confronted with conflicting results.

5 CONCLUSIONS

With the aim of determining the effect of different filler types, sizes, amounts and dispersion quality on silicone elastomers, in this work six fillers in the submicron scale were added to a pure high temperature vulcanized (HTV) silicone rubber matrix as well as standard grade alumina trihydrate (ATH) filled HTV. These submicron scale fillers were added in loading levels up to 5 wt% and their influence was investigated on electric, chemical, thermal an mechanical properties.

Results of the tests according to IEC 61621 (high voltage arcing) and IEC 60587 (tracking and erosion) were successfully explained by the Interphase Volume Model, which suggests that changes in material properties are related to the interphase content. The model was expanded to account for the occurrence of particle clusters, being able to accurately estimate interphase content for particle cluster amounts lower than 60%; additionally, in this range, it was found that the influence of clusters on the peak of interphase content can be neglected.

Lower loading levels were found to improve high voltage arcing and tracking and erosion with the lowest compromise of tensile strength, tear resistance and acid and UV resistance. In fact, at 1 wt% tensile strength and tear resistance were actually improved (5% and 6.5%, respectively). At 3 wt% tensile strength was reduced by 5.2% and tear strength 6%. The highest loading level of 5 wt% on the other hand led to better hydrophobicity (evaluated via Dynamic Drop Test and contact angle measurements).

Regarding the influence of standard grade ATH, compositions containing it displayed 144% higher time to end of the high voltage arcing test, with better tracking and erosion, acid and UV resistance. Nonetheless, mechanical properties were reduced (tensile strength: 59.2%; tear strength: 22.6%), and hydrophobicity was also compromised.

Although improvements could be seen when adding nanofillers to pure HTV, their exclusive application (as a substitute for ATH) is not realistic, since minimum requirements for outdoor insulating materials were not (or were barely) fulfilled. The minimum time to end of test of 180 s in IEC 61621, for example, was only reached for five out of six compositions at 1 wt% (Figure 13), and unachieved for all material at 3 wt% and 5 wt%. Therefore, the

application of standard grade ATH still seems critical, and the combination of nanofillers and ATH is rather recommended.

Concerning the comparison of the submicron fillers among themselves, results are graphically summarized in Figure 67 for the compositions without ATH and in Figure 68 for compositions containing it. Each material is graded from 1 to 5, with the higher values representing the best performances. In regard to the influence of surface treatment, octylsilane treated silica S2 performs better than S1, especially when associated to ATH, but that cannot be exclusively attributed to the chemical composition, since particle size is also different in the two fillers.

Compositions filled with titanium dioxide (T1) exhibit the best overall performance; compositions containing silica (S1 and S2) display very good electrical properties, particularly the hydrophobic silica S2; material filled with aluminium oxide A1 show very good mechanical properties; material filled with boehmite A3 possess particularly good hydrophobicity, and finally, material filled with A2 has an average performance in all tests, not standing out in any particular one.

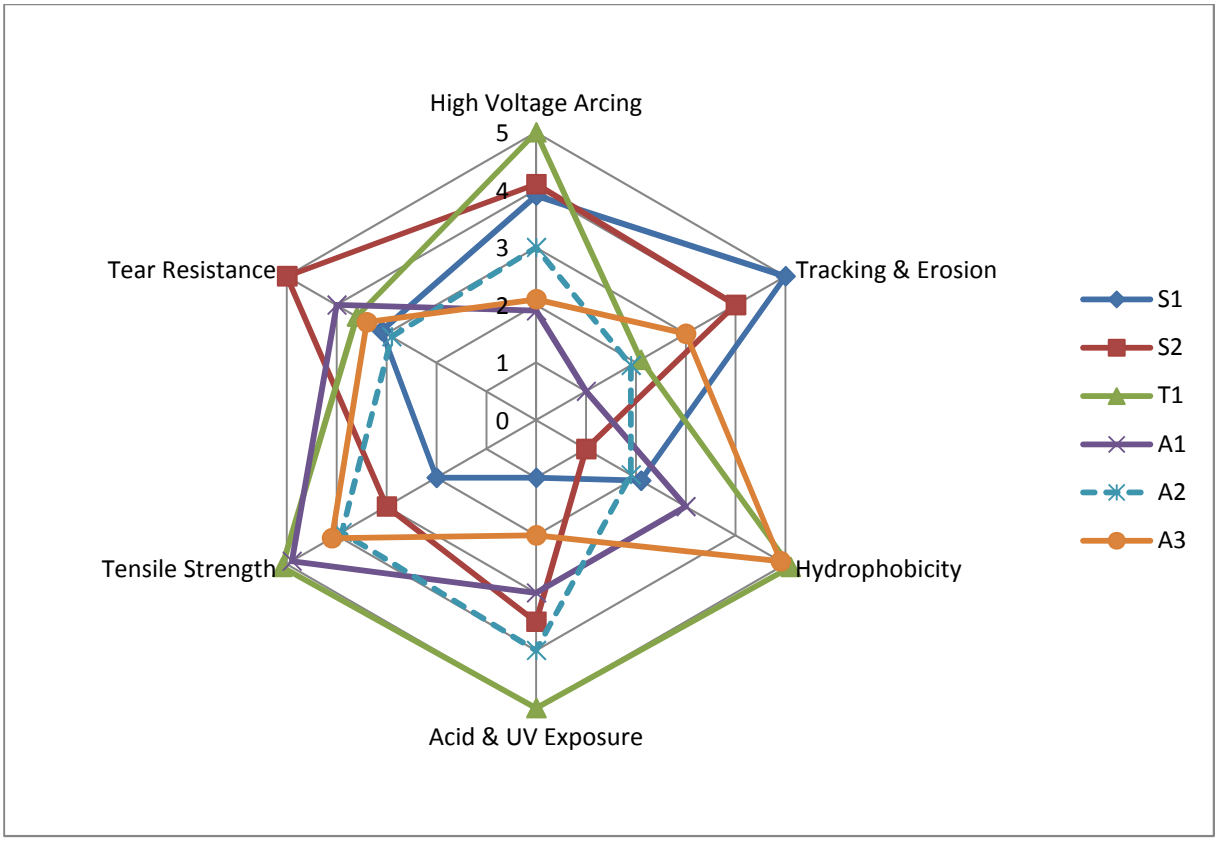

Figure 67. Radar chart summarizing properties of compositions without standard grade ATH.

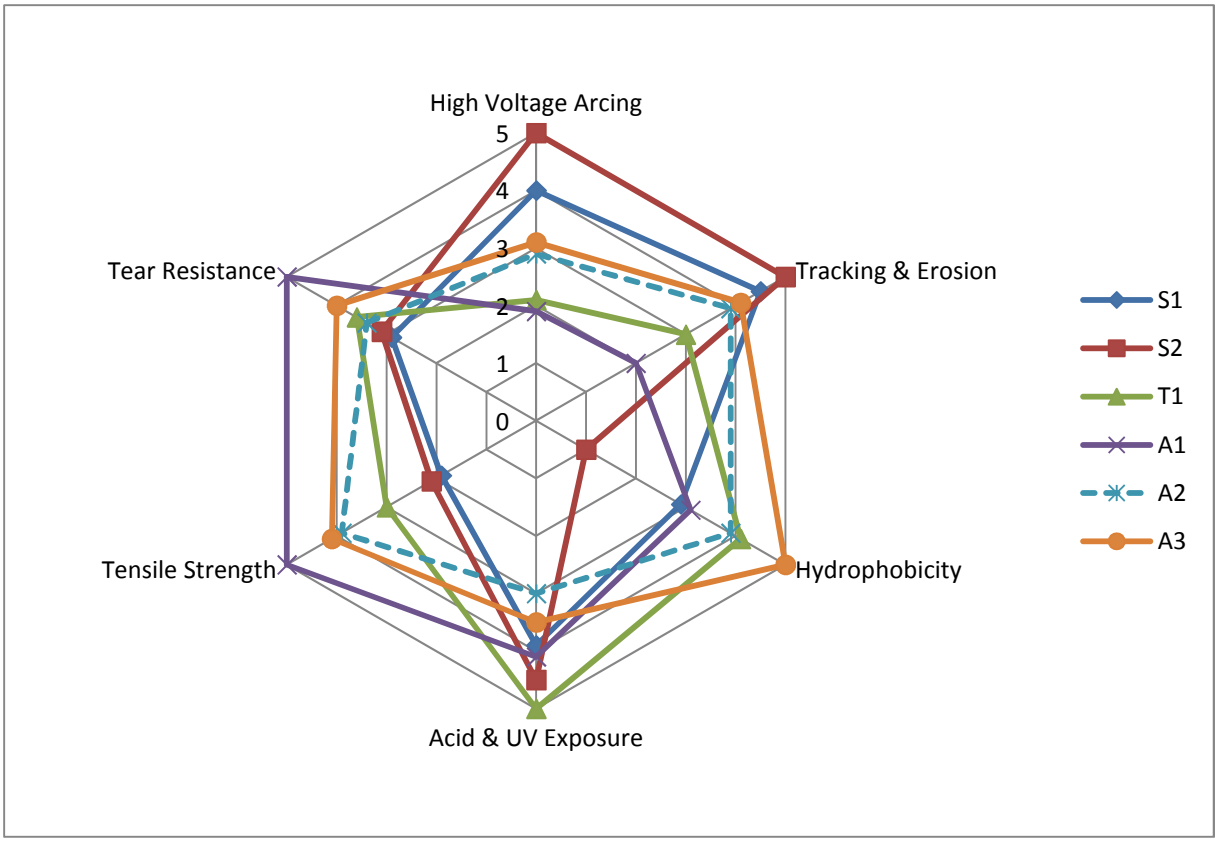

Figure 68. Radar chart summarizing properties of compositions containing standard grade ATH.

ACKNOWLEDGEMENTS

First and foremost I want to mention my parents, Sinha and Beto; this is as much their victory as it is mine. Without their education I would not have had the opportunities I did, or the wisdom to recognize and appreciate them. Still on the topic of family, I wish to thank all that gave emotional support, and apologize for the tears my parting brought them, especially Maíra, Tiago, Tânia, Inês and Paulo. For whatever mysticism left in me I wish to thank God for the many blessings and the drive to carry on.

For the financial support (under the process code 290037/2010-7), I express my gratitude to CNPq, an entity from the Brazilian government dedicated to scientific and technological development. I must also express my gratefulness to my advisor, Prof. Dr.-Ing. Kindersberger, for all the hours he dedicated to me and this project, even before I arrived in Germany. For the same reason I owe much to Dr.-Ing. Jens Seifert too, but also for welcoming me at Lapp Insulators and making available to me all I wished for. I wish to thank all at Lapp, but namely Heinz Denndörfer, Rainer Glück and Monika Wunderlich for the help with machinery and tests, as well as Fabian Lehretz, Jan Schulte-Fischedick, Martina Müller and Frau Wippenbeck.

For their time, discussions, instructions and general availability at the TUM, I want to thank all personnel, namely A. Hergert, J. Seiler, J. Niedernhuber, F. Dschung, M. Refaey, as well as Frau Rabenstein-Stoiber, for always dealing with my many questions and requests with the best of manners and giving all the help she could.

Finally, for the supplying of material samples to this research, I wish to acknowledge Dr. Annika Luks, Dr. Mario Scholz and Dr.-Ing. Jürgen Röper in the name of Nabaltec, Evonik, Heraeus and 3iP Consulting.

REFERENCES

[1] C. N. RAVERA, “Specification for composite insulators”, Eskom Specification NWS 1612, 1992.

[2] EPRI, “Application guide for transmission line non-ceramic insulators”, Electric Power Research Institute, Final Report No. TR-111566, 1998.

[3] T. ZHAO and R. A. BERNSTORF, “Ageing tests of polymeric housing materials for non-ceramic insulators”, IEEE Electrical Insulation Magazine, Vol. 14, No. 2, pp. 26-33, 1998.

[4] S. SIMMONS, M. SHAH, J. MACKEVICH, and R. J. CHANG, “Polymer outdoor insulating materials. Part III – Silicone elastomer considerations”, IEEE Electrical Insulation Magazine, Vol. 13, No. 5, pp. 25-32, 1997.

[5] J. MACKEVICH and S. SIMMONS, “Polymer outdoor insulating materials. Part II – Material considerations”, IEEE Electrical Insulation Magazine, Vol. 13, No. 4, pp. 10-16, 1997.

[6] J. MACKEVICH and M. SHAH, “Polymer outdoor insulating materials. Part I – Comparison of Porcelain and Polymer Electrical Insulation”, IEEE Electrical Insulation Magazine, Vol. 13, No. 3, pp. 5–12, 1997.

[7] “History of Composite Insulators”, Hoechst CeramTec Communique, Wunsiedel, 05.06.1990, V/H-Dr.Ki/GO.

[8] J. F. HALL, “History and Bibliography of polymeric insulators for outdoor applications”, IEEE Transactions on Power Delivery, Vol. 8, No. 1, pp. 376-385, 1993.

[9] M. EHSANI, H. BORSI, E. GOCKENBACH, G. R. BAKHSHANDEH and J. MORSHEDIAN, “Improvement of electrical, mechanical and surface properties of silicone insulators”, CEIDP, 2004 Annual Report, pp. 623-626, Boulder, USA, 2004.

[10] R. HACKAM, “Outdoor HV Composite Polymeric Insulators”, IEEE Transactions on Dielectrics and Electrical Insulation, Vol. 6, No. 5, pp. 557-585, 1999.

[11] J. S. T. LOOMS, “Insulators for High Voltage”, Peter Peregrinus Ltd., London, United Kingdom, 1990.

[12] S. FANG, Z. JIA, H. GAO, and Z. GUAN, “Influence of fillers on silicone rubber for outdoor insulation”, CEIDP, 2007 Annual Report, pp. 300-303, Vancouver, Canada, 2007.

[13] H. JAHN, “Zur Bewertung stofflicher und herstellungsbedingter Einflußgrößen auf das Hydrophobie- und Erosionsverhalten von Silikonelastomeroberflächen”, PhD Thesis, TU Dresden, 2003 (in German).

[14] S. REINER, “New ATH developments drive flame retardant cable compounding”, Plastics Additives and Compounding, Vol. 12, pp. 22-29, 2002.

[15] Z. HAN, C. DIAO, L. DONG and X. ZHANG, “Effect of Surface-treated Nano-silica on Thermal Behavior and Flame Retardant Properties of EVA/ATH composites”, IEEE International Conference on Solid Dielectrics, pp. 330-332, Winchester, United Kingdom, 2007.

[16] J. K. NELSON, Y. HU and J. THITICHAROENPONG, “Electrical properties of TiO2 nanocomposites”, CEIDP, 2003 Annual Report, pp. 719-722, Albuquerque, USA, 2003.

[17] S. H. KIM, E. A. CHERNEY and R. HACKAM, “Effects of filler level in RTV silicone rubber coatings used in HV insulators”, IEEE Transaction on Electrical Insulation, Vol. 27, No. 6, pp. 1065-1072, 1992.

[18] H. DENG, R. HACKAM and E. A. CHERNEY, “Role of the size of particles of alumina trihydrate filler on the life of RTV silicone rubber coating”, IEEE Transactions on Power Delivery, Vol. 10, No. 2, pp. 1012-1024, 1995.

[19] S. KUMAGAI and N. YOSHIMURA, “Tracking and erosion of HTV silicone rubber and suppression mechanism of ATH”, IEEE Transactions on Dielectrics and Electrical Insulation, Vol. 8, No. 2, pp. 203-211, 2002.

[20] T. TANAKA, G. C. MONTANARI and R. MÜHLHAUPT, “Polymer nanocomposites as dielectrics and electrical insulation-perspectives for processing technologies, material characterization and future applications”, IEEE Transactions on Dielectrics and Electrical Insulation, Vol. 11, No. 5, pp. 763-784, 2004.

[21] KOZAKO, R. KIDO, N. FUSE, Y. OHKI, T. OKAMOTO and T. TANAKA, “Difference in surface degradation due to partial discharges between polyamide nanocomposite and microcomposite”, CEIDP, 2004 Annual Report, pp. 398-401, Boulder, USA, 2004.

[22] AGORIS et al., “Emerging Nanocomposite Dielectrics”, CIGRE Task Force Report, Electra No. 226, pp. 24-31, June 2006.

[23] M. ROY, J. K. NELSON, R. K. MacCRONE, L. S. SCHADLER, C. W. REED and R. KEEFE, “Polymer nanocomposite dielectrics – The role of the interface”, IEEE Transactions on Dielectrics and Electrical Insulation, Vol. 12, No. 4, pp. 629-643, 2005.

[24] B. VENKATESULU and M. J. THOMAS, “Studies on the Tracking and Erosion Resistance of RTV Silicone Rubber Nanocomposite”, CEIDP, 2008 Annual Report, pp. 204-207, Québec City, Canada, 2008.

[25] M. F. FRÉCHETTE, M. TRUDEAU, H. D. ALAMDARI, S. BOILY, “Introductory remarks on nanodielectrics”, CEIDP, 2001 Annual Report, pp. 92–99, Kitchener, Canada, 2001.

[26] I. RAMIREZ, S. JAYARAM, E. A. CHERNEY, “Analysis of temperature profiles and protective mechanism against dry-band arcing in silicone rubber nanocomposites”, IEEE Transactions on Dielectrics and Electrical Insulation, Vol. 17, No. 2, pp. 597-606, 2010.

[27] S. SINGHA, M. J. THOMAS, “Polymer composite/nanocomposite processing and its effect on the electrical properties”, CEIDP, 2006 Annual Report, pp. 557-560, Kansas City, USA, 2006.

[28] I. RAMIREZ, E. A. CHERNEY, S. JAYARAM, M. GAUTHIER, “Nanofilled silicone dielectrics prepared with surfactant for outdoor insulation applications”, IEEE Transactions on Dielectrics and Electrical Insulation, Vol. 15 , No. 1, pp. 228-235, 2008.

[29] I. RAMIREZ, S. JAYARAM, E. CHERNEY, M. GAUTHIER and L. SIMON, “Erosion resistance and mechanical properties of silicone nanocomposite insulation”, IEEE Transactions on Dielectrics and Electrical Insulation, Vol. 16, No. 1, pp. 52-59, 2009.

[30] S. W. REED, “Self-Assembly of Polymer Nanocomposites for Dielectrics and HV Insulation”, IEEE International Conference on Solid Dielectrics, pp. 397-400, Winchester, United Kingdom, 2007.

[31] S. RAETZKE and J. KINDERSBERGER, “Erosion Behaviour of Nano Filled Silicone Elastomers”, Proceedings of the XIVth International Symposium on High Voltage Engineering, Paper No. C-09, Beijing, China, 2005.

[32] S. RAETZKE and J. KINDERSBERGER, “Role of interphase on the resistance to high-voltage arcing, on tracking and erosion of silicone/SiO2 nanocomposites”, IEEE Transactions on Dielectrics and Electrical Insulation, Vol. 17, No. 2, pp. 607-614, 2010.

[33] S. RAETZKE, Y. OHKI, T. IMAI, J. KINDERSBERGER, and T. TANAKA, “Enhanced performance of tree initiation V-t characteristics of epoxy/clay nanocomposite in comparison with neat epoxy resin”, CEIDP, 2008 Annual Report, Paper No. 6-2, Québec City, Canada, 2008.

[34] S. RAETZKE, Y. OHKI, T. IMAI, T. TANAKA, and J. KINDERSBERGER, “Tree Initiation Characteristics of Epoxy Resin and Epoxy/Clay Nanocomposite”, IEEE Transactions on Dielectrics and Electrical Insulation, Vol. 16, No. 5, pp. 1473–1480, 2009.

[35] P. MAITY, S. V. KASISOMAYAJULA, S. BASU, V. PARAMESWARAN and N. GUPTA, “Effect of particle dimensions and pre-processing of nanoparticles in improving surface degradation characteristics of nanodielectrics”, CEIDP, 2007 Annual Report, pp. 604-607, Vancouver, Canada, 2007.

[36] R. S. GORUR, J. MONTESINOS, L. VARADADESIKAN, S. SIMMONS, M. SHAH, “A laboratory test for tracking and erosion resistance of HV outdoor insulation”, IEEE Transactions on Dielectrics and Electrical Insulation, Vol. 4, No. 6, pp. 767-774, 1997.

[37] J. M. SEIFERT, H.-J WINTER, R. BAERSCH, A. BOGNAR, “Tracking and Erosion Performance of Liquid Silicone Rubber HV composite in Housings”, CEIDP, 2007 Annual Report, pp. 329–337, Vancouver, Canada, 2007.

[38] H. DENG, R. HACKAM and E. A. CHERNEY, “Influence of thickness, substrate type, amount of silicone fluid and solvent type on the electrical performance of RTV silicone rubber coatings”, IEEE Transactions on Power Delivery, Vol. 11, No. 1, pp. 431-443, 1996.

[39] Y. KOSHINO, I. UMEDA and M. ISHIWARI, “Deterioration of silicone rubber for polymer insulators by corona discharge and effect of fillers”, CEIDP, 1998 Annual Report, Vol. 1, pp. 72-79, Atlanta, USA, 1998.

[40] M. NOEL, J.-M. FOURMIGUE, G. RIQUEL, “Evaluation of diagnostic techniques for non-ceramic outdoor high voltage insulators”, CEIDP, 1994 Annual Report, pp. 639–644, Arlington, USA, 1994.

[41] X. LI, Y. WANG, F. LIU, “Study on improving the tracking and erosion resistance of silicone rubber”, Proceedings of the 6th International Conference on Properties and Applications of Dielectric Materials, Vol. 1, pp. 342-345, China, 2000.

[42] B. J. ASH, L. S. SCHADLER, R. W. SIEGEL, T. APPLE, B. C. BENICEWICZ, D. F. ROGER, and C. J. WIEGAND, “Mechanical Properties of Al2O3/Polymethylmethacrylate Nanocomposites”, Polymer Composites, Vol. 23, pp. 1014-25, 2002.

[43] J. WU, B. HEIL and A. SCHNETTLER, “Study on durability of nanostructured superhydrophobic insulating surfaces under simultaneous climatic and electrical stresses”, Proceedings of the XVth International Symposium on High Voltage Engineering, Paper No. T4-166, Ljubljana, Slovenia, 2007.

[44] J. WU and A. SCHNETTLER, “Degradation assessment of nanostructured superhydrophobic insulating surfaces using multi-stress methods”, IEEE Transactions on Dielectrics and Electrical Insulations, Vol. 15, No. 1, pp. 73-80, 2008.

[45] S. RAETZKE and J. KINDERSBERGER, “The effect of interphase structure in nanodielectrics”, IEEJ Trans. XX, Vol. 126, No. 1, pp. 1-6, 2006.

[46] I. RAMIREZ, S. JAYARAM, E. A. CHERNEY, “Aging evaluation of silicone rubber nanocomposites”, CEIDP, 2009 Annual Report, pp. 279-273, Virginia Beach, USA, 2009.

[47] L. H. MEYER, S. H. L. CABRAL, E. ARAUJO, E., G. CARDOSO, G. and N. LIESENFELD, “Use of nano-silica in silicone rubber for ceramic insulators coatings in coastal areas”, Conference Record of the 2006 IEEE International Symposium on Electrical Insulation, pp. 474-477, Toronto, Canada, 2006.

[48] S. RAETZKE and J. KINDERSBERGER, “Resistance to high voltage arcing and the resistance to tracking and erosion for silicone/SiO_2 nanocomposites”, Proceedings of the 16th International Symposium on High Voltage Engineering, Paper No. F-10, Johannesburg, South Africa, 2009.

[49] L. H. MEYER, S. H. L. CABRAL, G. E. CARDOSO, M. R. DE LIMA and F. H. MOLINA, “Use of Nanosilica in Silicone Rubber Coatings for Ceramic Insulators in Coastal Areas - Field Results”, Conference Record of the 2008 IEEE International Symposium on Electrical Insulation, pp. 676-679, Vancouver, Canada, 2008.

[50] E. TUNCER, C. CANTONI, K. L. MORE, D. R. JAMES, G. POLIZOS, I. SAUERS, A. R. ELLIS, “Breakdown properties of epoxy nanodielectrics”, CEIDP, 2010 Annual Report, pp. 1-4, West Lafayette, USA, 2010.

[51] E. TUNCER, G. POLIZOS, I. SAUERS, D. R. JAMES, A. R. ELLIS, K. L. MORE, “Electrical properties of a polymeric nanocomposite with in-situ synthesized nanoparticles”, CEIDP, 2009 Annual Report, pp. 527-530, Virginia Beach, USA, 2009.

[52] S. LI, G. YIN, F. NI, S. BAI, J. LI, T. ZHANG, “Investigation on the dielectric properties of nano-titanium dioxide — Low density polyethylene composites”, 2010 10th IEEE International Conference on Solid Dielectrics (ICSD), pp. 1-4, Potsdam, Germany, 2010.

[53] BIRTWHISTLE et al., “Material properties for non-ceramic outdoor insulation – State of the art”, CIGRE Working Group WG D1.14, Technical Brochure No. 255, 2004

[54] ISO 4287: Geometrical Product Specifications (GPS) - Surface texture: Profile method - Terms, definitions and surface texture parameters. International Organization for Standardization, 1997.

[55] ISO 4288: Geometrical Product Specifications (GPS) - Surface texture: Profile method - Rules and procedures for the assessment of surface texture. International Organization for Standardization, 1996.

[56] IEC 61621. Dry, solid insulating materials - Resistance test to high-voltage, low-current arc discharges. International Electrotechnical Commission, 1997.

[57] IEC 60587. Electrical insulating materials used under severe ambient conditions - Test methods for evaluating resistance to tracking and erosion. International Electrotechnical Commission, 2007.

[58] A. H. EL-HAG, L. H. MEYER, A. NADERIAN, “Experience with salt-fog and inclined-plane tests for aging polymeric insulators and materials”, IEEE Electrical Insulation Magazine, Vol. 26, No. 2, pp. 42-50, 2010.

[59] L. H. MEYER, E. A. CHERNEY, S. H. JAYARAM, “The role of inorganic fillers in silicone rubber for outdoor insulation alumina tri-hydrate or silica”, IEEE Electrical Insulation Magazine, Vol. 20, No. 4, pp. 13-21, 2004.

[60] IEC/TS 62073. Guidance on the measurement of wettability of insulator surfaces. International Electrotechnical Commission, 2003.

[61] “Dynamic contact angle measurement” by Guillaume Paumier (guillom), licensed under Creative Commons Attribution, Share Alike 3.0 via Wikimedia Commons, http://commons.wikimedia.org/wiki/File:Dynamic_contact_angle_measurement.svg#mediaviewer/File:Dynamic_contact_angle_measurement.svg. File accessed on 2014-08-12.

[62] J. HOFMANN, “Elektrische TE- und Ableitstrommessungen mit Impulsspannung an polymeren Isolierstoffoberflächen mit Tropfenbelägen zur Diagnose des Oberflächenzustandes – am Beispiel von Elastomeren”, PhD Thesis, TH Zittau, 1995 (in German).

[63] R. BAERSCH, “Bewertung der Hydrophobie sowie des Kriechstromverhaltens von Silikonelastomeren für Hochspannungs-Freiluftisolatoren”, ETG Technical Report 93, pp. 97-108, Berlin, 2003 (in German).

[64] KINDERSBERGER et al., “Evaluation of dynamic hydrophobicity properties of polymeric materials for non-ceramic outdoor insulation – Retention and transfer of hydrophobicity”, CIGRE Working Group WG D1.14, Technical Brochure No. 442, 2009.

[65] ISO 37. Rubber, vulcanized or thermoplastic - Determination of tensile stress-strain properties. International Organization for Standardization, 2011.

[66] ISO 34-1. Rubber, vulcanized or thermoplastic - Determination of tear strength - Part 1: Trouser, angle and crescent test pieces. International Organization for Standardization, 2010.

[67] M. AMIN, M. AHMED, “Effect of UV Radiation on HTV-Silicon Rubber Insulators with Moisture”, IEEE Multitopic Conference (INMIC ’07), pp. 1-5, Lahore, Pakistan, 2007.

[68] M. KUMOSA, L. KUMOSA, D. ARMENTROUT, “Causes and Potential Remedies of Brittle Fracture Failure of Composite (Non-Ceramic) Insulators, IEEE TDEI, Vol. 11, No. 6, pp. 1037-1048, 2004.

[69] J. MONTESINOS, R. S. GORUR, B. MOBASHER, “Mechanical performance of GRP rods used in nonceramic insulators after exposure to acid attack”, Eleventh International Symposium on High Voltage Engineering, Vol. 4, pp. 1-4, Johannesburg, South Africa, 1999.

[70] T. J. LEWIS, “Interfaces are the dominant feature of dielectrics at the nanometric level”, IEEE Transactions on Dielectrics and Electrical Insulation, Vol. 11, No. 5, pp. 739-753, 2004.

[71] T. TANAKA, M. KOZAKO, N. FUSE, Y. OHKI, “Proposal of a multi-core model for polymer nanocomposite dielectrics”, IEEE Transactions on Dielectrics and Electrical Insulation, Vol. 12, No. 4, pp. 669-681, 2005.

[72] T. ANDRITSCH, R. KOCHETOV, P. H. F. MORSHUIS, J. J. SMIT, “Proposal of the polymer chain alignment model”, CEIDP, 2011 Annual Report, pp. 624-627, Cancun, Mexico, 2011.

[73] S. RAETZKE, “Zur Wirkungsweise von nanoskaligen Füllstoffpartikeln in polymeren Isolierwerkstoffen der Hochspannungstechnik”, PhD Thesis, TU München, 2009 (in German).

[74] N. TAGAMI, M. OKADA, N. HIRAI, T. TANAKA, Y. OHKI, T. IMAI, M. HARADA, AND M. OCHI, “Effects of Curing and Filler Dispersion Methods on Dielectric Properties of Epoxy Nanocomposites”, CEIDP, 2007 Annual Report, pp. 232-235, Vancouver, Canada, 2007.

[75] I. RAMIREZ, E. A. CHERNEY, S. JAYARAM, M. GAUTHIER, “Silicone Rubber Nanocomposites for Outdoor Insulation Applications”, CEIDP, 2007 Annual Report, pp. 384-387, Vancouver, Canada, 2007.

[76] D. SHIIBARA, K. HAJI, T. SAKODA, M. OTSUBO, “Fundamental research on characteristics of hydrophobicity disappearance of silicone rubber surface in Dynamic Drop Test”, International Symposium on Electrical Insulating Materials (ISEIM ‘08), pp. 99-102, Japan, 2008.

[77] J. LAMBRECHT, “Über Verfahren zur Bewertung der Hydrophobieeigenschaften von Silikonelastomer-Formstoffen”, PhD Thesis, TU Dresden, 2000 (in German).

[78] R. S. GORUR, E. A. CHERNEY, R. HACKAM, T. ORBECK, “The electrical performance of polymeric insulating materials under accelerated aging in a fog chamber”, IEEE Transactions on Power Delivery, Vol. 3, No. 3, pp. 1157-1164, 1988.

[79] M. M. S. SHIRAZI, H. BORSI, E. GOCKENBACH, “Effect of TiO2 nanofillers on electrical, thermal and mechanical parameters of epoxy resin”, Conference Record of the 2012 IEEE International Symposium on Electrical Insulation (ISEI ‘12), pp. 69-72, San Juan, USA, 2012.

[80] G. B. SOHONI, J. E. MARK, “Thermal Stability of In Situ Filled Siloxane Elastomers”, Journal of Applied Polymer Science, Vol. 45, pp. 1763-1775, 1992.

[81] G. CAMINO. S. M. LOMAKIN. M. LAZZARI, “Polydimethylsiloxane thermal degradation. Part 1. Kinetic aspects”, Polymer, No. 42, pp. 2395-2402, 2001.

[82] G. CAMINO. S. M. LOMAKIN. M. LAGEARD, “Polydimethylsiloxane thermal degradation. Part 2. The degradation mechanisms”, Polymer, No. 43, pp. 2011-2015, 2002.